ABSTRACT

DUMARIEH, RANIA A. Fast-Time-Scale Methods (Stopped-Flow UV-visible and Electron Paramagnetic Resonance Spectroscopies) for Elucidating the Role of Protein Radicals in Multifunctional Peroxidases. (Under the direction of Dr. Reza A. Ghiladi).

It was thought previously that protein radicals are short-lived and too reactive to be catalytic intermediates. However, with the development of fast-time-scale spectroscopic methods, it became possible to observe these protein-radical intermediates and characterize them. The systems we became interested in studying are multifunctional heme peroxidases. In this work, we employ biochemical assays and spectroscopic techniques (stopped-flow UV-visible and EPR spectroscopies) to elucidate mechanistic insight and to help us gain a better understanding of the heme enzymes *Mycobacterium tuberculosis* KatG and dehaloperoxidase (DHP). KatG is involved in the activation of the prodrug isoniazid, and dehaloperoxidase catalyzes the oxidation of toxic trihalophenols to the less toxic dihaloquinones We used mutagenesis and the spectroscopic techniques mentioned above to gain further insight into the role of the sulfonium ion in the Met-Tyr-Trp crosslink in KatG. We also incorporated unnatural amino acids with various electronic properties into the crosslink to explore the possibility of obtaining KatG mutants with enhanced catalytic activity. In the peroxidase cycle of DHP, we identified the catalytically-competent intermediate Compound ES [Fe(IV)=O, AA$^{\bullet}$], and we identified the location of the protein radical by mutagenesis. Our findings regarding the position of the radical in DHP Compound ES support those reported by Thompson et al. [*J. Am. Chem. Soc.*, 2010], who obtained similar results by the simulation of DHP EPR spectra.

Fast Time Scale Methods (Stopped-Flow UV-visible and Electron Paramagnetic Resonance Spectroscopies) for Elucidating the Role of Protein Radicals in Multifunctional Peroxidases

by
Rania A. Dumarieh

A dissertation submitted to the Graduate Faculty of
North Carolina State University
in partial fulfillment of the
requirements for the degree of
Doctor of Philosophy

Chemistry

Raleigh, North Carolina

2011

APPROVED BY:

_____	_____
Dr. Reza A. Ghiladi Committee Chair	Dr. Stefan Franzen
_____	_____
Dr. Tatyana Smirnova	Dr. David Shultz
_____	
Dr. Lucian Lucia	

BIOGRAPHY

Rania Dumarieh was born January 9, 1980 in Jeddah, Saudi Arabia to Amna and Ameen Dumarieh. She came to the United States of America in 2001 and obtained her undergraduate degree then Master's degree in 2006 from the University of North Carolina at Charlotte. While there she worked as a research and teaching assistant. It was there that she began performing scientific research in the field of bioanalytical chemistry, spending three years in the laboratory of Dr. Brian Cooper. Upon graduation in 2006, Rania moved to Raleigh, North Carolina to attend graduate school at North Carolina State University. She joined the laboratory of Dr. Reza Ghiladi. Under the supervision of Dr. Ghiladi she obtained her Ph.D. in the field of bioinorganic chemistry.

ACKNOWLEDGMENTS

First, I would like to thank my advisor Dr. Reza Ghiladi for his help and guidance. I want to also thank my committee members Dr. Stefan Franzen, Dr. Tatyana Smirnova, Dr. David Shultz, and Dr. Lucian Lucia. Dr. Franzen and Dr. Smirnova also offered very useful discussions, and their insight was important to the progress of the research. The current postdocs in Dr. Smirnov's group, Dr. Saritha Nellutla and Dr. Maxim Voynov, put much time and effort into training me on the EPR instruments. Many thanks to all the previous and current members of the Ghiladi group, especially David Barrios, Jennifer D'Antonio, and Elke Feese for their help and their friendship. I would also like to thank my family for all their love and support throughout the years and my husband, Ali Yasar, for his love and the joy he brought into my life.

TABLE OF CONTENTS

LIST OF TABLES

LIST OF FIGURES

CHAPTER I

Introduction

It is now believed that protein radicals play an important role in the catalysis of some of the most vital processes that occur in the cell. This realization, however, came after a misconception held for a long time that radicals are too short-lived and reactive to mediate enzyme catalysis. Advanced techniques, such as stopped-flow UV-visible and electron paramagnetic resonance (EPR) spectroscopies, have contributed greatly to the observation, study and characterization of protein radical intermediates. The interest in protein radicals also grew significantly after finding that pyrroloquinoline quinone (PQQ), a cofactor found in bacterial dehydrogenases, is not responsible for the redox processes in eukaryotes and prokaryotes as was previously thought (*2*). Some of the important catalytic reactions catalyzed by protein radicals will be presented later.

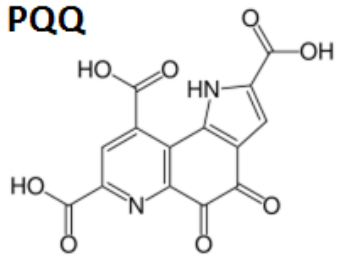

Radicals in proteins are usually located on the amino acids that are most easily oxidized: tyrosine, post-translationally modified tyrosine, tryptophan, cysteine and glycine. These redox-active amino acids can be easily oxidized by the available biological oxidants. For a comparison of the reduction potentials of these amino acids, see Table I.1. It is important to note that the local protein environment of a residue can shift its reduction potential significantly.

Table I.1: Reduction potentials and UV-visible properties of redox-active amino acids (*3*)

radical	$E^{o'}$ (V)	λ_{max} (nm) [ε_{max} (M^{-1} cm^{-1})]	g values
$Tyr^{\bullet}$	0.93-0.94	407 [3200]	2.0067, 2.0042, 2.0023
$Trp^{\bullet}$	1.01-1.05	320 [2800]	
		325 [3670]	
		510 [1750-2300]	
$TrpH^{+\bullet}$	1.15	335 [4750]	
	(pH 2, 3)	340 [3900]	
		560 [3000]	
		580 [2600]	
$Gly^{\bullet}$	1.22		2.0042, 2.0035, 2.0032
	(pH 10.5)		
$Cys^{\bullet}$	1.33	300-330 [400-1200]	2.2441, 2.0006, 1.9837

Pyruvate-formate lyase is an example of the importance of protein radicals in the chemistry of life processes. During the anaerobic catabolism of glucose, the conversion of pyruvate to acetyl CoA and formate is catalyzed by a stable radical on a glycine residue in pyruvate-formate lyase (see Figure I.1) (*3*). One of the proposed mechanisms for this reaction suggests that after the thiolate of Cys^{419} on the enzyme adds to the carbonyl of pyruvate, the radical is transferred from $Gly^{734\bullet}$ to Cys^{418}. Then the Cys^{418} radical reacts with the carboxylate group on pyruvate to form a covalent adduct with it. Upon the transfer of a hydrogen atom, an alkoxy radical **1** is formed followed by the homolytic cleavage of the C-C bond in the substrate leading to the formation of radical **2**. Radical **2** then rearranges to form radical **3**, which disproportionates into formic acid and $Cys^{418\bullet}$. Finally, formate is released leaving an acetyl-enzyme behind and the radical is restored on Gly^{734}.

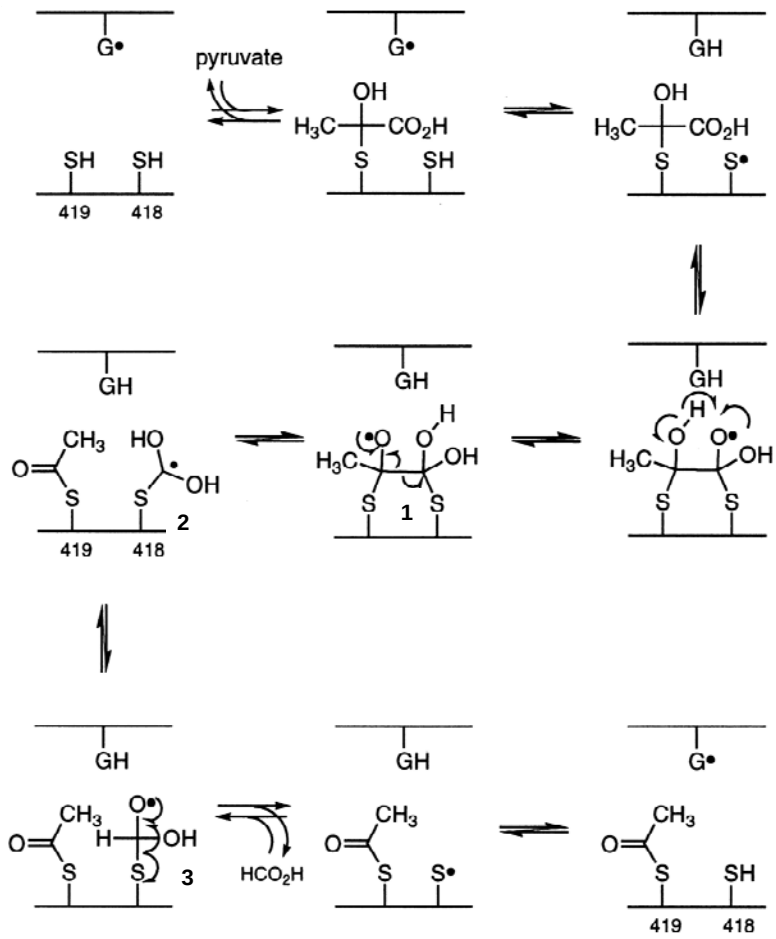

Figure I.1: A suggested mechanism for pyruvate-formate lyase (taken from Ref. (*4*)).

The reduction of ribonucleotides to deoxyribonucleotides (the building blocks of DNA) as catalyzed by ribonucleotide diphosphate reductase (RNR) is another prime example of a critically important life process that is protein-radical mediated. The process first involves the formation of a $Tyr^{122\bullet}$-diferric cluster cofactor, a self-catalytic biosynthesis that requires iron, oxygen and a reducing agent. The fact that the tyrosine residue is buried inside the protein contributes to the stability of that radical. Through a series of redox active residues, an electron is transferred from Cys^{439} in the active site to Tyr^{122}, and a thiyl radical is formed (see Figure I.2). It is interesting to note that based on the reduction potentials of these residues, the electron transfer process is predicted to be thermodynamically unfavorable. However, the environment surrounding them in the protein modifies their

reduction potentials and makes it easier for the electron to be transferred. After that, $Cys^{439\bullet}$ abstracts a hydrogen atom from the C3′ of ribose. As a result, the 2′-OH is activated and becomes a good leaving group upon receiving a proton from one of the thiol groups on the enzyme, and at the same time, 3′-OH is deprotonated. After the 2′-OH leaves, an α-keto radical is produced. The reduction of this activated substrate via the oxidation of two cysteines to the disulfide generates the 3′-deoxynucleotide radical, which then abstracts a hydrogen atom from Cys^{439} regenerating the thiyl radical. At first, there was some resistance to the idea that thiyl radicals can participate in catalysis mainly because RSH compounds can donate a hydrogen with a rate that is 4 orders of magnitude higher than that with which they can abstract a hydrogen. However, if the hydrogen abstraction process is coupled to another fast reaction, then it can proceed further to the right and go to completion (*4*).

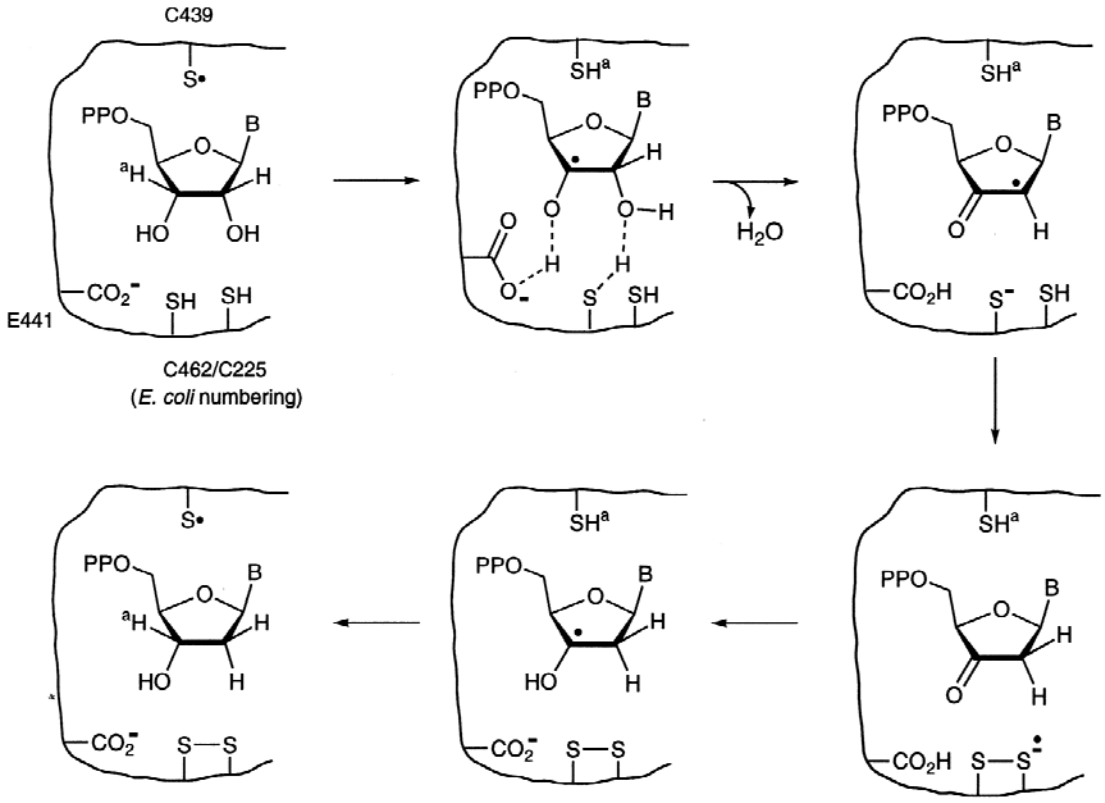

Figure I.2: Mechanism of the reduction of ribonucleotides to deoxyribonucleotides by RNR (taken from Ref. (*4*))

Peroxidases and catalases are also important classes of enzymes whose reaction mechanisms involve radicals. For example, mammalian peroxidases play important roles in defense against infection, hormone biosynthesis and pathogenesis. The peroxidase in its resting state [Fe(III) heme] reacts with a molecule of hydrogen peroxide (H_2O_2), which then undergoes heterolytic cleavage to form H_2O and an oxygen atom with six valence electrons "oxene". The highly reactive "oxene" oxidizes the iron as well as the porphyrin. The two-electron-oxidized species is Called compound I [Fe(IV)=O, porphyrin π-cation radical] (see Figure I.3). Compound I can then react with a molecule of the substrate in a one-electron process to form Compound II [Fe(IV)=O or Fe(III)-OH, aa$^{\bullet}$), which is only a single oxidizing equivalent above the resting state. Finally, Compound II is reduced by a second electron to the resting state. Catalases also react with H_2O_2 to form Compound I. However, in catalases Compound I is converted back to the resting state via a two-electron reduction step not via two sequential one-electron reduction steps (see Figure I.3).

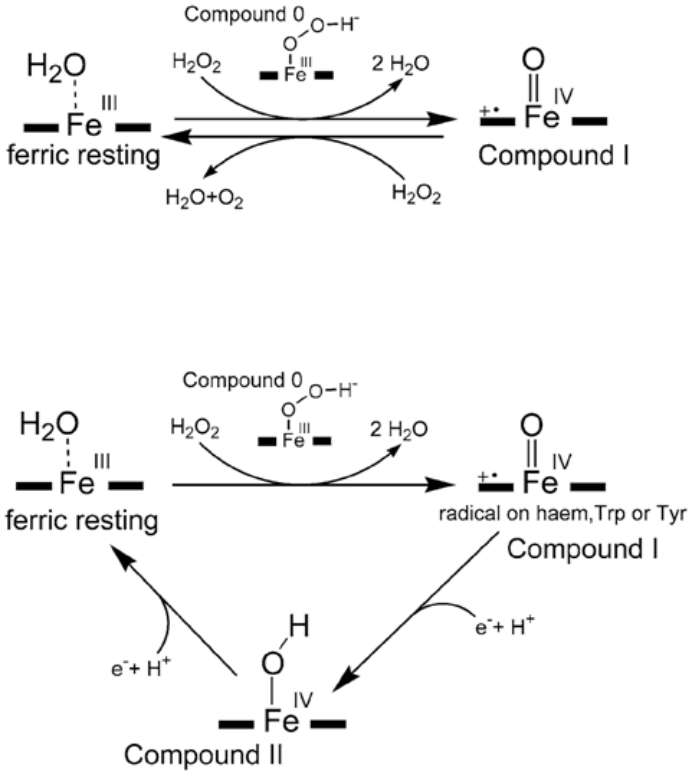

Figure I.3: Mechanisms of catalases (top) and peroxidases (bottom)

Cytochrome c peroxidase (CcP) was the first heme peroxidase to be crystallized 31 years ago. It differs from most peroxidases in that the radical in Compound I is not on the porphyrin but on Trp^{191} (see Figure I.3). This species that is two oxidizing equivalents above the resting state and has one oxidizing equivalent residing on an amino acid residue will be hereafter referred to as Compound ES instead of Compound I. Compound ES in CcP is remarkably stable ($t_{1/2}$ = 6.6±1.4 h) because of the negative potential surrounding $Trp^{+\bullet}$, and because deprotonation of the proximal His by Asp^{235} increases the electron density on the iron and stabilizes the oxoferryl moiety. It took a long time to discover the identity of the organic radical of CcP-Compound ES because the EPR signal was too broad and didn't resemble that of an organic radical. However, through mutagenesis it was discovered that Trp^{191} is the site of radical formation and that the shape of the signal was due to an exchange interaction between the unpaired electrons in the heme and in $Trp^{+\bullet}$. So, why is CcP the only known peroxidase to date to form a radical on Trp^{191} and not on the porphyrin? CcP differs from other peroxidases in that in most peroxidases there is a phenylalanine in the position of Trp^{191}. Why is the porphyrin radical more stable in some peroxidases like horse radish peroxidase (HRP) and does not decay into an amino acid radical? The reasons for that are still subject for debate, but there is a hypothesis that when the heme propionates are not hydrogen bonded (like in CcP), then the increased electron density can fill the "hole" in the porphyrin π-cation radical, and it becomes destabilized. The substrate of CcP, which is cytochrome c, binds to the surface of CcP to facilitate the transfer of an electron to the Trp^{191} radical. It was found that CcP can catalyze the reduction of up to 10 H_2O_2 molecules in the absence of a reducing substrate, which suggested that H_2O_2 is reduced to H_2O by the oxidation of amino acid residues in CcP. Reduction of additional H_2O_2 molecules by Compound ES in the absence of substrate requires the electron transfer from a redox-active amino acid residue to the Fe(IV)=O moiety and the formation of a new protein-based radical. Upon the reaction of H_2O_2 with Fe(III)-OH, Fe(IV)=O is regenerated and an additional protein radical is formed. Figure I.4 shows the active site of CcP where the heme is surrounded by a number of readily oxidizable residues (Tyr, Trp, Met).

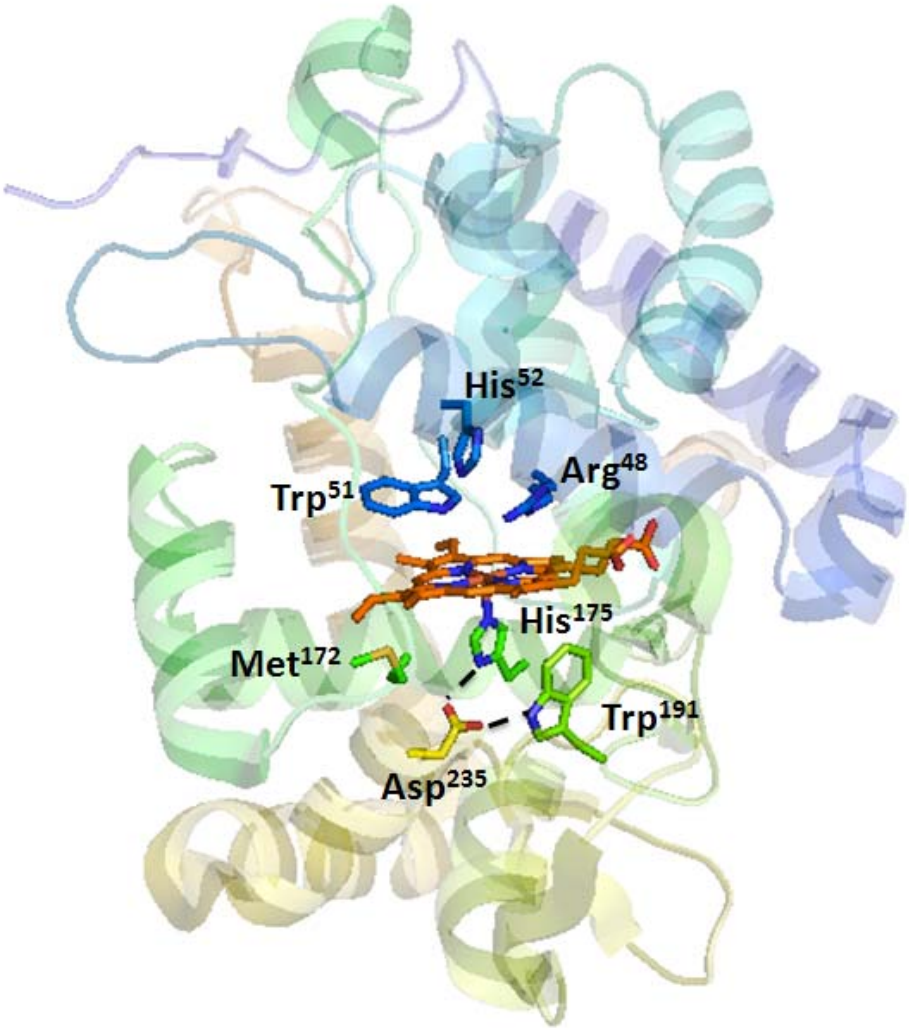

Figure I.4: Active site of CcP

The importance of protein radicals in human health and disease can readily be considered in tuberculosis (TB). Tuberculosis is an airborne bacterial infection caused by *Mycobacterium tuberculosis (Mtb)*. Eight million people every year are infected with active tuberculosis, and upwards of two million people die of tuberculosis annually. Most of the individuals who are infected with active tuberculosis do not show symptoms, and they face the risk of activation (2%-23%) when their immune systems get compromised. Although a number of antibiotics, such as isoniazid discovered in the 1940-50s, have slowed the spread of tuberculosis considerably, the alarming increase in multiple drug-resistant strains of TB

since the 1980s has led to the World Health Organization issuing multiple health alerts on tuberculosis.

The role of a single peroxidase in the rise of drug-resistant strains of TB has been now well established. *Mycobacterium tuberculosis* KatG is a bifunctional enzyme that acts as both a catalase and a peroxidase. In the presence of small amounts of H_2O_2, KatG Compound I [Fe(IV)=O, $Por^{+\bullet}$] is formed. This two-electron-oxidized intermediate has been shown to react with isonicotinic acid hydrazide (INH), a prodrug used for the treatment of tuberculosis. Oxidized INH reacts with NAD^+ to form an INH-NAD adduct, which subsequently binds very tightly to InhA and acts as an inhibitor. InhA is an enoyl-acyl carrier protein reductase, an enzyme involved in the biosynthesis of mycolic acid, which is an important component of the mycobacterial cell wall.

Since KatG is responsible for the peroxidative activation of one of the frontline drugs (INH), and because it is the only catalase in *Mycobacterium tuberculosis*, many studies have been undertaken to understand its structure-function relationship. Smeluvich et al. (*5*) reviewed the work that has been done in this area until 2005. Through the examination of four KatGs (*Haloarcula marismortui*, *Burkholdeia pseudomallei*, *Mycobacterium tuberculosis*, and *Synechococcus*), it was noted that KatGs have a sequence homology to class I plant peroxidases, and they have a catalase activity comparable to that of monofunctional catalases (k_{cat} = 3500-6000 s^{-1}, K_M = 3.7-8 mM and k_{cat}/K_M = 2.4×10^5-8.9×10^6 M^{-1} s^{-1}). Crystal structures of the four KatGs (*6-8*) show that there are conserved amino acids in the proximal and distal heme sides at the same positions as in class I peroxidases. For example, one conserved proximal triad is His-Asp-Trp. The hydrogen bonds between Asp^{402} and His^{290} and between His^{290} and Trp^{311} (*Synechocystis* numbering used in the review) play a major role in maintaining the stability of KatG architecture. In mutants where these hydrogen bonds were completely lost, the heme binding to the protein decreased significantly (*9-11*). Also, these bonds are part of the hydrogen-bonding network that exists between the proximal and distal residues. Another conserved triad is Arg-His-Trp, which is located on the distal side of the heme. The Arg^{119}/His^{123} pair is important for the heterolytic cleavage of the O-O bond in H_2O_2 for Compound I formation, which is the initial step in the

catalase and peroxidase cycles. His^{123} is also hydrogen-bonded to Asn^{153}. Mutation of Asn^{153} makes His^{123} less basic and affects its ability to act as an acid-base catalyst in the formation of Compound I. Moreover, Asn^{153} is adjacent to Asp^{152} which is important for catalase activity.

Despite the sequence homology between KatG and peroxidases, there are some residues that are KatG-specific. One of those residues is the distal Asp^{152} which forms a hydrogen bond with Ile^{248}. Ile^{248} is part of the KatG-specific insertion LL1 (see Figure I.5) which links the distal side with the proximal E and F helices with the latter carrying the proximal His^{259}. Therefore, mutation of the distal Asp^{152} affects the proximal His-Asp hydrogen bond mentioned above. Asp^{152} is also located at the entrance of the substrate channel and guides the substrate H_2O_2 to its oxidation site.

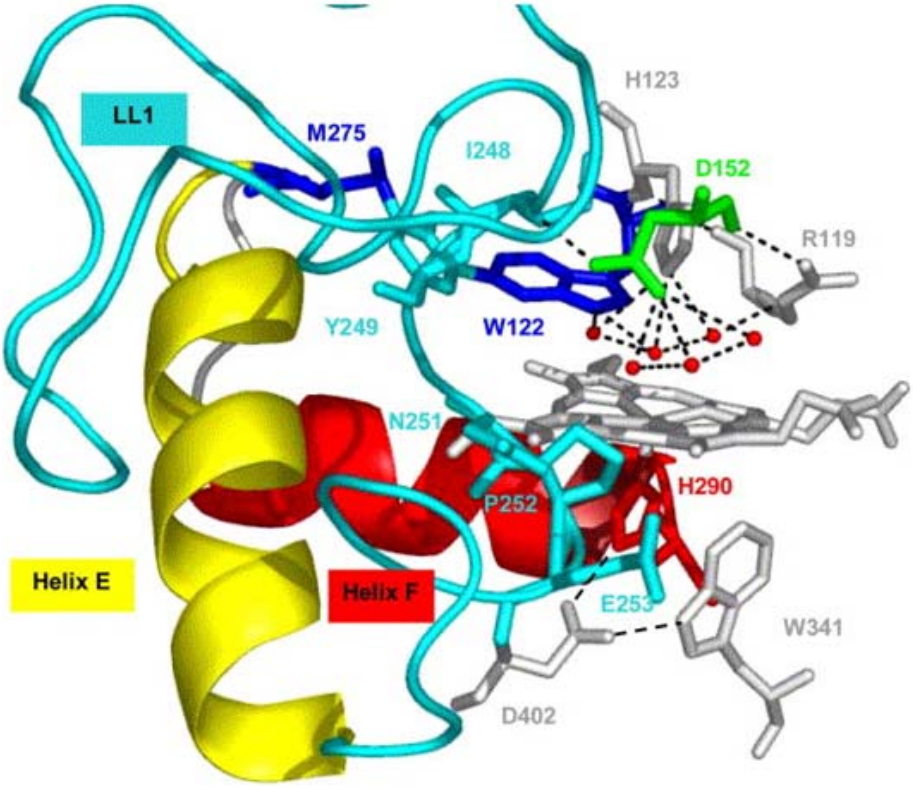

Figure I.5: LL1 connecting the distal side with helices E and F. Numbering is for *Synechocystis.* Typical peroxidase residues are in grey, the proximal His is in red, and the crosslink residues are in blue (Figure taken from Ref. (*5*)).

What is also unique in KatGs is that they have covalent bonds between Trp^{122}, Tyr^{249} and Met^{275} (*Synechocystis* numbering). Mutation of Tyr or Trp prevents the crosslink from forming but mutation of Met still allows a bond to be formed between Trp and Tyr. The Met-Tyr-Trp crosslink has been found to be crucial for catalase activity. Overall, the integrity of the distal side and of the substrate channel is important for catalase activity but does not influence the peroxidase activity significantly. Also, the hydrogen-bonding network maintains the reduction potentials of redox-active residues, which is an important factor in the formation of protein radicals which are very important catalytic intermediates.

Singh et al. (*12*) identified the intermediates in the peroxidase cycle of *Mtb* KatG. By using multifrequency EPR spectroscopy, selective deuterium labeling, and mutagenesis, they identified two Trp radicals as well as a Tyr radical upon the reaction of KatG with peroxyacetic acid (PAA). One of the Trp radicals was assigned to Trp^{321} and believed to be in an exchange interaction with the heme center. When KatG was reacted with PAA, a 400-G signal that was temperature dependent was observed. Due to the shape of the signal, it was believed to be due to an organic radical in an exchange interaction with the heme as in CcP. Because the W107F and W91F mutants have the same wide signal as the WT enzyme, Trp^{107} and Trp^{91} cannot be the sites of the radical. However, since the position of the Trp radical in CcP is conserved in KatG and corresponds toTrp^{321}, the W321F mutant was expressed and tested. The W321F mutant did not show the broad EPR signal leading to the conclusion that it is the site of the 400-G radical signal. At higher temperatures and upon the reaction with PAA, a narrower signal was observed. To decide whether the narrow signal was due to Tyr or Trp, first the Tyr residues were deuterated and the signal became narrower indicating the contribution of a Tyr radical to the narrow signal. Interestingly, when the Trp residues were deuterated, the same effect on the signal was observed. Therefore, both a Tyr and a Trp radical contribute to the narrow signal. High field data, where the g values are better resolved, also confirmed that conclusion. Also, the W91F and W107F mutants showed the contribution of both a Tyr and a Trp radical to the narrow signal suggesting that Trp^{91} and Trp^{107} are not the sites of the radical. Upon incubation of WT KatG with INH and reaction with PAA, the broad signal did not disappear at 4 K, indicating that [Fe(IV)=O, $Trp_{321}^{+\bullet}$] is

not the reactive species with INH. However, the narrow signal disappeared. Following this study, the W321F mutant was preincubated with NIH and reacted with PAA. Like in the WT enzyme, the Trp and Tyr radicals contributing to the 20-G signal were absent. However, a new very broad signal (2000 G) corresponding to Compound I appeared in the 4 K spectrum. This suggested that Compound I does not react with INH, and that the Trp or Tyr radicals that form subsequently are responsible for the fast reaction with INH.

In an effort to understand the catalase mechanism of KatG, Zhao et al. (*13*) used stopped-flow UV-visible spectroscopy and mutagenesis to identify the intermediates involved in that mechanism. They proposed an important role for a radical located on the Met-Tyr-Trp adduct, which is unique to KatG. They also showed that the loss of catalase activity in the KatG mutant W107F is linked to loss of the protein radical signal and greater stability of the oxyferrous intermediate which has a longer life-time in the W107F mutant than in the WT enzyme during the turnover of H_2O_2. Interestingly, a significant amount of the W107F mutant was isolated in the oxyferrous form after purification, and more abundant amount of 6-coordinate heme was present in KatG(W107F) compared to the WT enzyme. So, what is the role of the protein radical and the oxyferrous intermediate in the catalase cycle? The conclusion that the oxyferrous intermediate is reactive in KatG is based on the observation that the turnover of H_2O_2 occurs in the presence of this intermediate. However, because the oxyferrous form that is produced from the photolysis of the carbonyl enzyme is inactive, then there must be another additional feature that participates in catalysis. Since the lifetime of the protein radical (narrow doublet) corresponds with the time required to consume H_2O_2, this intermediate was thought to be catalytically competent. The enhanced oxyferrous stability in the W107F mutant may be due to better hydrogen bonding of His^{108} to dioxygen. Moreover, the presence of Trp in the WT enzyme may be destabilizing for 6-coordinate species probably to avoid the formation of a dead end intermediate. It was finally concluded that the narrow doublet species is important for catalase activity, and that mutation of the adduct eliminates the narrow doublet and catalase activity and improves the stability of the oxyferrous intermediate.

In a companion paper to the one mentioned above, Suarez et al. (*1*) proved theoretically that the protein radical that is required for catalase activity is located on the Met-Tyr-Trp crosslink. Rapid freeze-quench EPR at X band and D band was used to detect the protein radical in order to perform simulations that allowed the prediction of the radical location. During the turnover of H_2O_2, a narrow doublet with an 11-G hyperfine splitting was observed. D-band EPR shows a signal with two g_x values (2.00550 and 2.00606) and unique g_y (2.00344) and g_z (2.00186) values (for native tyrosyl radicals, g_y and g_z are between 2.0020 and 2.0042). The crystal structure coordinates of the Met-Tyr-Trp adduct were used in DFT calculations, and the predicted signal matched the one obtained experimentally. Therefore, the tyrosyl radical was assigned to the adduct. The two g_x values reflect variation in the electronic environment around the tyrosine due to hydrogen bonding: the larger the g_x value the weaker the hydrogen bonding. Based on these findings, a role for the adduct radical was proposed. Upon reaction with H_2O_2, Compound I is formed but not detected. Then the porphyrin radical in Compound I is reduced, and a radical is formed on the Met-Tyr-Trp adduct. Upon the reaction with another H_2O_2 molecule, Compound III [Fe(III)-O_2^-] with an adduct radical is formed. The adduct radical was proposed to regenerate the ferric form of the enzyme by aiding in the release of O_2 from Compound III (see Figure I.6).

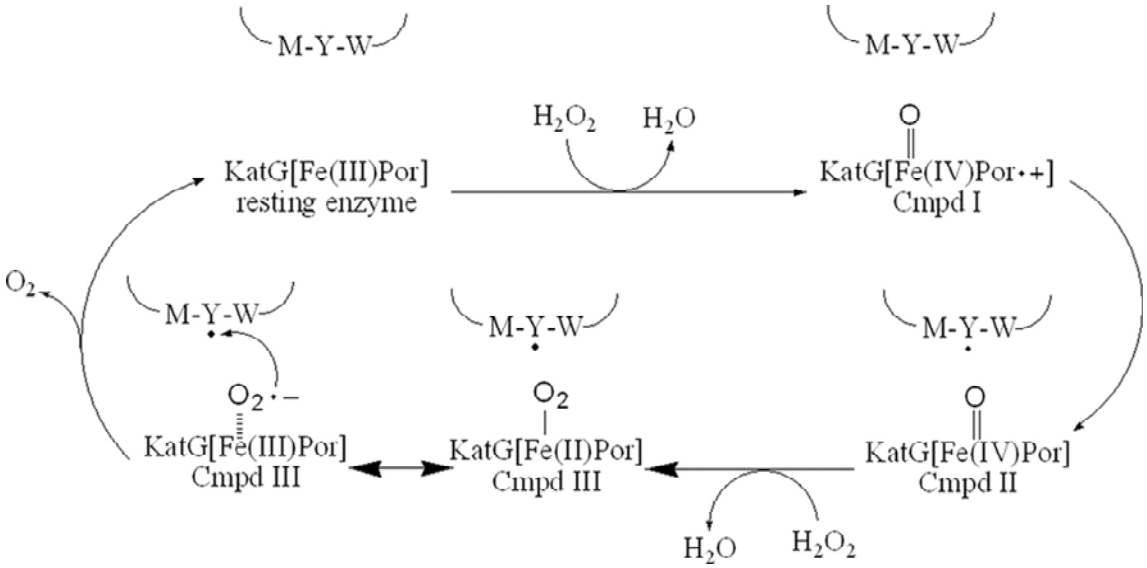

Figure I.6: The mechanism proposed by Suarez et al. (*1*) for the catalase activity of KatG

As mentioned above, a radical signal (narrow doublet) at g = 2.0034 during the turnover of KatG with H_2O_2 was observed. From the anisotropy of that radical signal, it was thought to be due to a Tyr radical that is important for catalase activity. Since any mutation in the MYW adduct eliminated that radical as well as the catalase activity, and after some simulation studies by Suarez et al (*1*), the radical was assigned to Tyr^{229}. To confirm this conclusion experimentally, Zhao et al. (*14*) prepared two KatG samples, one grown in a medium containing tyrosine deuterated at the beta-methylene position and another grown in a medium containing tyrosine deuterated at the 3 and 5 positions. In the first sample, the doublet became a singlet with a width of 11 G instead of 17 G, while the spectrum of the second sample with the 3 and 5 positions on tyrosine deuterated didn't show any change. This result indicates that the radical position in the undeuterated sample is a Tyr which has the 3 and 5 positions not available making the Tyr in the crosslink a plausible candidate. Also, 21 Tyr mutants were expressed, and they all showed the radical formation except for Y229F supporting their assignment.

Another metalloenzyme where radicals play an important mechanistic role is *Amphitrite ornata* dehaloperoxidase (DHP). This bifunctional heme protein possesses both hemoglobin and peroxidase activity, and has been suggested to protect *A. ornata* from toxic substances (brominated phenols) that are secreted by other organisms, such as *Thelespus crispis* and *Nomastus lobatus*, as part of their defense mechanism. DHP catalyzes the oxidative dehalogenation of trihalophenol to less toxic dihaloquinones. Understanding the mechanism of DHP is an important step towards using this enzyme for bioremediation in the future.

A number of mechanistic studies have been undertaken on DHP in order to determine the origins of its bifunctional activity. Davydov (*15*) et al. used 77 K cryoreduction EPR/ENDOR to study the peroxidase and hemoglobin functions of DHP. The observation of Compounds I, II and ES in the absence and presence of the substrate analog trifluorophenol (F_3PhOH) confirms that the oxidative dehalogenation of trihalophenols by DHP proceeds through two consecutive one-electron steps. The oxyferrous form of DHP was cryoreduced at 77 K resulting in peroxoferric species [Fe(III)-O_2^{2-}] that is paramagnetic but preserves the

structure of the diamagnetic precursor. The peroxoferric species is a mixture of two forms A and B (whose abundance is slightly pH dependent) indicating that the oxyferrous precursor exists in two forms. The presence of these two forms might be due to the flexibility of the distal His^{55}. Upon annealing of the peroxoferric species above 170 K, it abstracts a proton and forms hydroperoxoferric DHP, which upon further annealing leads to the formation of a signal with a g value equal to 3.75 that was assigned to Compound I where the porphyrin radical is ferromagnetically coupled to the ferryl center. Compound ES is not observed in the cryoreduction and annealing process perhaps due to the formation of strong residual radicals by the cryoreduction process. However, Compound II was observed. The decrease in the accumulation of Compound I during the annealing of cryoreduced oxyferrous DHP in the presence of F_3PhOH suggests that the substrate reduces Compound I to Compound II and a substrate radical is formed. The absence of peaks in the ^{19}F ENDOR spectrum of DHP incubated with F_3PhOH suggested that the fluorine atoms are farther than 5 Å away from the paramagnetic center. Therefore, the substrate most probably binds close to the heme but outside the distal pocket.

After the detection of Compound ES in DHP by Feducia et al. (*16*), Thompson et al. (*17*) identified the location of the Tyr radical in Compound ES by simulating the EPR spectra. They also monitored and characterized the ferric forms of the enzyme as well as the free radicals at different incubation times with H_2O_2 and at varying pH values. Two high-spin (HS) ferric forms were observed for DHP in the resting state. One of the forms displays a rhombic signal (R1HS) and is more abundant at low pH (pH 5) while the other form displays a near-axial signal (NAHS) and is more abundant at high pH (pH 7). The two forms are thought to correspond to the open and closed conformations of the distal His^{55}, respectively. Because the axial state in globins (Hb and Mb) corresponds to a water molecule being bound to the heme in the sixth position and hydrogen-bonded to the distal His, the NAHS signal was assigned to DHP having His^{55} in the closed conformation. And since the binding of 4-iodophenol induces a rhombic EPR signal and the crystal structure of DHP-4-iodophenol complex shows the distal His pushed out of the distal pocket, the R1HS signal was assigned to a 5-coordinate species of DHP having His^{55} in the open conformation. The protonation of

the distal His at low pH disrupts its hydrogen bonding with the water molecule on the distal side of the heme, and the distal His is pushed out of the active site. Also, the higher positive charge on His^{55} at low pH disfavors the His^{55} being close to the positively-charged heme.

The protein radical EPR signal at pH 5 was clearly different from that at pH 7. Upon simulation of both spectra and comparing the obtained rotation angles with published crystal structures, it was concluded that the "principal radical" is located on Tyr^{34} while the other radical which is more observable at low pH is located on Tyr^{38} and called the "pH 5 radical". However, only the Tyr^{34} is associated with Compound ES because at higher pH, the His is in the closed conformation and DHP has peroxidase activity. Also, when the ferryl is in the protonated state (pK_a=4.7), then it is more reactive. The reason for the enhanced reactivity is that the protonated oxoferryl is in resonance with a ferric heme coordinated by a hydroxyl radical (a very strong oxidizing agent). Interestingly, a crosslink between the heme and the protein was detected, and Compound RH that forms in the absence of substrate is believed to be a ferric heme with a crosslink to the protein. Formation of Compound RH and of the Tyr^{38} radical are believed to be two pathways for the decay of Compound ES depending on the conformation of His^{55}. In the open conformation at low pH, the reactive potonated oxoferryl abstracts a proton from the nearest oxidizable site (the porphyrin) forming a neutral porphyrin radical that combines with the neutral Tyr^{34} radical (located close to the active site). In the closed conformation, which is more abundant at high pH, the reactive protonated oxoferryl abstracts a proton from the imidazole of His^{55}, which is in close proximity to the heme center in this case. But what happens next? In the closed conformation, His^{55} is very close to Tyr^{38}, so after the His^{55} is oxidized by the protonated oxoferryl, a radical on Tyr^{38} is formed. It was finally concluded in this study that the path of decay for Compound ES in DHP depends on whether the distal His is in the closed or open conformation and that the formation of Compound RH in the absence of substrate is a safe way to terminate two oxidizing equivalents and prevent the unwanted propagation of radicals.

In the following chapters, we employ biochemical assays and spectroscopic techniques (stopped-flow UV-visible and EPR spectroscopies) to elucidate mechanistic insight and to help us gain a better understanding of the heme enzymes KatG and DHP. We

used mutagenesis and the spectroscopic techniques mentioned above to gain further insight into the role of the sulfonium ion in the Met-Tyr-Trp crosslink in KatG. We also incorporated unnatural amino acids with various electronic properties into the crosslink to explore the possibility of obtaining KatG mutants with enhanced catalytic activity. In the peroxidase cycle of DHP, we identified the catalytically-competent intermediate Compound ES [Fe(IV)=O, AA$^{\bullet}$], and we identified the location of the protein radical by mutagenesis. Our findings regarding the position of the radical in DHP Compound ES support those reported by Thompson et al. (*17*), who obtained similar results by the simulation of DHP EPR spectra.

REFERENCES

1. Suarez, J., Ranguelova, K., Jarzecki, A. A., Manzerova, J., Krymov, V., Zhao, X. B., Yu, S. W., Metlitsky, L., Gerfen, G. J., and Magliozzo, R. S. (2009) An Oxyferrous Heme/Protein-based Radical Intermediate Is Catalytically Competent in the Catalase Reaction of Mycobacterium tuberculosis Catalase-Peroxidase (KatG), *Journal of Biological Chemistry 284*, 7017-7029.

2. Pedersen, J. Z., and Finazziagro, A. (1993) Protein-Radical Enzymes, *Febs Letters 325*, 53-58.

3. Stubbe, J., and van der Donk, W. A. (1998) Protein Radicals In Enzyme Catalysis, *Chemical Reviews 98*, 705-762.

4. Stubbe, J., and van der Donk, W. A. (1998) Protein Radicals in Enzyme Catalysis, *Chemical Rreviews 98*, 705-762.

5. Smulevich, G., Jakopitsch, C., Droghetti, E., and Obinger, C. (2006) Probing the Structure and Bifunctionality of Catalase-Peroxidase (Katg), *Journal of Inorganic Biochemistry 100*, 568-585.

6. Yamada, Y., Fujiwara, T., Sato, T., Igarashi, N., and Tanaka, N. (2002) The 2.0 Angstrom Crystal Structure of Catalase-Peroxidase from *Haloarcula marismortui*, *Nature Structural Biology 9*, 691-695.

7. Bertrand, T., Eady, N. A. J., Jones, J. N., Nagy, J. M., Jamart-Gregoire, B., Raven, E. L., and Brown, K. A. (2004) Crystal Structure of *Mycobacterium tuberculosis* Catalase-Peroxidase, *Journal of Biological Chemistry 279*, 38991-38999.

8. Carpena, X., Loprasert, S., Mongkolsuk, S., Switala, J., Loewen, P. C., and Fita, I. (2003) Catalase-peroxidase KatG of *Burkholderia pseudomallei* at 1.7 A Resolution, *Journal of Molecular Biology 327*, 475-489.

9. Santoni, E., Jakopitsch, C., Obinger, C., and Smulevich, G. (2004) Comparison between Catalase-Peroxidase and Cytochrome *c* Peroxidase. The Role of the Hydrogen-Bond Networks for Protein Stability and Catalysis, *Biochemistry 43*, 5792-5802.

10. Hillar, A., Peters, B., Pauls, R., Loboda, A., Zhang, H. M., Mauk, A. G., and Loewen, P. C. (2000) Modulation of the Activities of Catalase-Peroxidase HPI Of *Escherichia coli* by Site-Directed Mutagenesis, *Biochemistry 39*, 5868-5875.

11. Jakopitsch, C., Regelsberger, G., Furtmuller, P. G., Ruker, F., Peschek, G. A., and Obinger, C. (2002) Engineering the Proximal Heme Cavity of Catalase-Peroxidase, *Journal of Inorganic Biochemistry 91*, 78-86.

12. Singh, R., Switala, J., Loewen, P. C., and Ivancich, A. (2007) Two Fe(IV)=O Trp(center dot) Intermediates in *M-tuberculosis* Catalase-Peroxidase Discriminated by Multifrequency (9-285 Ghz) EPR Spectroscopy: Reactivity Toward Isoniazid, *Journal of the American Chemical Society 129*, 15954-15963.

13. Zhao, X., Yu, S., Ranguelova, K., Suarez, J., Metlitsky, L., Schelvis, J. P. M., and Magliozzo, R. S. (2009) Role of the Oxyferrous Heme Intermediate and Distal Side Adduct Radical in the Catalase Activity of *Mycobacterium tuberculosis* KatG Revealed by the W107F Mutant, *Journal of Biological Chemistry 284*, 7030-7037.

14. Zhao, X. B., Suarez, J., Khajo, A., Yu, S. W., Metlitsky, L., and Magliozzo, R. S. (2010) A Radical on the Met-Tyr-Trp Modification Required for Catalase Activity in Catalase-Peroxidase Is Established by Isotopic Labeling and Site-Directed Mutagenesis, *Journal of the American Chemical Society 132*, 8268-+.

15. Davydov, R., Osborne, R. L., Shanmugam, M., Du, J., Dawson, J. H., and Hoffman, B. M. (2010) Probing the Oxyferrous and Catalytically Active Ferryl States of Amphitrite ornata Dehaloperoxidase by Cryoreduction and EPR/ENDOR Spectroscopy. Detection of Compound I, *Journal of the American Chemical Society 132*, 14995-15004.

16. Feducia, J., Dumarieh, R., Gilvey, L. B. G., Smirnova, T., Franzen, S., and Ghiladi, R. A. (2009) Characterization of Dehaloperoxidase Compound ES and Its Reactivity with Trihalophenols, *Biochemistry 48*, 995-1005.

17. Thompson, M. K., Franzen, S., Ghiladi, R. A., Reeder, B. J., and Svistunenko, D. A. (2010) Compound ES of Dehaloperoxidase Decays via Two Alternative Pathways Depending on the Conformation of the Distal Histidine, *Journal of the American Chemical Society 132*, 17501-17510.

CHAPTER II

Catalytic Relevance of the Sulfonium Ion in the Met-Tyr-Trp Crosslink of *Mycobacterium tuberculosis* Catalase-Peroxidase (KatG)

Rania Dumarieh, Katalin F. Medzihradszky, Paul R. Ortiz de Montellano and Reza A. Ghiladi.

Abstract

The Met-Tyr-Trp adduct has been shown to be a unique protein crosslink that imparts catalatic activity to the bifunctional catalase-peroxidases (KatGs). To further probe the impact that this crosslink has on the mechanism of KatG, we have investigated recombinant *Mycobacterium tuberculosis* KatG(M255C), whose Met→Cys mutation leads to the formation of a Cys-Tyr-Trp protein crosslink as confirmed by mass spectrometric studies. Stopped-flow UV-visible and rapid-freeze-quench electron paramagnetic resonance spectroscopies were employed to characterize Compounds I, II and III. Interestingly, as one progresses in the series: crosslink-absent [KatG(Y229F)], Tyr-Trp [KatG(M255I)], Cys-Tyr-Trp [KatG(M255C)], and Met-Tyr-Trp crosslink (WT KatG), it was observed that: i) the rate of formation of Compound II (oxoferryl) intermediate was increasingly attenuated, suggesting that a possible role of the crosslink is to avoid formation of this catalase-inactive species; and ii) conversion of Compound II to Compound PR, a putative one-electron oxidized species (protein radical), became progressively accelerated, indicating that the crosslink may facilitate the reduction of Compound II. The combined effects of slower Compound II formation and accelerated Compound II reduction likely minimize the amount of time that this catalase-inactive species has to react with additional H_2O_2, thus favoring catalase activity. Both of these effects correlate well with the observed trend in catalase activity of KatG (WT > M255C > M255I > Y229F), and further support a ferryl avoidance role for the Met-Tyr-Trp crosslink. Additional insight into the overall contribution of the Met-Tyr-Trp crosslink to the catalase-peroxidase mechanism is also presented.

II.1. Introduction

KatG is a bifunctional enzyme that acts as a catalase ($H_2O_2 \rightarrow H_2O + 1/2O_2$) and as a peroxidase ($2\ AH + H_2O_2 \rightarrow 2A^{\bullet} + 2H_2O$) and belongs to Class I of the peroxidase superfamily (plants, fungi and bacteria). KatG shares significant sequence homology with prokaryotic peroxidases (*1*), and as such possesses substantial peroxidase activity. However, although KatG shares little sequence homology with catalases (*2*), it exhibits catalase activity that is equivalent to that of monofunctional catalases. Interestingly, the crystal structures of the KatGs identified to date show the presence of a unique structural feature, the Met-Tyr-Trp crosslink. The crosslink (*3-6*), which is located on the distal side of the heme, and the integrity of the supporting hydrogen-bonding network (*7-10*) have proved to be important for the catalase activity of KatG.

We have previously shown that the presence or absence of the crosslink leads to two different one-electron oxidized intermediates. In WT KatG (crosslink present), the one-electron reduction of Compound I leads to the formation of Compound PR (protein radical) [Fe(III)-OH, $AA^{\bullet}$]. However in KatG(Y229F) (crosslink absent and no catalase activity), the one-electron reduction of Compound I leads to the formation of Compound II. Compound II, upon the reaction with another molecule of H_2O_2, forms Compound III, which is inactive in the catalase cycle. Therefore, the structure-function relationship in KatG is different than that in other peroxidases; the presence of the crosslink corresponds with catalase activity and Compound PR formation, whereas the absence of the crosslink corresponds with peroxidase activity only and formation of Compound II.

The catalytic function of the Met-Tyr-Trp crosslink in KatG has been subject to many studies. Magliozzo et al. (*11, 12*) recently proposed a mechanism for the catalatic activity of KatG. They proposed that ferric KatG reacts with a molecule of H_2O_2 to form the two-electron oxidized intermediate Compound I [Fe(IV)=O, $Por^{+\bullet}$]. Then the porphyrin radical is reduced by Tyr^{229} in the crosslink to form a ferryl intermediate [Fe(IV)=O, $Tyr^{\bullet}$]. Compound ES then reacts with another H_2O_2 molecule to form oxyferrous KatG with a radical on Tyr^{229} [Fe(II)-O_2, $Tyr^{\bullet}$]↔[Fe(III)-O_2^-, $Tyr^{\bullet}$]. Finally, quenching of the protein radical via electron

transfer from the oxyferrous intermediate yields dioxygen and regenerates the ferric resting state of the enzyme.

Despite the progress that has been made in understanding the relationship between the structure of KatG, its enzymatic function, and the spectroscopic features of the intermediates, more needs to be understood about the role of the Met-Tyr-Trp crosslink in the peroxidase and catalase cycles of KatG. Supporting Magliozzo's conclusions, we present here evidence that the crosslink imparts catalase activity by avoiding the formation of Compound II [Fe(IV)=O], the iron(IV)-oxo (ferryl) intermediate which is inactive in the catalase cycle. In this paper we performed biochemical and spectroscopic investigations of KatG(M255C). The mutation Met→Cys leads to the formation of a Cys-Tyr-Trp crosslink, which mimics the crosslink in WT KatG but lacks the sulfonium ion. We employed UV-visible stopped-flow spectroscopy and EPR to detect compounds I, II, III and PR of this mutant. When the data is viewed in light of those obtained for WT KatG (Met-Tyr-Trp crosslink) and other mutants: KatG(M255I) (Tyr-Trp crosslink) and KatG(Y229F) (no crosslink), we find that correlations can be made with the rates of formation and reduction of Compound II, catalase activity, and the extent of the crosslink present. As one progresses in the series: KatG(Y229F) (no crosslink), KatG(M255I) (Tyr-Trp crosslink), KatG(M255C) (Cys-Tyr-Trp crosslink), WT KatG (Met-Tyr-Trp crosslink), slower rates of compound II formation and higher rates of compound II reduction to Compound PR are observed. These effects correlate with catalase activity [Y229F<M255I<M255C<WT]. Therefore, we concluded that the role of the Met-Tyr-Trp crosslink is to reduce the time that Compound II has to react with H_2O_2 so that it does not form Compound III which is inactive in the catalase cycle.

II.2. Materials and Methods

The QuikChange XL® site-directed mutagenesis kit and XL-10 Gold and BL-21(DE3)pLysS competent *E. coli* cells were purchased from Stratagene. Buffer salts and acetonitrile (HPLC grade) were purchased from Fisher Scientific. All other reagents and biochemicals, unless otherwise specified, were purchased from commercial sources and were of reagent or molecular-biology grade.

Plasmid Preparation, Protein Expression, and Purification: Mutagenesis was performed per manufacturer's protocols using the QuikChange XL site-directed mutagenesis kit from Stratagene. Mutagenesis [melt (94 °C, 90 s), anneal (57 °C, 90 s), extension (68 °C, 7 min); 35 cycles] was performed directly on the template pKatG(M255I) (*13*) using the mutagenic primers 5'-CGGCGC**TGC**GCCATGAACGACGTCGAAACAGCGG-3' (sense), and 5'-AAACGTCTCGCGAATGTCGACCGCCGCGGCCATGGGG-3' (antisense). Parental DNA was digested with DPN1 (New England Biolabs) and the mutated plasmids were transformed into XL-10 Gold *E. coli* cells and grown on LB agar plates containing 100 mg/L ampicillin. Cultures containing LB and 100 mg/L ampicillin were inoculated with individual colonies, grown 16 hours, and centrifuged. DNA was extracted and purified from the bacterial pellet using the Qiagen QiaPrep Spin Miniprep kit. Sequencing of double-stranded plasmid pKatG(M255C) by the Sanger method was used to confirm the desired nucleotide substitution and the absence of secondary mutations (University of Michigan Sequencing Core Facility, Ann Arbor, MI).

The plasmid pKatG(M255C) was transformed into BL-21(DE3)pLysS *E. coli* cells (heat shock), and protein overexpression was performed in a protocol modified from that previously employed for WT KatG (*14-16*). Specifically, the transformed cells were plated onto LB-agar-ampicillin (0.1 mg/mL) plates, and grown overnight at 37 °C. Starter cultures (~5 mL each) were inoculated with a single colony in LB-ampicillin (0.1 mg/mL) containing chloramphenicol (50 μg/mL), and grown for 8-12 h at 37 °C. Each starter culture was further used to inoculate 1.5 L of LB media (2 flasks, 3 L total) containing 0.1 mg/mL ampicillin, 30 mg/L hemin (dissolved in 0.2 N NaOH), and chloramphenicol (50 μg/mL). Cultures were grown with orbital shaking (250 rpm) for 8 h (37 °C), induced with IPTG (1.5 mM final concentration), and grown overnight (~15 h) at 30 °C. After centrifugation (5000 g, 10 min), the cell pellet was re-suspended in 100 mM potassium phosphate, 300 mM NaCl, and 20 mM imidazole (pH 8.0; 2.5 mL/g cell pellet) containing protease inhibitors (minimum of 10 mg/L TPCK, 75 mg/L PMSF, 10 mg/L soybean trypsin inhibitor, and 1 mg/L leupeptin) and lysed by sonication (6x; 50% duty cycle) in the presence of lysozyme (2 mg/mL) in an ice bucket.

Cellular debris was pelleted at 30,000 *g* for 30 min, resulting in a viscous, red-brown crude extract, which was first purified by affinity chromatography employing a HisTrap HP pre-packed Ni-sepharose column (Amersham Biosciences, 5 mL column volume). Non-bound proteins and hemin were removed by washing (5 mL/min) with 200 mL 100 mM potassium phosphate buffer (pH 8.0) containing 1 M NaCl, 20 mM imidazole, and 0.1% SDS. KatG was eluted with 100 mM potassium phosphate buffer (pH 8.0) containing 1 M NaCl and 200 mM imidazole. Fractions containing KatG, identified by their red/brown color and the presence of an 85-kDa band on a 10-12% SDS-polyacrylamide gel, were pooled and concentrated using an Amicon Diaflow concentrator equipped with a 50,000–molecular weight cutoff membrane (BioMax-50). The concentrate was further purified by size-exclusion chromatography (Sephacryl S300-HR, 5.0 i.d. x 80 l, cm; 5 mL/min flow rate) equilibrated with 50 mM potassium phosphate and 300 mM NaCl (pH 7.5). Fractions containing KatG exhibiting no impurities by SDS-PAGE analysis were pooled and concentrated as above, and frozen at -80 °C in 10% glycerol for storage. Due to the report of an observed instability found in frozen KatG samples (*17*), only fresh samples that were stored for less than two weeks were used in this study.

Spectroscopic Studies: Optical spectra were recorded on a Cary-50 Spectrophotometer equipped with a thermostated cell holder at 25 °C. Protoheme content was measured by the pyridine hemochrome assay using $\Delta\varepsilon_{557}$ = 20.7 $mM^{-1}cm^{-1}$ (reduced - oxidized) for iron protoporphyrin IX.

Enzyme Assays: All measurements were performed with minor modification from published procedure (*14-16*). Specifically, measurements were performed in octiplet using a SpectraMax Plus384 UV-visible plate reader equipped with 96-well plates. Assays were carried out at 25 °C in 100 mM NaP_i buffer (pH 7.5) containing 5 μM EDTA (200 μL total volume). Catalase activity was measured spectrophotometrically by following the decrease over 60 s (linear least-squares fittings) of the hydrogen peroxide concentration (1.5, 5, 10, 15, 30, and 50 mM) at 240 nm (ε_{240} = 43.6 $M^{-1}cm^{-1}$) (*18*) with a fixed KatG concentration of 20 M. Peroxidase activity was measured by following the increase (linear least-squares fittings) in absorbance for 1.0 mM ABTS (ε_{405} = 36.8 $mM^{-1}cm^{-1}$) (*19*) in the presence of *tert*-

butyl hydroperoxide (1, 10, 25, 100, 200, and 500 mM) over 60 seconds at a fixed enzyme concentration of 500 nM. Kinetic parameters (K_m, V_{max}) were obtained from non-linear regression (least squares fitting) of Michaelis-Menton plots using the Grafit kinetics software package.

Stopped-flow UV-Visible Spectrophotometric Studies: Experiments were performed on a Bio-Logic SFM-400 Triple Mixing Stopped-Flow instrument equipped with a J & M TIDAS MCS 500-3 diode array UV-visible spectrophotometer, and were carried out at 25 °C in 100 mM KPi (pH 7.5) containing 5 μM EDTA. Constant temperature was maintained using a circulating water bath. Data was collected (900 scans total) over a three time-domain regime (2.5 ms, 25 ms, 250 ms; 300 scans each) using the Bio Kinet32 software package (Bio-Logic). Experiments were performed in double-mixing mode using an aging line prior to the second mixing step. The final (post-mixing) concentrations were: [KatG] = 10 μM, [MPPH] = [PAA] = 10, 25, 100 or 1000 μM, and [H_2O_2] = 0.01, 0.1, 1, and 10 mM. All data were evaluated using the Specfit Global Analysis System software package (Spectrum Software Associates) as pseudo-first-order reactions and fit with SVD analysis from one to three exponential curves where applicable. Kinetics data were baseline corrected using the Specfit autozero function.

Preparation of EPR Samples by Freeze-Quench Methods: Rapid freeze-quench experiments were performed with a BioLogic SFM 400 Freeze-Quench apparatus by mixing a 50 μM enzyme solution (final concentration) with a 10-fold excess of peroxyacetic acid solution in 100 mM potassium phosphate buffer (pH 7.5) at 25 °C. Reaction quench times were varied as a function of the enzyme, and are reported in Figure II.5. A standard 4 mm O.D. quartz EPR tube was connected to a Teflon funnel, and both the tube and the funnel were completely immersed in an isopentane bath at -120 °C. The reaction mixtures were quenched by spraying them into the cold isopentane, and the frozen material so obtained was packed at the bottom of the quartz tube using a packing rod equipped with a Teflon plunger. Samples were then transferred temporarily to a liquid nitrogen storage dewar until analyzed.

X-band EPR Spectroscopy: EPR spectra were recorded with an X-band (9 GHz) Varian E-9 EPR spectrometer (Varian, El Palo, CA). A standard 4 mm quartz EPR tube was

filled as described above and placed into a quartz finger dewar insert filled with liquid nitrogen. The temperature of the samples was maintained at 77 K for the duration of the data acquisition, which required periodic refilling of the dewar due to the evaporation of the liquid nitrogen during longer acquisition runs. The typical spectrometer settings were as follows: field sweep 200 G, modulation frequency 100 KHz, modulation amplitude 4.0 G, and microwave power 2 mW. The exact resonant frequency of each EPR experiment was measured by an EIP-578 (PhaseMatrix, San Jose, CA) in-line microwave frequency counter and is indicated in the figures. Typically, 20 to 200 individual scans were averaged to achieve sufficient signal-to noise for the spectra. Experimental spectra were simulated using WINEPR (Bruker Biospin, Billerica, MA) software package.

II.3. Results

UV-visible Spectroscopic Analysis of KatG(M255C) – The electronic absorption spectrum of KatG(M255C) (Cys-Tyr-Trp crosslink) is shown in Figure II.1, and is contrasted against those observed for WT KatG (Met-Tyr-Trp crosslink), KatG(M255I) (Tyr-Trp crosslink) and KatG(Y229F) (no crosslink). Relevant spectral features and UV-visible analysis are presented in Table II.S1. When compared to 6-c HS hemes, a 5-c HS heme generally exhibits a slightly blue shifted and hypochromic Soret band with a shoulder at 380 nm and a CT1 feature at ~640 nm (or higher). 6-c HS hemes often have this CT1 band closer to 630 nm, whereas 6-c LS heme systems lack it entirely, exhibit a red-shifted Soret, and have visible features at 565 and 580 nm. Thus, comparison of the A_{Soret}/A_{380} and A_{614}/A_{645} ratios can provide insight into the electronic nature of the heme prosthetic group (*17*). Here, KatG(M255C) (A_{614}/A_{645} = 0.96) (Table II.S1) has a significantly lower relative population of 6-c HS heme than KatG(M255I), and is intermediate between WT KatG (1.05) and KatG(Y229F) (0.85). A relatively small feature at 580 nm, not observed in the other three KatGs, may suggest the presence of a minor amount of low spin heme present in KatG(M255C). The narrow range of the A_{Soret}/A_{380} ratio (1.68 – 1.79) precludes any relative population assignments. The optical purity ratio (Reinheitzahl or R_z, defined as A_{Soret}/A_{280}) for KatG(M255C) was found to be 0.56, identical to that observed for KatG(M255I). A

pyridine hemochrome assay of KatG(M255C) yielded 0.97 ± 0.04 heme/monomer, indicating stoichiometric heme incorporation, suggesting that the slightly lower Rz value when compared to WT KatG (0.63) or KatG(Y229F) (0.59) is most likely due to a lower heme extinction and not the presence of apo-enzyme.

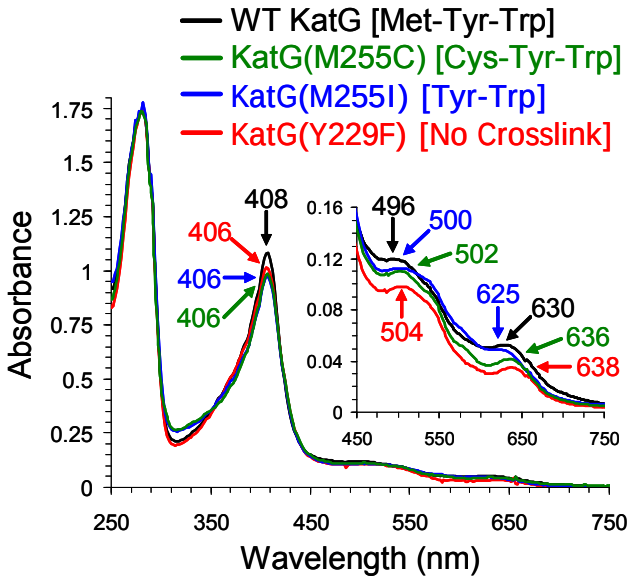

Figure II.1: UV-visible spectra of KatG(M255C) (green), WT KatG (black), KatG(M255I) (blue) and KatG(Y229F) (red). Conditions: 10 µM enzyme in 100 mM potassium phosphate, pH 7.5, 25 °C.

Catalase and Peroxidase Activities of KatG(M255C) – Kinetic parameters (k_{cat}, K_m, and catalytic efficiency, k_{cat}/K_m) for the catalase and peroxidase activities of KatG(M255C) are presented in Table II.1. As conventional catalases do not follow typical Michaelis-Menten kinetics (lack of a detectable enzyme-substrate complex and inability to reach saturation with H_2O_2 before inactivation), kinetic constants reported here for catalase activity are 'apparent' values. KatG(M255C) exhibited saturable catalase activity under the conditions employed for this kinetic study. The k_{cat} (20.6 ± 1.0 s^{-1}) and K_m (20.1 ± 2.4 mM) values are marginally better than those reported for KatG(M255I) (Tyr-Trp crosslink; 1.1 s^{-1}, 40.2 mM) and KatG(Y229F) (no crosslink; 0.1 s^{-1}, 39.8 mM), but are significantly poorer than those observed for WT KatG (Met-Tyr-Trp crosslink present; 6000 s^{-1}, 2.5 mM).

Comparison of the catalytic efficiencies (k_{cat}/K_m) reveals that the loss of the sulfonium ion in KatG(M255C) results in an enzyme ~10^3 more attenuated in activity than WT KatG, and accounts for roughly half the loss in log units for catalase activity when comparing WT enzyme with KatG(Y229F) (~10^6 lower). Thus, the presence of a carbon-sulfur bond in the Cys-Tyr-Trp crosslink itself is not sufficient for imparting catalase activity, but there is an apparent requirement of a sulfonium ion as in the Met-Tyr-Trp crosslink. The result that catalase activity is severely disrupted for KatG(M255C) versus WT KatG is consistent with literature observations (*4-6*) that an intact Met-Tyr-Trp crosslink, including the presence of the sulfonium ion, is essential for a catalatic competency of ~$k_{cat}/K_m > 10^3$ $M^{-1}s^{-1}$. One other possible interpretation is that the M255C mutation significantly disrupts the active site H-bonding network that has also been identified as critical for catalase activity.

Table II.1: Kinetic Parameters for Catalase and Peroxidase Activities of KatG(M255C). For comparison, the values for WT KatG (*20, 21*), KatG(M255I) (*22*), and KatG(Y229F) (*20*) are also provided.

	WT KatG Met-Tyr-Trp	KatG(M255C) Cys-Tyr-Trp	KatG(M255I) Tyr-Trp	KatG(Y229F) No Crosslink
		Catalase Activity		
k_{cat}, s^{-1}	6000 ± 70	20.6 ± 1.0	1.1 ± 0.1	0.1 ± 0.05
K_m, mM	2.5 ± 0.2	20.1 ± 2.4	40.2 ± 6.1	39.8 ± 6.4
k_{cat}/K_m, ($M^{-1}s^{-1}$)	(2.40 ± 0.03) x 10^6	1026 ± 49	27.0 ± 4.1	2.5 ± 1.3
		Peroxidase Activity		
k_{cat}, s^{-1}	0.062 ± 0.001	0.170 ± 0.004	0.164 ± 0.002	0.843 ± 0.056
K_m, mM	8.4 ± 0.5	2.8 ± 0.2	3.40 ± 0.08	2.7 ± 0.7
k_{cat}/K_m, ($M^{-1}s^{-1}$)	7.3 ± 0.4	60.7 ± 4.3	48.1 ± 1.2	316 ± 39

Peroxidase activities (saturable) were measured for the one-electron oxidation of 2,2'-azino-bis(3-ethylbenzothiazoline-6-sulfonate) (ABTS) to the corresponding radical cation $ABTS^{\bullet+}$ by KatG in the presence of *tert*-butylhydroperoxide. KatG(M255C) exhibited an increase in k_{cat} (0.170 ± 0.004 s^{-1}) and decrease in K_m (2.8 ± 0.2 mM) as compared to WT KatG (0.062 s^{-1} and 8.4 mM, respectively). These findings are similar to those reported for KatG(M255I) (0.164 s^{-1}, 3.40 mM), and indirectly suggests that the presence of the sulfonium ion lowers the peroxidase activity of the wild-type enzyme when compared to these two mutants. An increase in peroxidase activity for crosslink-disrupted KatGs has been

noted previously by Magliozzo and co-workers (*4*), who suggested that upon loss of the covalent adduct the increase in peroxidase activity (with concomitant loss of catalase function) is due to enhanced formation and/or increased stabilization of the Compound II intermediate, which plays a role in the peroxidase, but not catalase, cycle. This is most apparent in KatG(Y229F) (0.843 s^{-1}, 2.7 mM), in which the complete lack of the Met-Tyr-Trp crosslink leads to an increase in peroxidase catalytic efficiency of ~20-fold in comparison to WT KatG.

Stopped-Flow UV-visible Characterization of Compounds I and III in KatG(M255C) – Stopped-flow UV-visible spectroscopic methods were employed to detect the high valent iron-oxo Compound I and oxyferrous Compound III intermediates of KatG(M255C). For characterization of Compound I, rapid mixing (2 ms) of a solution of ferric KatG(M255C) [UV-visible spectrum: 406 (Soret, ε = 98 $mM^{-1}cm^{-1}$), 502, 542 (sh) nm] (Figure II.2A) with 10 equivalents H_2O_2 yielded a new species [UV-visible spectrum: 408 (Soret, ε = 60 $mM^{-1}cm^{-1}$), 520, 555 (sh) nm] (Figure II.2B) whose spectral features are consistent (with respect to λ_{max} and extinction coefficient) to the previously characterized Compound I intermediates of *Mtb* KatG(M255I) [UV-visible spectrum: 407 (Soret, ε □= 74 $mM^{-1}cm^{-1}$), 518, 560 (sh) nm] (*13*), *Synechocystis* PCC 6803 KatG(M275I) [UV-visible spectrum: 407 (Soret exhibits ~20% hypochromicity), ~522, ~570 (sh) nm] (*23*), and *Mtb* KatG(Y229F) [UV-visible spectrum: ~408 (Soret, ε □= 59 $mM^{-1}cm^{-1}$), 528, 555 (sh) nm] (Table II.2) (*24, 25*). Furthermore, the spectral features matched neither those for Compound II [UV-visible spectrum: PR, WT KatG – 410 (Soret), 628 nm; II, KatG(Y229F) - 417 (Soret), 531, 561 nm] (*24*), nor for Compound III [UV-visible spectrum: WT KatG – 418 (Soret), 545, 580 nm; KatG(M255I) – 417 (Soret), 538, 578 nm; KatG(Y229F) – 418 (Soret), 545, 581 nm] (*25*). Based on these spectral observations, as well as the distinct hypochromicity of the Soret band, we assign this intermediate observed here as *Mtb* KatG(M255C) Compound I. Values of k_{obs} for Compound I formation were linearly dependent on [H_2O_2] (10 – 100 fold excess per heme), giving a bimolecular rate constant of (1.5 ± 0.2) x 10^6 $M^{-1}s^{-1}$. This rate is approximately 100-fold faster than that found for WT KatG (1.21 x 10^4 $M^{-1}s^{-1}$) (*26*), and on a par with that found for KatG(Y229F) (4 x 10^6 $M^{-1}s^{-1}$) (*4*) (Table II.2). We surmise that the

faster formation of Compound I in these mutants may be due to the lack of the sulfonium ion that is present in the active site of WT KatG, whose presence may hinder the formation of a second positive charge in the form of the porphyrin π-cation radical. Additionally, the Q-band region of the UV-visible spectrum of WT KatG Compound I is shifted (550, 590 nm) compared to those of mutants where the crosslink is perturbed [M255C, M255I, Y229F: ~518-520, 555-560 nm], suggesting that the loss of the sulfonium ion in the crosslink does alter the electronics of this intermediate.

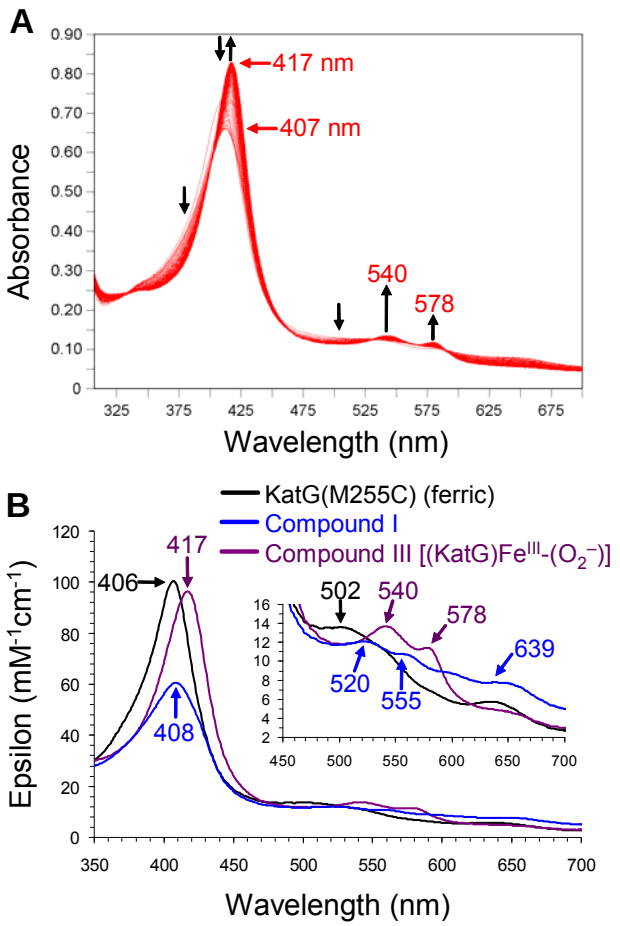

Figure II.2: (A) Stopped-flow UV-visible spectroscopic monitoring of the reaction (300 scans, 0.6 sec) between KatG(M255C) (10 μM) and a 10-fold excess of H_2O_2. See experimental for details. (B) Calculated UV-visible spectra for resting (black), Compound I (blue), and Compound III (purple) KatG(M255C) are shown; the rapid-scanning data from A were compiled and fitted to a double exponential reaction model using Specfit program.

Table II.2: UV-visible spectroscopic data and kinetic parameters for the oxidized intermediates of KatG(M255C), KatG(M255I), WT KatG, and KatG(Y229F)

	λ_{max} (ε, $mM^{-1}cm^{-1}$)	k_{obs}($M^{-1}s^{-1}$)	Ref.
KatG(M255C); Cys-Tyr-Trp CLPF			
Ferric (resting)	406 (98), 602, 542, 636	n/a	[a]
Compound I	408 (60), 520, 555 (sh)	$(1.5 \pm 0.2) \times 10^6$	[a]
Compound II - [(KatG•)Fe^{III}-OH]	409 (105), 500, 565, 623	$(3.1 \pm 0.1) \times 10^4$ [b] $(9.3 \pm 0.8) \times 10^4$ [c]	[a]
Compound II - [(KatG)Fe^{IV}=O]	417 (89), 531, 561	$(6.4 \pm 0.4) \times 10^3$ [d]	[a]
Compound III	417 (96), 540, 578	$(2.5 \pm 0.1\ s^{-1})$ [e]	[a]
KatG(M255I); Tyr-Trp CLPF			
Ferric (resting)	406 (101), 500, 540, 620	n/a	(*22*)
Compound I	407 (74), 518, 560 (sh)	$(3.8 \pm 0.3) \times 10^5$	(*22*)
Compound II - [(KatG•)Fe^{III}-OH]	408 (110), 500, 556, 615	$(1.0 \pm 0.2) \times 10^4$ [b]	(*22*)
Compound II - [(KatG)Fe^{IV}=O]	415 (82), 531, 560	$(1.4 \pm 0.1) \times 10^5$ [c] $(1.8 \pm 0.4) \times 10^4$ [d]	(*22*)
Compound III	417 (94), 538, 578	$(3.7 \pm 0.4\ s^{-1})$ [e]	(*22*)
WT KatG; Met-Tyr-Trp CLPF			
Ferric (resting)	408 (107), 496, 540 (sh) 630	n/a	(*20, 27*)
Compound I	411 (64), 550, 590, 655	1.21×10^4 [e]	(*20, 27*)
Compound II - [(KatG•)Fe^{III}-OH]	410 (118), 628	$(4.8 \pm 0.4) \times 10^4$	(*20, 27*)
Compound III	418 (98), 545, 580	$>10^9$	(*21*)
KatG(Y229F); no crosslink			
Ferric (resting)	406 (101), 504, 538	n/a	(*20, 28*)
Compound I	408 (59), 528, 555	4×10^6	(*20, 28*)
Compound II - [(KatG)Fe^{IV}=O]	417 (108), 531, 561	$(5.8 \pm 0.7) \times 10^6$	(*20, 28*)
Compound III	418 (94), 545, 581	$(9.2 \pm 0.2) \times 10^5$	(*21*)

[a] = this work; n/a = not applicable; [b] = when formed with MPPH; [c] = when formed with 1 eq. H_2O_2; [d] = when formed with PAA; [e] = measurement of Compound I to Compound III conversion

Under these conditions of excess peroxide, the Compound I intermediate was found to be unstable at pH 7.5 and 25 °C, and rapidly converted ($2.5 \pm 0.1\ s^{-1}$) to a second intermediate whose spectral features [417 (Soret), 540, 578 nm] (Figure II.2B) match well to those previously assigned to as KatG Compound III [413-418 (Soret), 538-545, 578-582 nm]

(*13, 25*) (Table II.2). A similar conversion of Compound I to Compound III under conditions of excess peroxide has been noted by others for both *Mtb* KatG(Y229F) (*4*) and *Synechocystis* PCC 6803 KatG(Y249F) (*22*). The oxyferrous intermediate was also found to be unstable under these conditions, with either a slow decay (~0.01 s^{-1}) back to the resting enzyme at low [H_2O_2] (100 μM), or bleaching of the Compound III spectrum at intermediate [H_2O_2] (1 – 10 mM). At the highest concentrations of H_2O_2 investigated (1000-fold excess), the reaction with KatG(M255C) proceeded at such an accelerated rate that Compound I was formed within the mixing time of the stopped-flow apparatus.

Observation of the Compound II Ferryl [(KatG)Fe^{IV}=O] Intermediate in KatG(M255C) – In contrast to the observations of Compounds I and III with excess hydrogen peroxide, stopped-flow rapid mixing of a 10 μM solution of KatG(M255C) (Figure II.3A) with an excess of peracetic acid (PAA) first revealed the formation of Compound I [UV-visible spectrum: 409, 520, and 555 nm], followed by rapid formation of a new intermediate [UV-visible spectrum: 417 (Soret, ε = 89 $mM^{-1}cm^{-1}$), 531, and 561 nm] (Figure II.3B) whose spectral features matched neither those of KatG(M255C) Compounds I or III (*vide supra*, Table II.2). The spectral features (λ_{max}, ε) match well to the previously characterized ferryl-type [(KatG)Fe^{IV}=O] Compound II intermediate of KatG(M255I) [UV-visible spectrum: 415 (Soret), 531, 560 nm], KatG(Y229F) [UV-visible spectrum: ~417 (Soret), ~531, ~561 nm] (*4, 24*), with the Compound II spectrum of *Synechocystis* PCC 6803 KatG(Y249F) [UV-visible spectrum: 418 (Soret), 530, 558 nm] (*6*), as well as for the classical ferryl Compound II intermediates observed in HRP and other peroxidases. Thus, we assign this intermediate as KatG(M255C) Compound II. Values of k_{obs} for this species were linearly dependent on [PAA] (10 – 100 fold excess per heme), giving a bimolecular rate constant of (6.4 ± 0.4) x 10^3 $M^{-1}s^{-1}$.

Observation of a Compound II intermediate for KatG(M255C) is consistent with studies that have shown its formation in mutants that lack a fully intact (including sulfonium ion) Met-Tyr-Trp crosslink. An interesting trend is noted for the rate of formation of this species in KatG: Y229F (no crosslink, 5.8 x 10^6 $M^{-1}s^{-1}$) > M255I (Tyr-Trp, 0.18 – 1.4 x 10^5 $M^{-1}s^{-1}$) > M255C (Cys-Tyr-Trp, 6.4 x 10^3 $M^{-1}s^{-1}$) > WT KatG (Met-Tyr-Trp, no formation

observed). This trend is inversely correlated with their catalase activities (Y229F < M255I < M255C < WT), and suggests that as components of the crosslink are added to the active site of KatG, formation of Compound II becomes progressively less favored, culminating in its lack of formation in the wild-type enzyme when the Met-Tyr-Trp crosslink is fully intact. As this intermediate is inactive in the catalase (but not peroxidase) cycle, we have previously hypothesized that KatG maintains its catalatic activity via a Compound II 'ferryl avoidance' mechanism, and the data presented here (and below) for KatG(M255C) support this hypothesis.

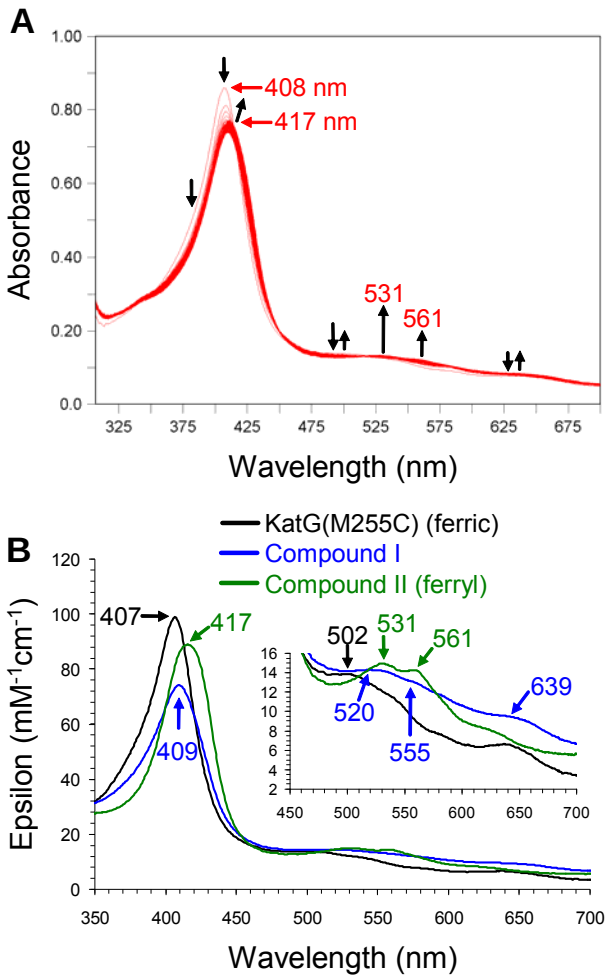

Figure II.3: (A) Stopped-flow UV-visible spectroscopic monitoring of the reaction (300 scans, 0.6 sec) of KatG(M255C) (10 µM) with a 10-fold excess of PAA. See experimental for details. (B) Calculated UV-visible spectra for resting (black), Compound I (blue), and Compound II [(KatG)(Por)Fe^{IV}=O] KatG(M255C) (green) are shown; the rapid-scanning data from A were compiled and fitted to a double exponential reaction model using the Specfit global analysis program.

The Compound II intermediate was found to be unstable under the above conditions, converting (0.061 ± 0.002 s^{-1}) to a new species whose spectral features [408 (Soret), 556 (sh), 615 nm] (Fig. S1) matched those of Compound PR [(KatG•)(Por)Fe^{III}-OH] (*vide infra*) (Fig. II.4B). The rate of formation of this species from II also exhibits an interesting trend: WT KatG (Met-Tyr-Trp, no II observed; 4.8×10^4 $M^{-1}s^{-1}$ or 0.48 s^{-1} if calculated as a unimolecular k_{obs}) > M255C (Cys-Tyr-Trp, 0.061 s^{-1}) > M255I (Tyr-Trp, 0.011 s^{-1}) > Y229F

(no crosslink, Compound PR not observed). This trend directly correlates with their observed calatase activities, WT > M255C > M255I > Y229F. Thus, not only does the crosslink slow the formation of the catalase inactive Compound II, it also speeds its transformation to the isoelectronic, catalase-active Compound PR. Decay (0.005 ± 0.001 s^{-1}) of this intermediate resulted in reformation of the resting enzyme.

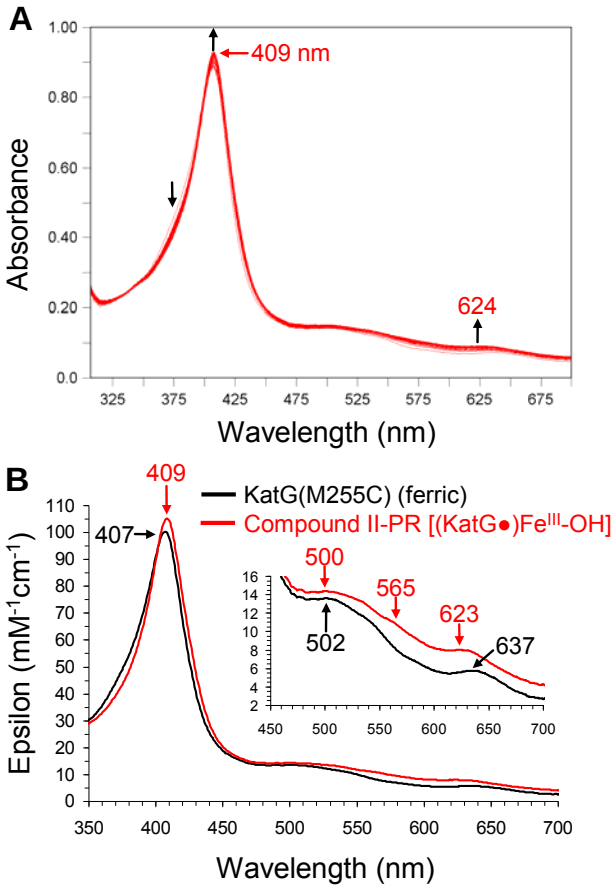

Figure II.4: (A) Stopped-flow UV-visible spectroscopic monitoring of the reaction (300 scans, 60 sec) between KatG(M255C) (10 µM) and a 10-fold excess of MPPH. See experimental for details. (B) Calculated UV-visible spectra for both resting (black) and Compound PR [(KatG•)(Por)Fe^{III}-OH] KatG(M255C) (red) are shown; the rapid-scanning data from A were compiled and fitted to a single exponential reaction model using the Specfit global analysis program.

Direct Observation of Compound PR [(KatG•)(Por)Fe^{III}-OH] in KatG(M255C) – Upon stopped-flow rapid mixing (2 ms) of a solution of ferric KatG(M255C) with 2-methyl-

1-phenyl-2-propyl hydroperoxide (MPPH) (Figure II.4A), a new species was observed [UV-visible spectrum: 409 (Soret, ε □= 105 $mM^{-1}cm^{-1}$), 500, 565 and 623 nm] (Figure II.4B) whose spectral features matched neither those of KatG(M255C) Compounds I, II, or III (*vide supra*, Table II.2). The spectral features, however, were highly consistent (with respect to λ_{max} and extinction) to the previously characterized [(KatG•)(Por)Fe^{III}-OH] Compound PR intermediates of WT KatG (*24*), KatG(M255I) (*13*), KatG(R418L) (*25*), KatG(S315T) (*25*), *Synechocystis* PCC 6803 KatG (*29*), and *Anacystis nidulans* KatG (*21*). Values of k_{obs} for formation of this new species were linearly dependent on [MPPH] (2.5 – 10 fold excess per heme), giving a bimolecular rate constant of (3.1 ± 0.1) x 10^4 $M^{-1}s^{-1}$, on a par with that determined for WT KatG under identical conditions (4.8 x 10^4 $M^{-1}s^{-1}$). The intermediate was found to be unstable under these conditions, with a slow decay (0.004 s^{-1}) resulting in re-formation of resting (ferric) enzyme, concomitant with a slight bleaching (< 5%) of the heme Soret band that increased at higher oxidant concentrations. MPPH has been previously shown to undergo homolytic O-O bond cleavage (*30*), predominantly at pH values above 6.0 (*31*), resulting in Compound II formation (as opposed to Compound I intermediates which are derived from heterolytic cleavage of the O-O bond in most alkylhydroperoxides). Based on these UV-visible spectroscopic observations and on the known chemical reactivity of the MPPH oxidant, we assign the new species detected under the conditions employed here as the Compound PR intermediate, [(KatG•)(Por)Fe^{III}-OH], of *Mtb* KatG(M255C).

EPR Spectroscopic characterization of the Protein Radical in Compound PR [(KatG•)(Por)Fe^{III}-OH]. Rapid-freeze-quench methods were employed to stabilize the intermediates of the reaction between KatG (50 μM final) and a 10-fold excess of PAA at pH 7 for subsequent characterization by continuous wave (CW) EPR. For comparison purposes, X-band CW EPR spectra of WT KatG, KatG(M255C), and KatG(M255I) samples containing the putative Compound PR intermediate obtained at pH 7.0 with various quench times are shown in Figure II.5. The EPR spectra collected for WT KatG, KatG(M255C) and KatG(M255I) had an average g-value of ~ 2.004, and a peak-to-trough width of ~ 16 G. The shape of the EPR signal for WT KatG changed slightly over time but remained unchanged after 2 minutes. The shapes of the EPR signals for KatG(M255C) and KatG(M255I) became

slightly narrower over time. Based on the *g*-factor and the width of the signals, these EPR signals were assigned to tyrosyl radicals (*28*).

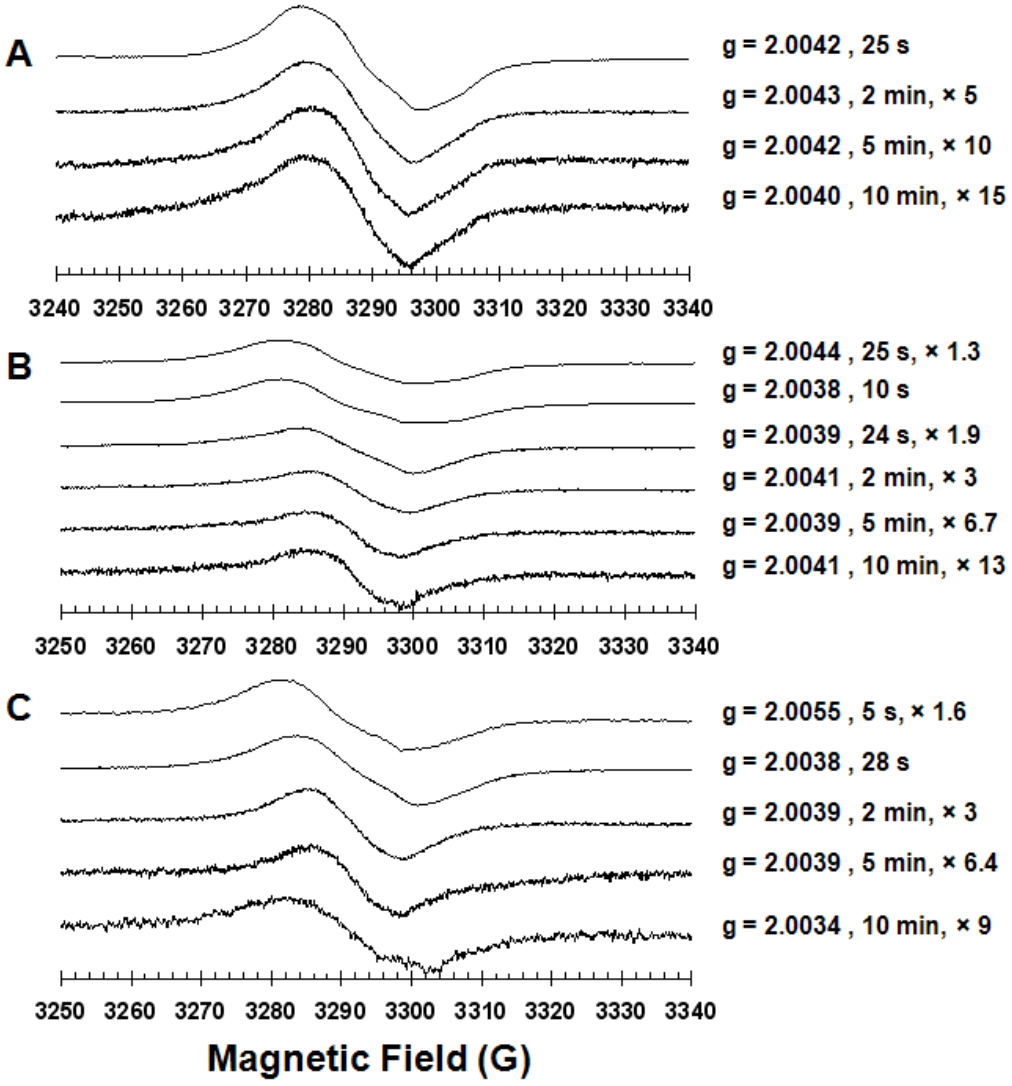

Figure II.5: EPR spectra monitoring the reaction between (A) WT KatG, (B) KatG(M255C), and (C) KatG(M255I) with 10 equivalents of PAA

These signals differ from those obtained by Zhao et al. (*12*) upon the reaction of WT KatG with H_2O_2 and assigned to a radical located on Tyr^{229}, which is part of the distal Met-Tyr-Trp adduct. Zhao et al. (*12*) described the signal they obtained as a narrow doublet with a peak-to-trough width of 17 G at g=2.0034. In a study performed by Chouchane et al. (*32*),

WT KatG was reacted with PAA and the intermediates were studied using X-band EPR spectroscopy at 77 K. A doublet characterized by a line width of 30 G was observed within 6.4 ms of mixing and lasted for 500 ms. After that, a singlet appeared at g~2.004 with a linewidth of 27 G. Chouchane et al. (*32*) concluded that the initial doublet and the following singlet belong to tyrosyl radical(s) as suggested by deuterium labeling and simulation studies. The sites of the radicals were identified in a later study by Ranguelova et al. (*33*) who used using EPR spectroscopy, the three-dimensional crystal structure of KatG, and electron transfer couplings. They first observed an initial wide doublet signal (WD), which was then replaced by a wide singlet (WS) (20 G) over 10 s. When the incubation times were extended up to several minutes, further transition to a singlet with a linewidth of ~15 G was observed. No hyperfine splitting was detectable for this signal even under optimized spectrometer conditions. Ranguelova et al. (*33*) concluded that within the first few milliseconds of turnover, a tyrosyl radical is formed on residue Tyr ^{229}. This is followed by a mixture of tyrosyl and tryptophanyl radical species and finally by only a tyrosyl radical on residue Tyr^{353}, which lies more distant from the heme (14 Å). The EPR signals obtained in this study are more similar to the singlet signals described by Ranguelova et al., and the changes in signal shapes over time might be due to the transfer of the unpaired electron from one residue to another, namely from a mixture of Tyr and Trp residues to a Tyr residue located father away from the heme. Jakopitch et al. (*23*) also identified the presence of Tyr and Trp radicals after *Synechocystis* WT KatG reacts with PAA by using EPR spectroscopy, deuterium labeling and site-directed mutagenesis. Later, Jakopitch et al. (*34*) identified Trp^{106} (*Synechocystis* numbering) as the site of the Trp radical, but mutation of the equivalent Trp site in *Mtb* KatG did not suppress the Trp$^{\bullet}$ signal. However, the M275I (*Synechocystis* numbering, corresponds to M255I here) did not form the Trp radical because of the dramatic changes in the heme distal side induced by the repositioning of the Trp-Tyr adduct. When Ivancich (*10*) collected the X-band EPR spectra of samples of *Mtb* WT KatG with PAA at 77K (similar to the conditions we used in this study), they observed a signal composed of a mixture of Tyr and Trp radicals with a line width of 20 G at g~2.004.

II.4. Discussion

In previous work done by Ghiladi et al. (*13, 15, 16*), the role of the Met-Tyr-Trp crosslink was investigated by studying the reactivity of WT KatG (Met-Tyr-Trp), KatG(M255I) (Tyr-Trp), and KatG(Y229F) (no crosslink). While the role of the Tyr-Trp bond in the crosslink formation became more understood, questions still remained about the role of the sulfonium ion in the Met-Tyr bond. To gain further insight into the role of this species, the mutant KatG(M255C) was expressed, and its reactivity with H_2O_2 and PAA was studied and compared to those of WT KatG, KatG(M255I), and KatG(Y229F). The Met→Cys mutation resulted in the formation of the Cys-Tyr-Trp adduct and the absence of the sulfonuim ion.

The UV-visible features of Compound III in WT KatG (Met-Tyr-Trp), KatG(M255C) (Cys-Tyr-Trp), KatG(M255I) (Tyr-Trp), and KatG(Y229F) (no crosslink) were similar (see Table II.2) indicating that the presence or absence of the crosslink(s) does not affect the electronic structure of Compound III. However, the UV-visible features of Compound I formed in WT KatG differ from those of Compound I formed in the mutants where the Met-Tyr-Trp adduct was disrupted. This is probably because mutation of the crosslink disrupted the hydrogen-bonding to the ferryl moiety in compound I, thus, modifying its UV-visible features slightly. More importantly, the UV-visible features of the one-electron oxidized intermediate (Compound PR vs. Compound II) were different in these four enzymes. Ghiladi et al. (*13, 24*) previously reported that the spectral features of the one-electron oxidized intermediate correlate to enzyme function: WT KatG (Met-Tyr-Trp) has catalase and peroxidase activity and exhibits the formation of Compound PR (not Compound II). Compound PR has spectral features that are similar to the resting state of the enzyme (slight hyperchromicity of the Soret band, little to no shift in the Soret peak relative to the ferric form, and the presence of ~ 625 nm feature). However, in KatG(Y229F) (no crosslink), which has only peroxidase activity, Compound II is formed (not Compound PR). Compound II has a Soret band that is red-shifted by ~ 10 nm relative to that of the ferric enzyme and has two prominent bands at 530 and 560 nm. In KatG(M255C) (Cys-tyr-Trp) and KatG(M255I) (Tyr-Trp), which have only peroxidase activity, both Compounds PR and II were observed.

Therefore, the presence of Compound PR does not indicate the presence of catalase activity, but the complete absence of Compound II is required for the KatG enzyme to be active as a catalase.

The spectral differences between Compound II and Compound PR may be explained by the fact that they are two resonance forms of the one-electron oxidized intermediate: Compound II [Fe(IV)=O]↔Compound PR [Fe(III)-OH, KatG$^{\bullet}$]. While the former is the ferryl intermediate observed in monofunctional peroxidases, the latter is observed in catalase-peroxidases and has a UV-visible spectrum similar to that of the resting enzyme (*21, 29*). Compounds II and PR can be directly formed, while only Compound II interconverts to Compound PR indicating that the formation of PR is favorable. But why do catalse-peroxidases favor the formation of Compound PR over Compound II? Compound II is inactive in the catalase cycle because it reacts with H_2O_2 to form Compound III. Therefore, KatG avoids the formation of Compound II by transferring the oxidizing equivalent to an amino acid residue. In Compound PR [Fe(III)-OH, KatG$^{\bullet}$], the heme center is in the ferric state and can react with H_2O_2 to form Compound I, the common intermediate in the catalase and peroxidase cycles of KatG. We conclude that the function of the crosslink is to ensure that the heme cofactor remains in a catalytically competent state for both the catalase and peroxidase activities of KatG.

Another possible reason for the spectral differences observed for the one-electron oxidized intermediate in KatG is that the electronic absorption spectrum of the heme is affected by its environment. Perturbations in the Met-Tyr-Trp adduct may affect the geometry or the coordination of the heme, especially since Tyr^{229} is covalently linked to Trp^{107}, which is an important part of the hydrogen-bonding network on the distal side of the heme. It has been shown that some mutations in KatG may lead to the disruption of the hydrogen-bonding network (*35, 36*), which may result in changing the hydrogen bonding to the oxo moiety of the ferryl intermediate and change its UV-visible features. Magliozzo (*37*) also presented data indicating that loss of the adduct causes significant structural perturbations in the heme active site and the distal pocket. Their resonance raman (RR) spectra show that the distribution of heme spin and coordination states are significantly

altered by loss of the covalent adduct. While KatG (crosslink present) does not have detectable levels of low-spin (LS) heme, a significant amount of LS heme is present in KatG(Y229F) (no crosslink). Also, the RR spectra suggest that the heme in Y229F is more planar compared to WT KatG.

Upon comparing the data obtained for KatG(M255C) with those obtained for WT KatG, KatG(M255I), and KatG(Y229F), important trends are established regarding the kinetics of Compound II. These trends relate directly to the catalase activity of these enzymes. As one goes from crosslink absent [as in the case of KatG(Y229F)] to Met-Tyr-Trp crosslink present (as in WT KatG), it is observed that: i) formation of the catalase-inactive Compound II intermediate becomes progressively slower, suggesting that a possible role of the crosslink is to avoid formation of this one-electron oxidized ferryl species; and ii) conversion of Compound II to PR becomes progressively faster, indicating that the crosslink may have a role in reducing II. The combined effect of slower II formation and faster II reduction minimizes the amount of time that this species has to react with any additional H_2O_2 that may be present, thereby minimizing the amount of catalase-inactive Compound III that would result from such a reaction. Both of these effects correlate well with the observed trend in catalase activity of KatG (WT > M255C > M255I > Y229F), and further support a ferryl avoidance mechanism for Compound II, either by preventing its formation, or quickly reducing it in the event that it does form.

One interesting possibility is that WT KatG avoids the formation of the Compound II via a rapid two-electron reduction of Compound I. To test this hypothesis, WT KatG was reacted with one equivalent of H_2O_2 (similar results were obtained upon reaction with one equivalent of PAA). Under such "single turnover" conditions, catalase activity is not possible, and WT KatG can be compared to its mutants. For KatG(Y229F) (*4*), after the reaction with one equivalent of H_2O_2, Compound II was formed, presumably after the reduction of Compound I by Trp^{107}. For KatG(M255C), Compound II is also formed after the reaction with one equivalent of H_2O_2. This is most likely due to the reduction of Compound I by the Cys-Tyr-Trp crosslink. However, in KatG(M255C), Compound II slowly converts to Compound PR [Fe(III)-OH, $KatG^{\bullet}$]; this phenomenon has also been observed for

KatG(M255I) (*13*). For the WT enzyme, only Compound PR is observed perhaps due to the rapid two-electron reduction of Compound I. The first electron donor in this case is thought to be the Met-Tyr-Trp crosslink.

As to the origin of the second electron donor, several possibilities exist. Mutagenesis studies (*34, 38*) of *Synechocystis* PCC 6803 followed by EPR analysis, revealed that Trp^{106} (Trp^{91} in *Mtb* KatG) might be the second electron donor. Trp^{91} is part of the hydrogen bonding network that includes Trp^{107} in the crosslink, several waters, and the catalytically important distal histidine (His^{108}) and arginine (Arg^{104}), making it a good candidate for reducing Compound II. However, mutation of Trp^{91} in Mtb KatG did not suppress the $Trp^{\bullet}$ EPR signal observed in WT KatG (*39*). Magliozzo and coworkers found evidence for the presence of a tyrosyl radical in WT KatG (*32*) and Kat(Y229F) (*4*). Mutagenesis studies suggested that the radical is located on Tyr^{353}.

One intermediate in the peroxidase cycle of KatG that Ivancich and coworkers observed (*10*) but Magliozzo did not observe was [Fe(IV)=O, $Trp_{321}^{+\bullet}$], where Trp^{321} has a strong exchange coupling interaction with the heme, which was displayed by a 400-G signal that is temperature dependent as in CcP. This suggests that the first electron donor in the peroxidase cycle is Trp^{321} and not Tyr^{229} as in the catalase cycle. Colin et al. (*39*) suggest that the ferryl intermediate with the second oxidizing equivalent located on the proximal Trp or other Trp sites farther away from the heme, forming at the expense of the short-lived species Fe=O $Por^{+\bullet}$, may be considered as a way to differentiate between the peroxidase and the catalase functions of KatG. While a restrained access channel and a fine-tuned heme pocket are required for the catalase activity of KatG, the presence of alternative oxidizing sites for the one-electron oxidation of substrates (ditant from the heme) might be important for the peroxidase activity of KatG.

We have been able to show that a Cys-Tyr-Trp crosslink forms in KatG(M255C), that it alters the spectral features of the one-electron oxidized intermediate (Compound II or PR) which forms during catalysis, and that this correlates well to catalase activity. The data presented here for KatG(M255C) help to establish a trend which was not readily apparent from previous results, e. g. the Met-Tyr-Trp crosslink plays a role in protecting KatG against

catalase inactivation by minimizing the lifetime of the catalase-inactive Compound II intermediate (see diagram below). This is achieved by both retarding the formation of Compound II and hastening its conversion to the catalase-active Compound PR species.

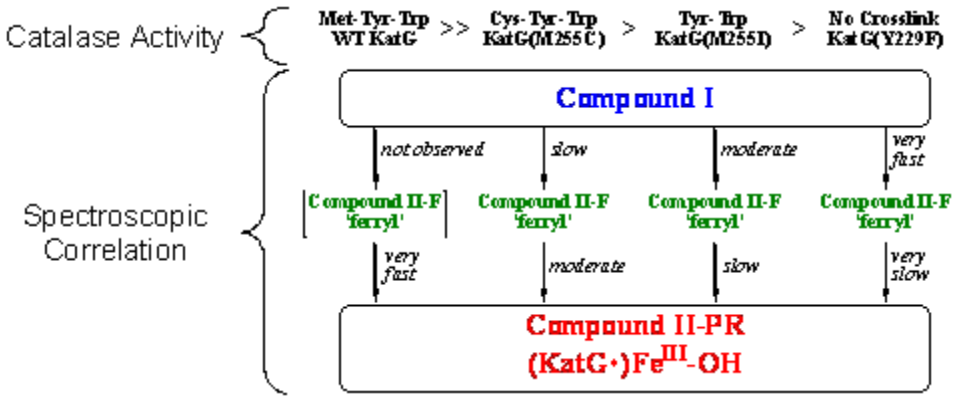

It is clear from this work that an enzyme structure-spectroscopy-activity relationship is readily observed in the catalase-peroxidases which is solely attributed to the presence of the Met-Tyr-Trp crosslink, and that the sulfonium ion plays a crucial role in mitigating the catalytic function of this system. Further studies are in progress to help deduce the electrochemical contributions of the sulfonium ion to the reduction potential of the crosslink. More recently, however, Magliozzo and co-workers have posited an elegant mechanism for catalase activity in KatG (*12*) with an important role for a radical located on the Me-Tyr-Trp crosslink. In this novel catalase reaction pathway, formation of a radical on the Met-Tyr-Trp crosslink (specifically Y229) is then followed by the transfer of an electron from oxyferrous KatG, leading to the release of dioxygen and a return to the resting form of the enzyme. While not specifically intended to address the mechanistic questions surrounding the origins of catalase activity in the bifunctional catalase-peroxidases, our results here provide further support for the necessity of both the Met-Tyr-Trp crosslink and the extended H-bonding network for maintaining catalase activity in KatG.

Supporting Information

Catalytic Relevance of the Sulfonium Ion in the Met-Tyr-Trp Crosslink of *Mycobacterium tuberculosis* Catalase-Peroxidase (KatG)

Contents

Table II.S1: UV-visible Spectroscopic Data for KatG(M255C), KatG(M255I), KatG(Y229F), and WT KatG.

	R_z	λ_{max} (Soret)	β	CT2	CT1 (LMCT)	A_{Soret}/A_{380}	A_{614}/A_{645}	Ref.
M255C	0.56	407	502	540	636	1.77	0.96	[a]
M255I	0.56	406	500	540	620	1.71	1.19	(*22*)
Y229F	0.59	406	504	540	638	1.68	0.85	(*20*)
WT	0.63	408	496	540	630	1.79	1.05	(*20*)

[a] = This work.

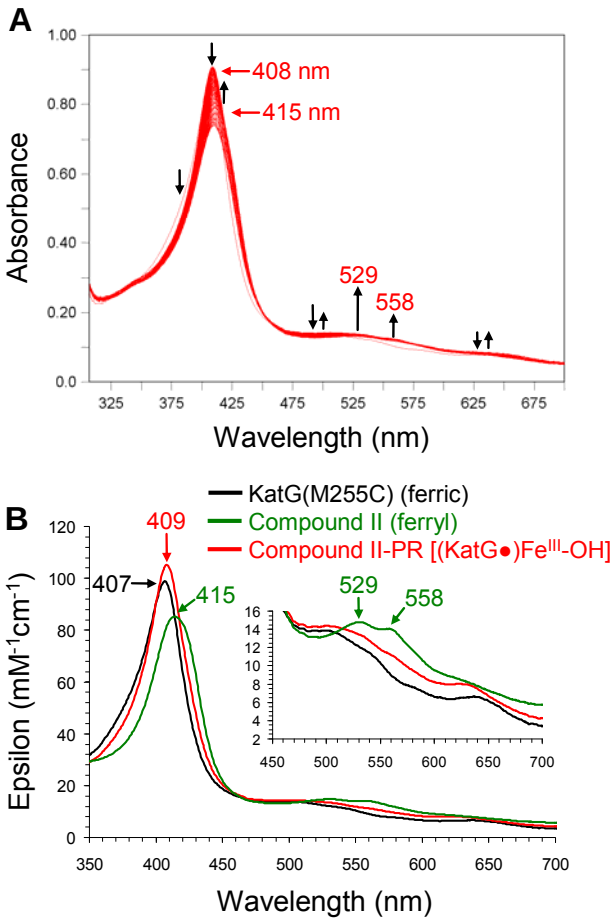

Figure II.S1: (A) Long time-scale (300 scans, 6 sec) UV-visible spectroscopic monitoring of the stopped-flow reaction between KatG(M255C) (10 µM) and 10-fold excess of PAA. See experimental for details. (B) Calculated UV-visible spectra for resting (black), [(KatG)(Por)Fe^{IV}=O] Compound II-F KatG(M255C) (green), and [(KatG•)(Por)Fe^{III}-OH] Compound II-PR KatG(M255C) (red) are shown; the rapid-scanning data from A were compiled and fitted to a double exponential reaction model using the Specfit global analysis program.

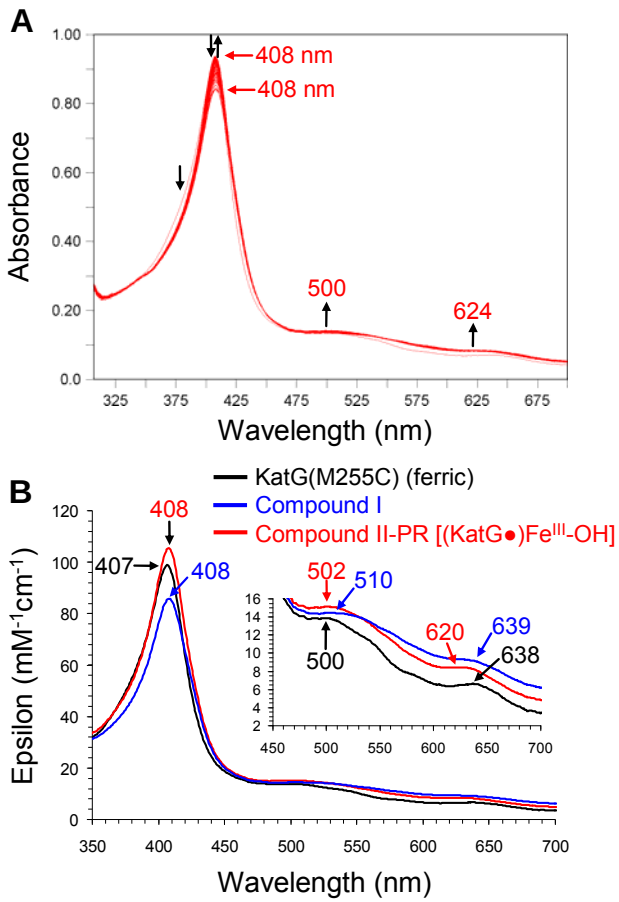

Figure II.S2: (A) Stopped-flow UV-visible spectroscopic monitoring of the reaction (300 scans, 0.6 sec) between KatG(M255C) (10 μM) and one equivalent of PAA. See experimental for details. (B) Calculated UV-visible spectra for both resting (black), Compound I (blue), and [(KatG•)(Por)Fe^{III}-OH] Compound II-PR KatG(M255C) (red) are shown; the rapid-scanning data from A were compiled and fitted to a double exponential reaction model using the Specfit global analysis program.

REFERENCES

1. Welinder, K. G. (1991) Bacterial Catalase-Peroxidases are Gene Duplicated Members of the Plant Peroxidase Superfamily, *Biochimica Et Biophysica Acta 1080*, 215-220.

2. Zamocky, M., Regelsberger, G., Jakopitsch, C., and Obinger, C. (2001) The Molecular Peculiarities of Catalase-Peroxidases, *Febs Letters 492*, 177-182.

3. Bertrand, T., Eady, N. A. J., Jones, J. N., Nagy, J. M., Jamart-Gregoire, B., Raven, E. L., and Brown, K. A. (2004) Crystal Structure of *Mycobacterium tuberculosis* Catalase-Peroxidase, *Journal of Biological Chemistry 279*, 38991-38999.

4. Yu, S. W., Girotto, S., Zhao, X. B., and Magliozzo, R. S. (2003) Rapid Formation of Compound II and a Tyrosyl Radical in the Y229F Mutant of *Mycobacterium tuberculosis* Catalase-Peroxidase Disrupts Catalase but Not Peroxidase Function, *Journal of Biological Chemistry 278*, 44121-44127.

5. Jakopitsch, C., Ivancich, A., Schmuckenschlager, F., Wanasinghe, A., Poltl, G., Furtmuller, P. G., Ruker, F., and Obinger, C. (2004) Influence of the Unusual Covalent Adduct on the Kinetics and Formation of Radical Intermediates in *Synechocystis* Catalase Peroxidase - A Stopped-Flow and EPR Characterization of the MET275, TYR249, and Arg(349) Variants, *Journal of Biological Chemistry 279*, 46082-46095.

6. Jakopitsch, C., Auer, M., Ivancich, A., Ruker, F., Furtmuller, P. G., and Obinger, C. (2003) Total Conversion of Bifunctional Catalase-Peroxidase (Katg) to Monofunctional Peroxidase by Exchange of a Conserved Distal Side Tyrosine, *Journal of Biological Chemistry 278*, 20185-20191.

7. Smulevich, G., Jakopitsch, C., Droghetti, E., and Obinger, C. (2006) Probing the Structure and Bifunctionality of Catalase-Peroxidase (KatG), *Journal of Inorganic Biochemistry 100*, 568-585.

8. Deemagarn, T., Wiseman, B., Carpena, X., Ivancich, A., Fita, I., and Loewen, P. C. (2007) Two Alternative Substrate Paths for Compound I Formation and Reduction in Catalase-Peroxidase KatG from *Burkholderia pseudomallei*, *Proteins-Structure Function and Bioinformatics 66*, 219-228.

9. Carpena, X., Wiseman, B., Deemagarn, T., Herguedas, B., Ivancich, A., Singh, R., Loewen, P. C., and Fita, I. (2006) Roles for Arg426 and Trp111 in the Modulation of NADH Oxidase Activity of the Catalase-Peroxidase KatG from *Burkholderia pseudomallei* Inferred from pH-Induced Structural Changes, *Biochemistry 45*, 5171-5179.

10. Singh, R., Switala, J., Loewen, P. C., and Ivancich, A. (2007) Two Fe(IV)=O Trp(center dot) Intermediates in *M-tuberculosis* Catalase-Peroxidase Discriminated by Multifrequency (9-285 GHz) EPR Spectroscopy: Reactivity toward Isoniazid, *Journal of the American Chemical Society 129*, 15954-15963.

11. Suarez, J., Ranguelova, K., Jarzecki, A. A., Manzerova, J., Krymov, V., Zhao, X. B., Yu, S. W., Metlitsky, L., Gerfen, G. J., and Magliozzo, R. S. (2009) An Oxyferrous Heme/Protein-Based Radical Intermediate is Catalytically Competent in the Catalase Reaction of *Mycobacterium tuberculosis* Catalase-Peroxidase (KatG), *Journal of Biological Chemistry 284*, 7017-7029.

12. Zhao, X., Yu, S., Ranguelova, K., Suarez, J., Metlitsky, L., Schelvis, J. P. M., and Magliozzo, R. S. (2009) Role of the Oxyferrous Heme Intermediate and Distal Side Adduct Radical in the Catalase Activity of *Mycobacterium tuberculosis* KatG Revealed by the W107F Mutant, *Journal of Biological Chemistry 284*, 7030-7037.

13. Ghiladi, R. A., Medzihradszky, K. F., and Ortiz de Montellano, P. R. (2005) The Role of the Met-Tyr-Trp Crosslink in *Mycobacterium tuberculosis* Catalase-Peroxidase (KatG) as Revealed by KatG(M255I), *Biochem. 44*, 15093-15105.

14. Ghiladi, R. A., Cabelli, D. E., and de Montellano, P. R. O. (2004) Superoxide Reactivity of KatG: Insights into Isoniazid Resistance Pathways in TB, *Journal of the American Chemical Society 126*, 4772-4773.

15. Ghiladi, R. A., Medzihradszky, K. F., and de Montellano, P. R. O. (2005) Role of the Met-Tyr-Trp Cross-Link in *Mycobacterium tuberculosis* Catalase-Peroxidase (Katg) as Revealed by Katg(M255I), *Biochemistry 44*, 15093-15105.

16. Ghiladi, R. A., Knudsen, G. M., Medzihradszky, K. F., and de Montellano, P. R. O. (2005) The Met-Tyr-Trp cross-link in *Mycobacterium tuberculosis* Catalase-Peroxidase (KatG) - Autocatalytic Formation and Effect on Enzyme Catalysis and Spectroscopic Properties, *Journal of Biological Chemistry 280*, 22651-22663.

17. Chouchane, S., Girotto, S., Kapetanaki, S., Schelvis, J. P. M., Yu, S. W., and Magliozzo, R. S. (2003) Analysis of Heme Structural Heterogeneity in *Mycobacterium tuberculosis* Catalase-Peroxidase (Katg), *Journal of Biological Chemistry 278*, 8154-8162.

18. Beers, R. F., and Sizer, I. W. (1952) A Spectrophotometric Method for Measuring the Breakdown of Hydrogen Peroxide by Catalase, *Journal of Biological Chemistry 195*, 133-140.

19. Childs, R. E., and Bardsley, W. G. (1975) Steady-State Kinetics of Peroxidase with 2,2'-Azino-Di-(3-Ethylbenzthiazoline-6-Sulphonic Acid) as Chromogen, *Biochemical Journal 145*, 93-103.

20. Singh, R., Wiseman, B., Deemagarn, T., Donald, L. J., Duckworth, H. W., Carpena, X., Fita, I., and Loewen, P. C. (2004) Catalase-peroxidases (KatG) Exhibit NADH Oxidase Activity, *Journal of Biological Chemistry 279*, 43098-43106.

21. Engleder, M., Regelsberger, G., Jakopitsch, C., Furtmuller, P. G., Ruker, F., Peschek, G. A., and Obinger, C. (2000) Nucleotide Sequence Analysis, Overexpression in *Escherichia coli* and Kinetic Characterization of *Anacystis nidulans* Catalase-Peroxidase, *Biochimie 82*, 211-219.

22. Jakopitsch, C., Wanasinghe, A., Jantschko, W., Furtmueller, P. G., and Obinger, C. (2005) Kinetics of Interconversion of Ferrous Enzyme, Compound II and Compound III of Wild-Type Synechocystis Catalase-Peroxidase and Y249F. Proposal for the catalatic mechanism, *J Biol Chem*.

23. Jakopitsch, C., Ivancich, A., Schmuckenschlager, F., Wanasinghe, A., Poltl, G., Furtmuller, P. G., Ruker, F., and Obinger, C. (2004) Influence of the Unusual Covalent Adduct on the Kinetics and Formation of Radical Intermediates in S*ynechocystis* Catalase Peroxidase: A Stopped-Flow and EPR Characterization of the MET275, TYR249, And ARG439 Variants, *J Biol Chem 279*, 46082-46095.

24. Ghiladi, R. A., Knudsen, G. M., Medzihradszky, K. F., and Ortiz de Montellano, P. R. (2005) The Met-Tyr-Trp cross-link in *Mycobacterium tuberculosis* Catalase-Peroxidase (KatG): Autocatalytic Formation and Effect on Enzyme Catalysis and Spectroscopic Properties, *J. Biol. Chem. 280*, 22651-22663.

25. Ghiladi, R. A., Medzihradszky, K. F., Rusnak, F. M., and Ortiz de Montellano, P. R. (2005) Correlation between Isoniazid Resistance and Superoxide Reactivity in *Mycobacterium tuberculosis* KatG, *J Am Chem Soc 127*, 13428-13442.

26. Chouchane, S., Lippai, I., and Magliozzo, R. S. (2000) Catalase-peroxidase (*Mycobacterium tuberculosis* KatG) Catalysis and Isoniazid Activation, *Biochemistry 39*, 9975-9983.

27. Yu, S. W., Chouchane, S., and Magliozzo, R. S. (2002) Characterization of the W321F Mutant of *Mycobacterium tuberculosis* Catalase-Peroxidase KatG, *Protein Science 11*, 58-64.

28. Svistunenko, D. A., and Cooper, C. E. (2004) A New Method of Identifying the Site of Tyrosyl Radicals in Proteins, *Biophysical Journal 87*, 582-595.

29. Regelsberger, G., Jakopitsch, C., Engleder, M., Ruker, F., Peschek, G. A., and Obinger, C. (1999) Spectral and Kinetic Studies of the oxidation of Monosubstituted Phenols and Anilines by Recombinant *Synechocystis* Catalase - Peroxidase Compound I, *Biochemistry 38*, 10480-10488.

30. Nam, W., Han, H. J., Oh, S.-Y., Lee, Y. J., Choi, M.-H., Han, S.-Y., Kim, C., Woo, S. K., and Shin, W. (2000) New Insights into the Mechanisms of O-O Bond Cleavage of Hydrogen Peroxide and *tert*-Alkyl Hydroperoxides by Iron(III) Porphyrin Complexes, *J. Am. Chem. Soc. 122*, 8677-8684.

31. Nam, W., Choi, H. J., Han, H. J., Cho, S. H., Lee, H. J., and Han, S.-Y. (1999) Use of 2-Methyl-1-Phenylpropan-2-Yl Hydroperoxide (MPPH) as a Mechanistic Probel for the heterolytic versus homolytic O-O bond cleavage of Tert-Alkyl Hydroperoxide by Iron (III) Porphyrin Complex, *Chem Comm*, 387-388.

32. Chouchane, S., Girotto, S., Yu, S. W., and Magliozzo, R. S. (2002) Identification and Characterization of Tyrosyl Radical Formation in *Mycobacterium tuberculosis* Catalase-Peroxidase (KatG), *Journal of Biological Chemistry 277*, 42633-42638.

33. Ranguelova, K., Girotto, S., Gerfen, G. J., Yu, S., Suarez, J., Metlitsky, L., and Magliozzo, R. S. (2007) Radical Sites in *Mycobacterium tuberculosis* KatG Identified Using Electron Paramagnetic Resonance Spectroscopy, the Three-Dimensional Crystal Structure, and Electron Transfer Couplings, *Journal of Biological Chemistry 282*, 6255-6264.

34. Jakopitsch, C., Obinger, C., Un, S., and Ivancich, A. (2006) Identification of Trp106 as the Tryptophanyl Radical Intermediate in *Synechocystis* PCC6803 Catalase-Peroxidase by Multifrequency Electron Paramagnetic Resonance Spectroscopy, *Journal of Inorganic Biochemistry 100*, 1091-1099.

35. Santoni, E., Jakopitsch, C., Obinger, C., and Smulevich, G. (2004) Manipulating the Covalent Link Between Distal Side Tryptophan, Tyrosine, and Methionine in Catalase-Peroxidases: an Electronic Absorption and Resonance Raman Study, *Biopolymers 74*, 46-50.

36. Santoni, E., Jakopitsch, C., Obinger, C., and Smulevich, G. (2004) Comparison between Catalase-Peroxidase and Cytochrome *c* Peroxidase. the Role of the Hydrogen-Bond Networks for Protein Stability and Catalysis, *Biochemistry 43*, 5792-5802.

37. Kapetanaki, S. M., Zhao, X., Yu, S., Magliozzo, R. S., and Schelvis, J. P. M. (2007) Modification of the Active Site of *Mycobacterium tuberculosis* Katg after disruption of the Met-Tyr-Trp Cross-Linked Adduct, *Journal of Inorganic Biochemistry 101*, 422-433.

38. Ivancich, A., Jakopitsch, C., Auer, M., Un, S., and Obinger, C. (2003) Protein-Based Radicals in the Catalase-Peroxidase of *Synechocystis* PCC6803: A Multifrequency EPR Investigation of Wild-Type and Variants on the Environment of the Heme Active Site, *Journal of the American Chemical Society 125*, 14093-14102.

39. Colin, J., Wiseman, B., Switala, J., Loewen, P. C., and Ivancich, A. (2009) Distinct Role of Specific Tryptophans in Facilitating Electron Transfer or as Fe(IV)=O Trp(center dot) Intermediates in the Peroxidase Reaction of *Bulkholderia pseudomallei* Catalase-Peroxidase: A Multifrequency EPR Spectroscopy Investigation, *Journal of the American Chemical Society 131*, 8557-8563.

CHAPTER III

Enhanced Peroxidase Activity Displayed by KatG Containing Unnatural Amino Acids

III.1. Introduction

The incorporation of unnatural amino acids into proteins is a powerful tool for imparting new or enhanced catalytic activities to enzymes. Moreover, the incorporation of amino acids with defined steric or electronic properties enables us to use them as probes for exploring the structure and function of proteins. The methods used previously to obtain unnatural amino acid-containing proteins required the synthesis of the protein in vitro or the use of stoichiometric amounts of chemically-aminoacylated tRNAs. The latter resulted in low protein yields and the incorporation of the unnatural amino acid throughout the proteome. It also resulted in the competition between the unnatural amino acid and the existing 20 natural amino acids.

However, by the development of the Schultz method, unnatural amino acids can be included at specific sites with high fidelity and efficiency. This method was developed by Peter G. Schultz and reviewed by him in 2006 (*1*). The Schultz method has been used to incorporate over 30 unnatural amino acids into different proteins. These unnatural amino acids can contain spectroscopic probes, post-translational modifications, metal-chelating groups or photoaffinity labels. In order to incorporate unnatural amino acids into proteins with high fidelity and specificty, several requirements need to be met: a unique transfer RNA (tRNA):codon pair, the corresponding aminoacyl-tRNA synthetase, and sufficient levels of the unnatural amino acid in the cytoplasm of the host cells. The tRNA must be ortogonal to the system in which the unnatual amino acid is to be incorporated, i.e. not recognized by the endogenous aminoacyl-tRNA synthetases. Also, a unique codon that does not encode for any of the 20 natural amino acids is required. It is important that the cognate aminoacyl-tRNA synthetase aminoacylates only the ortogonal tRNA and not any of the endogenous tRNAs, and the tRNA has to be aminoacylated with the unnatural amino acid only and not with any of the natural amino acids. It is also required that the unnatural amino acid is not a substrate for any of the endogenous synthetases. The unnatural amino acid must be efficiently

transported to the cytoplasm of the host cells, and it has to be stable (not a substatee for metabolic enzymes).

To overcome the challenges listed above, Schultz and coworkers developed a method for including unnatural amino acids in prokaryotes (*2*) and then modified it slightly in order to be used for eukaryotes (*3*). In *E. coli*, the stop codon UAG was a suitable one for including unnatural amino acids because of its very low occurance in the genome. Unique (orthogonal) tRNA:aminoacyl-tRNA-synthetase pairs were taken from archea. The first pair was derived from tyrosyl-tRNA:tyrosyl-tRNA-synthetase pair from *Methanococcus jannaschii* (*Mj*tRNA^{Tyr}:*Mj*TyrRS) (*4*). The *Mj*tRNA^{Tyr} has distinct synthetase recognition elements. And the synthetase (*Mj*TyrRS) has minimalist anticodon loop binding domain so that the *Mj*tRNA^{Tyr} anticodon could be changed to CUA without affecting its affinity to the synthetase (*Mj*TyrRS). Unfortunately, the *Mj*tRNA^{Tyr} was aminoacylated by endogenous synthetases. Therefore, Schultz and coworkers made a library of tRNAs by mutating 11 amino acids in *Mj*tRNA^{Tyr} that do not interact directly wih the synthetase (*Mj*TyrRS). Then the mutants that were substrates for endogenous synthetases were removed from the library. Also, the tRNA needs to recognize the unnatural amino acid and not tyrosine or an endogenous amino acid. So, a library of synthetases modified in the active site was made. Then the synthetases that charge natural amino acids were removed from the library. It is important to mention that one of the methods that were used to include more than one unnatural amino acid into a protein was to develop quadruple codons and tRNAs with expanded anticodon loops.

One of the applications of Schultz's method is to include unnatural amino acids with chemically reactive groups, such as ketone (*5*), azide (*6*), acetylene or thioester groups. These groups can be then used to attach fluorophore tags or other reagents. For example, human growth hormone was modified with polyethylene glycol (PEG) to increase its lifetime in the serum, and the same technique can be used to increase the lifetime of other therapeutic proteins. Unnatural amino acids can also contain photoreactive groups that can form crosslinks upon irraditaion. This property is useful for mapping biomolecular interactions. In addition, photocaged amino acids have been used (*7, 8*). For example, in photocaged Cys,

Ser and Tyr, the hydroxy or thiol groups are blocked with a nitrobenzyl-group derivative that can be cleaved by irradiation at 365 nm. This property offers a great opportunity for the photoregultaion of enzymes. Some unntural amino acids can be used as biophysical probes. For example, flourescence probes can be used to visually monitor changes in protein structue and intermolecular interactions. These are more useful than Green Fluorescent Protein (GFP) because of their smaller size. Labelled unnatural amino acids can be included as NMR probes (*9, 10*), and nitrile groups can function as infrared probes to monitor local environment changes and protein dynamics. Another application of this method is using redox-active residues to manipúlate electron transfer processes, such as dihydroxyphenylalanine and 3-amino-L-tyrosine (*11*) which form the corresponding quinones upon their two-electron oxidation. 3-amino-L-tyrosine can also serve as a radical trap because of the high stability of its semiquinone form (*12*).

Interestingly, Wang et al. (*13*) expressed unnatural amino acids in *Mycobacterium Tuberculosis* as a way to facilitate the study of TB biology and the development of vaccines. For example, the photocrosslinkers p-iodophenylalanine and p-azidophenylalanine can help probe protein-protein or protein-nucleic acid interactions inside *Mtb* or between *Mtb* and the host cells. Also, the immunogenic amino acid p-nitrophenylalanine can be used to create novel TB vaccines.

In this work, we used the methodology developed by Schultz and coworkers for the incorporation of unnatural amino acids to gain further understanding of the role of the unique Met-Tyr-Trp crosslink in KatG, and to explore the possibility of creating mutants with enhanced catalytic activity. Mutations of the crosslink with other naturally-occuring amino acids have been shown to eliminate catalase activity in KatG but not the peroxidase activity. Here, we inserted unnatural amino acids with different electronic chracteristics in the position of Tyr^{229}, which has been shown to be a sensitive position, to explore the effect these modifications have on the catalytic activity of KatG and on the spectroscopic properties of the intermediates. The unnatural amino acids used in this study are presented in Figure III.1.

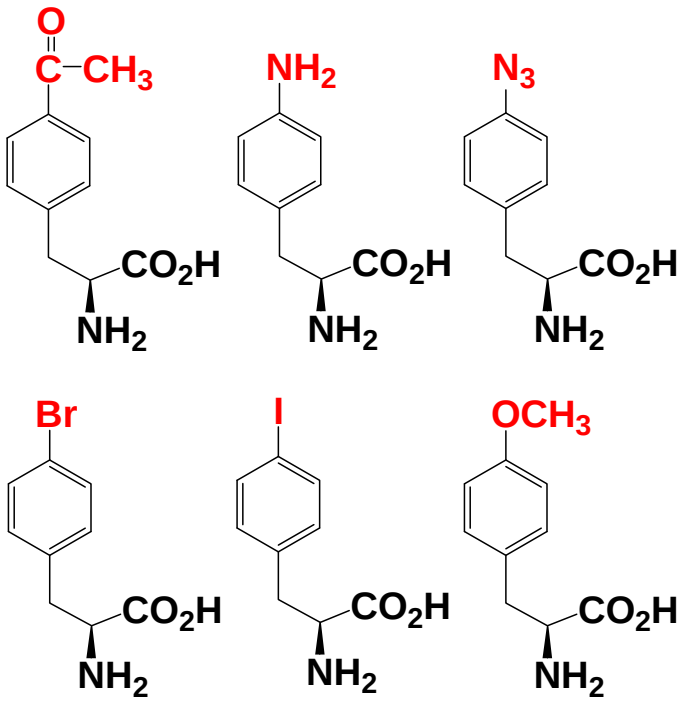

Figure III.1: The unnatural amino acids used in this study (the acetyl, amino, azido, bromo, iodo and methoxy derivatives of phenyl alanine).

III.2. Materials and Methods

Materials – *p*-Iodophenylalanine, *p*-aminophenylalanine, and *p*-azidophenylalanine were purchased from Bachem. All other reagents and biochemicals, unless otherwise specified, were of the highest grade available from commercial sources. Buffer salts and acetonitrile (HPLC grade) were purchased from Fisher Scientific. All other reagents and biochemicals, unless otherwise specified, were of the highest grade available from Sigma-Aldrich.

KatG(Y229TAG) Unnatural Amino Acid Protein Expression and Purification – The plasmid pKatG(Y229TAG) was co-transformed (heat shock) with the pSup vector containing the tRNA-synthetase pair for either *p*-iodophenylalanine, *p*-aminophenylalanine, *p*-azidophenylalanine, or *p*-acetylphenylalanine into competent *E. coli* BL21(Gold)DE3 cells, plated onto LB-agar plates containing 50 μg/mL ampicillin and 34 μg/mL chloramphenicol,

and grown overnight at 37 °C. Subsequent expression steps were performed the same way KatG(M255C) was expressed.

Stopped Flow UV-Visible Spectrophotometry – Experiments were performed on a Bio-Logic SFM-400 Triple Mixing Stopped-Flow System employing a diode array spectrophotometer, and were carried out at 25 °C in 100 mM KPi (pH 7.5) containing 5 μM EDTA. The initial (pre-mixing) concentrations were: $[KatG]_o$ = 20 μM, $[MPPH]_o$ = $[PAA]_o$ = $[H_2O_2]_o$ =20, 50, or 200 μM. Data was collected (900 scans total) over a two (750 ms, 300 scans; 1500 s, 600 scans) or three (750 ms, 7.5 s, 75 s; 300 scans each) time-domain regime using the Bio Kinet32 software package (Bio-Logic), and analyzed using the Specfit Global Analysis System software package (Spectrum Software Associates) as pseudo-first order reactions where applicable. Data was fit from one to three exponential curves where applicable.

III.3. Results and Discussion

Overexpression and Purification of Unnatural Amino Acid Containing KatGs – The plasmid encoding wild-type KatG with an N-terminal poly-His tag (pMRLB11) was obtained from Colorado State University under the TB Research Materials and Vaccine Testing Contract (NIH, NIAID NO1 AI-75320). PCR amplification of pMRLB11 using mutagenic primers produced KatG(Y229TAG) containing the amber stop codon in position 229. Hemin (80 mg/L) was added to the culture medium (prior to induction with IPTG) to assure stoichiometric incorporation of the heme cofactor during overexpression in *E.coli (14)*. The two-part purification strategy (affinity followed by size-exclusion chromatographies) resulted in purification levels > 95% homogeneity. Wild-type and mutant KatGs were indistinguishable by SDS-PAGE gels (data not shown). Yields of isolated, purified KatGs containing the unnatural amino acids ranged from 11 – 21 mg/L (Table III.1), below the typical 80 mg/L obtained for WT enzyme (*15*) but still in good yield considering this *in vivo* translation employs amber suppression which results in lower yields.

Table III.1: UV-visible spectral features and purification results for KatG(Y229UAA) mutants (3 L cultures)

Mutant	R_z	λ_{Max}	mg KatG	mg/L expression
KatG(Y229-p-Ac-F)	0.41	409	58	19
KatG(Y229-p-NH_2-F)	0.48	409	24	8
KatG(Y229-p-N_3-F)	0.47	409	62	21
KatG(Y229-p-Br-F)	0.48	409	56	19
KatG(Y229-p-I-F)	0.52	408	64	21
KatG(Y229-p-OMe-F)	0.51	409	61	20
KatG(Y229F)	0.59	408	194	65
WT KatG	0.62	408	240	80

UV-visible Spectroscopic Analysis of KatG(Y229UAA) – Relevant spectral features and analysis of the electronic absorption spectra of KatGs containing the unnatural amino acids are presented in Table III.2. The optical purity ratio (Reinheitzahl or R_z, defined as A_{Soret}/A_{280}) for KatG(Y229UAA) was found to range between 0.47 – 0.52, slightly below the value obtained for WT enzyme (*16*) but in a range that has been previously reported for other KatG mutants. Pyridine hemochrome assays yielded 0.82 – 0.91 ± 0.03 heme/monomer, indicating near stoichiometric heme incorporation, yet slightly below that found for WT enzyme (0.97) despite hemin supplementation in the growth medium.

Table III.2: Analysis of the UV-visible spectroscopic data for the four unnatural amino-acid containing (Y229UAA) mutants, and comparison with WT KatG and KatG(Y229F)

	λ_{max} (Soret)	A_{Soret}/A_{380}	A_{614}/A_{645}
WT KatG	408	1.79	1.05
KatG(Y229F)	406	1.68	0.85
KatG(Y229Iodo)	408	1.66	0.91
KatG(Y229Acetyl)	409	1.64	0.88
KatG(Y229Amino)	408	1.70	0.87
KatG(Y229Azido)	409	1.70	0.98

In lieu of electron paramagnetic or resonance Raman spectroscopic studies, analysis of the UV-visible spectrum of KatG(Y229UAA) by the methodology employed by Magliozzo and co-workers (*17*) provides insight into the electronic nature of the heme prosthetic group. Generally, 5-c HS hemes exhibit a slightly blue shifted and lower extinction coefficient Soret band than their 6-c HS counterparts, as well as a shoulder at 380 nm (denoted by a smaller A_{Soret}/A_{380} ratio). Additionally, the CT1 feature in a 5-c HS heme is found at ~640 nm (or higher), while that of a 6-c HS heme is generally closer to 630 nm (as revealed by an A_{614}/A_{645} ratio). LS heme systems exhibit a red-shifted Soret, the absence of a CT1 feature, and visible features at 565 and 580 nm. Thus, as can be seen from the data in Table III.2, the four KatG(Y229UAA) mutants exhibit a similar population of 5-c HS and 6-c HS hemes as does KatG(Y229F).

Catalase and Peroxidase Activities of KatG(Y229UAA) Mutants – Kinetic parameters (k_{cat}, K_m, and catalytic efficiency, k_{cat}/K_m) for the catalase and peroxidase activities of the KatG(Y299X) mutants are presented in Table III.3. As conventional catalases do not follow typical Michaelis-Menten kinetics (lack of a detectable enzyme-substrate complex and inability to reach saturation with H_2O_2 before inactivation), kinetic constants reported here for catalase activity are 'apparent' values. All the KatG(Y229UAA) mutants exhibited saturable catalase activity under the conditions employed for this kinetic study.

Table III.3: Kinetic parameters for the **catalase** activity of KatG(Y229UAA) mutants

	WT	**Acetyl**	**Amino**	**Azido**	**Iodo**	**Bromo**	**Methoxy**
k_{cat}, s^{-1}	6000±70	5.4±0.9	8.5±1.2	49.0±8.7	2.1 ±0.4	ND	1.0±0.2
K_m, mM	2.5±0.2	7.5±0.5	9.6±0.4	52.7±6.3	56.3 ±8.2	ND	47.2±6.7
k_{cat}/K_m, ($M^{-1}s^{-1}$)	$24\times10^5\pm 28\times10^3$	718 ± 126	895± 130	931 ± 166	37±7	ND	21 ± 4

ND: cannot be determined under the conditions used in this study

The k_{cat} values (2.1 – 49 s^{-1}) are slightly greater than that reported for KatG(Y229F) (0.1 s^{-1}), yet significantly less by 2 to 3 orders of magnitude compared to WT enzyme (6000

s^{-1}). The K_m values (7.5 - 56 mM) are also greater than that found for WT KatG (2.5 mM), although the extent of active site binding disruption appears to be mutant-dependent. The result that catalase activity is severely disrupted for KatG(Y299UAA) versus WT KatG (k_{cat}/K_m ~10^4 - 10^5 lower) suggests that none of the KatG(Y229UAA) mutants contains an intact Met-Tyr-Trp crosslink, a supposition that is supported by our tryptic digest studies.

Peroxidase activities (see Table III.4) (saturable) were measured for the one-electron oxidation of 2,2'-azino-bis(3-ethylbenzothiazoline-6-sulfonate) (ABTS) to the corresponding radical cation $ABTS^{\bullet+}$ by KatG in the presence of *tert*-butylhydroperoxide. KatG(Y229UAA) exhibited marked increases in k_{cat} (>2.35 ± 0.01 s^{-1}), with similar or lower values for K_m (2.60 – 9.20 mM) as compared to WT KatG (0.062 s^{-1} and 8.4 mM, respectively). The increase in peoxidase activity observed for the unnatural amino acid-containing mutants is significantly larger than the ~40-fold increase observed previously for KatG(Y229F) (k_{cat} = 0.843 s^{-1} and K_m = 2.7 mM).

Table III.4: Comparison of k_{cat}/K_m (**peroxidase** activity) of different KatG UAA mutants to WT KatG

	k_{cat}, s^{-1}	K_m, mM	k_{cat}/K_m, ($M^{-1}s^{-1}$)	Normalized
WT	0.062 ± 0.001	8.44 ± 0.45	7.3 ± 0.4	1
p-Br-F	1.27 ± 0.08	1.50 ± 0.21	849 ± 99	116
p-Ac-F	2.37 ± 0.01	2.60 ± 0.04	910 ± 12	124
p-I-F	1.70 ± 0.02	1.57 ± 0.08	1083 ± 55	148
p-NH_2-F	3.46 ± 0.23	2.37 ± 0.23	1461 ± 141	200
p-OMe-F	2.17 ± 0.07	1.13 ± 0.07	1920 ± 120	**263**
p-N_3-F	2.36 ± 0.03	1.09 ± 0.06	2155 ± 117	**295**

What are some of the possibilities that can be proposed for the enhanced peroxidase activity observed for these mutants? Stopped-flow UV-visible and EPR spectroscopies were used by Magliozzo and coworkers (*18*) to characterize the intermediates formed in the peroxidase cycle of KatG(Y229F). They found that k_{obs} for compound I formation is 4×10^6 M^{-1} s^{-1}, two orders of magnitude greater than k_{obs} obtained for WT KatG (1.2×10^4 M^{-1} s^{-1}). Therefore, one of the possibilities they suggested to account for the enhanced peroxidase activity of KatG(Y229F) is the faster formation of Compound I, which is the first intermediate in the peroxidase cycle. They proposed that the new orientation of Trp^{107} in the

mutant allows better interaction of the adjacent His with the hydroperoxide, and it becomes easier for His to act as a base and accept a proton from the hydroperoxide to form Fe^{III}-OOH, the first step in Compound I formation. Another possibility they proposed for the enhanced peroxidase activity in KatG(Y229F) is the greater stability of Compound II whose spectral features persisted for 6 min upon the reaction of KatG(Y229F) with 3 to 10 fold excess of PAA. Their reasoning was that because Trp^{107} is free (not involved in the crosslink), there is a possibility of hydrogen bond formation between the Trp^{107} indole ring and the oxygen atom of oxoferryl Compound II, which is an active intermediate in the peroxidase cycle but not the catalase cycle. Also, one of the reasons behind the marked decrease in the catalase activity of this mutant is that when Compound II is more stable, Compound III is more easily formed and the availability of the resting enzyme and compound I, which are important for the catalase cycle to continue, decreases.

While KatG(Y229F) displayed a 40-fold increase in peroxidase activity relative to WT KatG, our KatG(Y229UAA) mutants exhibited up to 300-fold increase in peroxidase activity relative to WT KatG due mainly to an increase in k_{cat}. One possibility for the increase in peroxidase activity relative for KatG(Y229UAA) compared to KatG(Y229F) is the greater stability of Compound II. Although the values of k_{obs} for Compound II formation for KatGY229F and KatG(Y229UAA) are comparable as can be seen from Table III.5, k_{obs} for Compound III formation (which is related to the rate of reaction of Compound II with H_2O_2) is two orders of magnitude smaller for KatG(Y229UAA) than it is for KatGY229F. The slower rate of formation of Compound III in KatG(Y229UAA) allows a longer lifetime for the Compound II intermediate, which is active in the peroxidase cycle. The slower rate of formation of Compound III might be due to a change in the position of Trp^{107} after the mutation of Tyr^{229}. As can be seen from Figure III.2, changes in the location of Trp^{107} might disrupt the hydrogen bonding between this residue and the water molecules in the substrate channel, therefore, hindering another H_2O_2 molecule from entering the active site and reacting with Compound II o form Compound III.

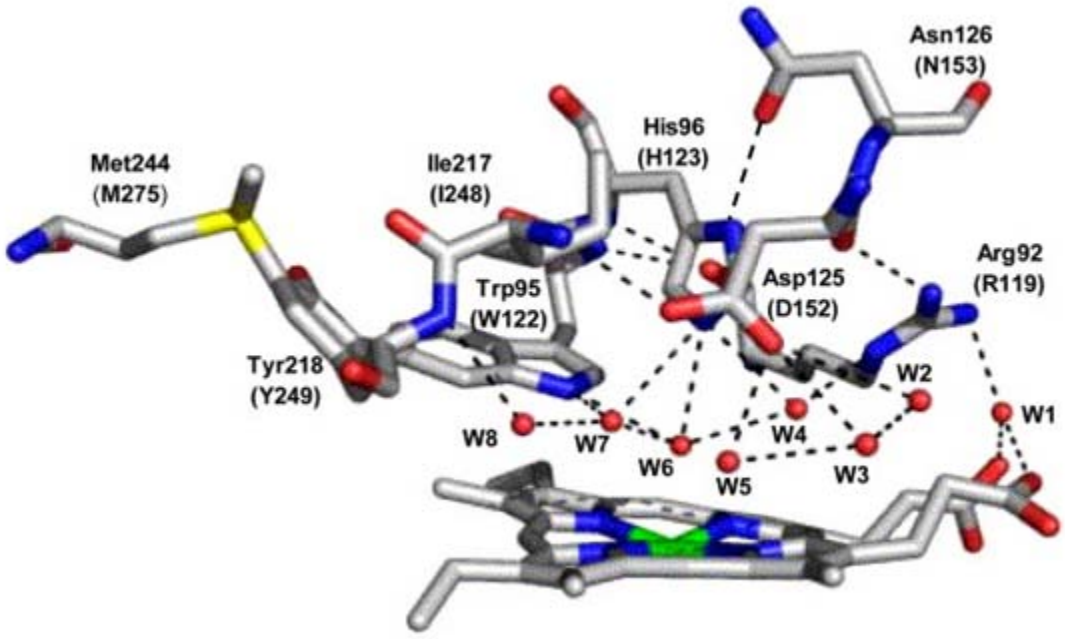

Figure III.2: A KatG figure showing the distal side of the heme and the substrate channel. Trp^{107} in *Mtb* KatG corresponds to Trp^{95} in *Haloarcula* KatG (*Synechocystis* numbering in parentheses) (figure taken from Ref. (*19*).)

Stopped-Flow UV-visible Characterization of Compounds I, II and III in KatG(Y229UAA) – Stopped-flow UV-visible spectroscopic methods were employed to detect the intermediates formed upon the reaction of KatG(Y229UAA) with H_2O_2 or PAA. Values for k_{obs} were determined by fitting exponential functions to the changes in absorbance with respect to time at the Soret band. Compound I was not observed for any of the KatG(Y229UAA) mutants because of its rapid conversion to compound(s) II and/or III. Figure III.3 shows an example of the spectral changes obtained upon the reaction of KatG(Y229Azido) and KatG(Y229Bromo) (8.9 μM) with 10 equivalents of PAA. Table III.5 provides a summary of the spectral features of the intermediates obtained with each of the KatG(Y229UAA) mutants examined here as well as the rates of formation and decay of these intermediates.

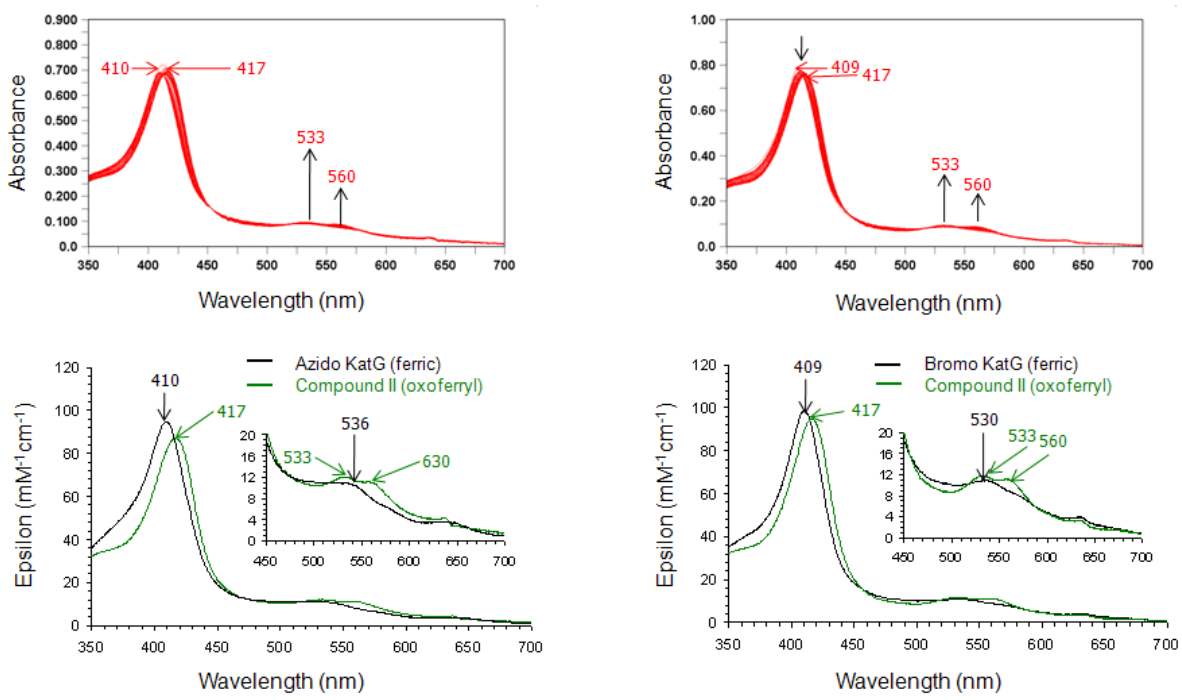

Figure III.3: Stopped-flow spectra of the reaction of azido and bromo KatG with 10 equivalents of PAA

In order to demonstrate the poor catalase activity of KatG(Y229UAA) mutants, Figure III.4 shows the reaction of KatG(Y229Azido) and KatG(Y229Bromo) (10 µM) with 100 equivalents of H_2O_2. At this excess concentration of H_2O_2, Compound III, which is a catalse-inactive intermediate, is observed [UV-visible spectrum: 418 (Soret), ~540, ~580 nm]. The values of k_{obs} for the formation of compounds II and III for the different mutants are listed in Table III.5. The spectrum of the ferric resting enzyme for KatG(Y229Azido) [UV-visible spectrum: 410 (Soret, ε=101 $mM^{-1}cm^{-1}$), 501, 536 (sh) nm] is not observed under the previous conditions (but included in Figure III.2 for comparison) because of the rapid conversion (within mixing time) of that species to oxoferryl compound II [UV-visible spectrum: 417 (Soret), ~530, ~560 nm].

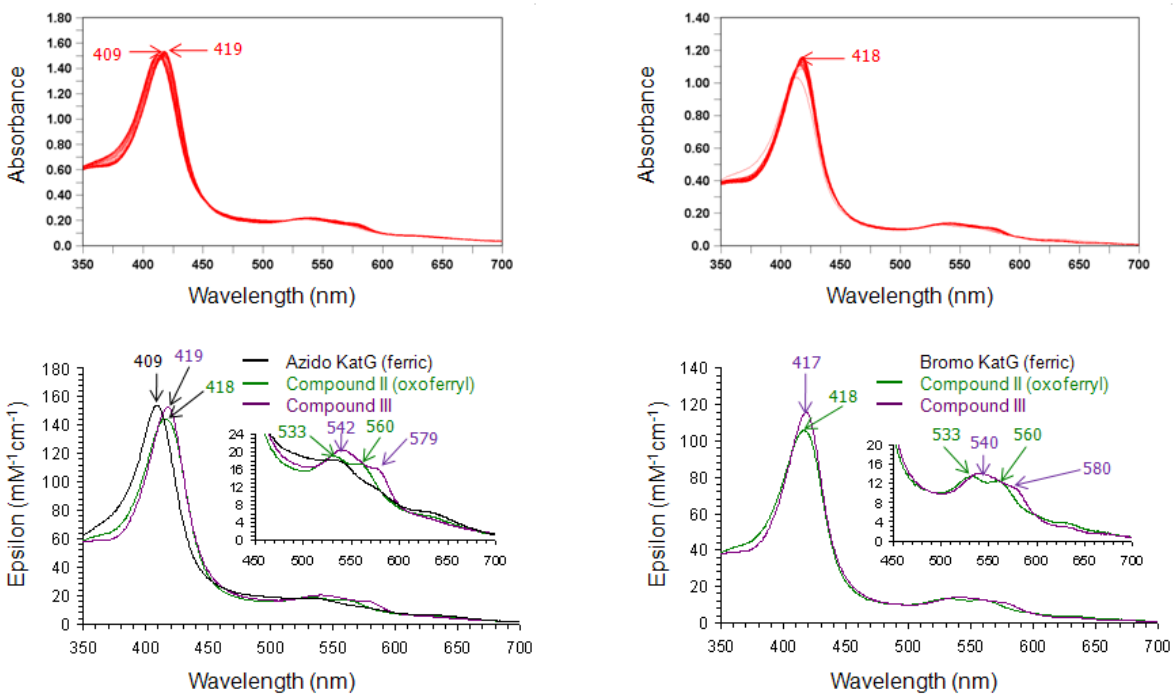

Figure III.4: Stopped-flow spectra of the reaction of azido and bromo KatG with 100 equivalents of H_2O_2

Table III.5: k_{obs} (formation constant) and k_d (decay constant) values of compounds II and III for KatG(Y229UAA) and comparison with KatG(Y229F).

Mutant	λ_{Max} (nm)	k_{obs} (M^{-1} s^{-1})	k_d (M^{-1} s^{-1})
KatG(Y229F)			
Ferric (resting)	408 (Soret), 504, 545 (sh)	$(5.8\pm0.7)\times10^{6}$	
Cmpd II-[(KatG)Fe^{IV}=O]	417 (Soret), 531, 561	$(9.2\pm0.2)\times10^{5}$	
Cmpd III	418 (Soret), 545, 581		
KatG(Y229-p-Br-F)			
Ferric (resting)	409 (Soret), 503, 530 (sh)	$(1.67\pm0.02)\times10^{6}$	$(1.88\pm0.04)\times10^{-2}$
Cmpd II-[(KatG)Fe^{IV}=O]	417 (Soret), 533, 560	$(6.1\pm0.2)\times10^{3}$	$(5.07\pm0.03)\times10^{-2}$
Cmpd III	419 (Soret), 540, 580		
KatG(Y229-p-Ac-F)			
Ferric (resting)	409 (Soret), 502, 543 (sh)	$(2.89\pm0.03)\times10^{6}$	$(2.61\pm0.02)\times10^{-2}$
Cmpd II-[(KatG)Fe^{IV}=O]	419 (Soret), 532, 561	$(2.17\pm0.03)\times10^{3}$	n/a
Cmpd III	419 (Soret), 543, 577		
KatG(Y229-p-I-F)			
Ferric (resting)	409 (Soret), 500, 533 (sh)	$(2.40\pm0.02)\times10^{6}$	n/a
Cmpd II-[(KatG)Fe^{IV}=O]	417 (Soret), 533, 561	$(2.43\pm0.06)\times10^{3}$	n/a
Cmpd III	418 (Soret), 541, 579		
KatG(Y229-p-NH_2-F)			
Ferric (resting)	410 (Soret), 500, 536 (sh)	n/a	$(1.77\pm0.01)\times10^{-1}$
Cmpd II-[(KatG)Fe^{IV}=O]	416 (Soret), 534, 562	$(1.99\pm0.04)\times10^{3}$	
Cmpd III	418 (Soret), 540, 576		
KatG(Y229-p-OMe-F)			
Ferric (resting)	410 (Soret), 500, 536 (sh)	$(2.11\pm0.03)\times10^{6}$	n/a
Cmpd II-[(KatG)Fe^{IV}=O]	416 (Soret), 534, 562	$(1.71\pm0.02)\times10^{3}$	n/a
Cmpd III	418 (Soret), 540, 576		
KatG(Y229-p-N_3-F)			
Ferric (resting)	410 (Soret), 501, 536 (sh)	$(5.88\pm0.12)\times10^{6}$	$(8.19\pm0.07)\times10^{-2}$
Cmpd II-[(KatG)Fe^{IV}=O]	417 (Soret), 533, 560	$(8.9\pm0.2)\times10^{3}$	$(1.37\pm0.03)\times10^{-2}$
Cmpd III	418 (Soret), 542, 579		

Conclusion

Tyr^{229} is one of the three residues (besides Trp^{107} and Met^{255}) that is involved in a unique crosslink that has been shown to impart catalase activity to KatGs. Although several KatG(Y229X) mutants lacking the Met-Tyr-Trp crosslink have been expressed and found to have enhanced peroxidase activity relative to WT KatG (*18*), the work described herein demonstrates the first example of enhanced enzymatic activity obtained via the use of unnatural amino acids. As can be seen from Table III.4, the extent of enhanced peroxidase activity depends on the structure of the unnatural amino acid with KatG(Y229Azido) displaying the most enhanced activity (~300 fold relative to WT KatG). Further studies will be performed in order to establish a relationship between the structure of the unnatural amino acid and its effect on the peroxidase activity of KatG.

REFERENCES

1. Xie, J., and Schultz, P. G. (2006) Innovation: A Chemical Toolkit for Proteins - An Expanded Genetic Code, *Nature Reviews Molecular Cell Biology 7*, 775-782.

2. Young, T. S., Ahmad, I., Yin, J. A., and Schultz, P. G. (2010) An Enhanced System For Unnatural Amino Acid Mutagenesis in *E. coli*, *Journal of Molecular Biology 395*, 361-374.

3. Chen, P. R., Groff, D., Guo, J. T., Ou, W. J., Cellitti, S., Geierstanger, B. H., and Schultz, P. G. (2009) A Facile System for Encoding Unnatural Amino Acids in Mammalian Cells, *Angewandte Chemie-International Edition 48*, 4052-4055.

4. Wang, L., Magliery, T. J., Liu, D. R., and Schultz, P. G. (2000) A New Functional Suppressor tRNA/Aminoacyl-tRNA Synthetase Pair for the in vivo Incorporation of Unnatural Amino Acids into Proteins, *Journal of the American Chemical Society 122*, 5010-5011.

5. Wang, L., Zhang, Z. W., Brock, A., and Schultz, P. G. (2003) Addition of the Keto Functional Group to the Genetic Code of *Escherichia coli*, *Proceedings of the National Academy of Sciences of the United States of America 100*, 56-61.

6. Tsao, M. L., Tian, F., and Schultz, P. G. (2005) Selective Staudinger Modification of Proteins Containing p-Azidophenylalanine, *Chembiochem 6*, 2147-2149.

7. Wu, N., Deiters, A., Cropp, T. A., King, D., and Schultz, P. G. (2004) A Genetically Encoded Photocaged Amino Acid, *Journal of the American Chemical Society 126*, 14306-14307.

8. Deiters, A., Groff, D., Ryu, Y. H., Xie, J. M., and Schultz, P. G. (2006) A Genetically Encoded Photocaged Tyrosine, *Angewandte Chemie-International Edition 45*, 2728-2731.

9. Jones, D. H., Cellitti, S. E., Hao, X. S., Zhang, Q., Jahnz, M., Summerer, D., Schultz, P. G., Uno, T., and Geierstanger, B. H. (2010) Site-Specific Labeling of Proteins with NMR-Active Unnatural Amino Acids, *Journal of Biomolecular Nmr 46*, 89-100.

10. Cellitti, S. E., Jones, D. H., Lagpacan, L., Hao, X. S., Zhang, Q., Hu, H. Y., Brittain, S. M., Brinker, A., Caldwell, J., Bursulaya, B., Spraggon, G., Brock, A., Ryu, Y., Uno, T., Schultz, P. G., and Geierstanger, B. H. (2008) In vivo Incorporation of Unnatural Amino Acids to Probe Structure, Dynamics, and Ligand Binding in a Large Protein by Nuclear Magnetic Resonance Spectroscopy, *Journal of the American Chemical Society 130*, 9268-9281.

11. Alfonta, L., Zhang, Z. W., Uryu, S., Loo, J. A., and Schultz, P. G. (2003) Site-Specific Incorporation of a Redox-Active Amino Acid into Proteins, *Journal of the American Chemical Society 125*, 14662-14663.

12. Seyedsayamdost, M. R., Xie, J., Chan, C. T. Y., Schultz, P. G., and Stubbe, J. (2007) Site-Specific Insertion of 3-Aminotyrosine Into Subunit Alpha 2 of *E-coli* Ribonucleotide Reductase: Direct Evidence for Involvement of Y-730 and Y-731 in Radical Propagation, *Journal of the American Chemical Society 129*, 15060-15071.

13. Wang, F., Robbins, S., Guo, J., Shen, W., and Schultz, P. G. (2010) Genetic Incorporation of Unnatural Amino Acids into Proteins in *Mycobacterium tuberculosis*, *Plos One 5*.

14. Ghiladi, R. A., Medzihradszky, K. F., Rusnak, F. M., and de Montellano, P. R. (2005) Correlation between Isoniazid Resistance and Superoxide Reactivity in *Mycobacterium tuberculosis* Katg, *Journal of the American Chemical Society 127*, 13428-13442.

15. Ghiladi, R. A., Medzihradszky, K. F., and de Montellano, P. R. O. (2005) Role of the Met-Tyr-Trp Cross-Link in *Mycobacterium tuberculosis* Catalase-Peroxidase (KatG) as Revealed by KatG(M255I), *Biochemistry 44*, 15093-15105.

16. Ghiladi, R. A., Knudsen, G. M., Medzihradszky, K. F., and de Montellano, P. R. O. (2005) The Met-Tyr-Trp Cross-Link in *Mycobacterium tuberculosis* Catalase-Peroxidase (Katg) - Autocatalytic Formation and Effect on Enzyme Catalysis and Spectroscopic Properties, *Journal of Biological Chemistry 280*, 22651-22663.

17. Chouchane, S., Girotto, S., Kapetanaki, S., Schelvis, J. P. M., Yu, S. W., and Magliozzo, R. S. (2003) Analysis of Heme Structural Heterogeneity in *Mycobacterium tuberculosis* Catalase-Peroxidase (KatG), *Journal of Biological Chemistry 278*, 8154-8162.

18. Yu, S. W., Girotto, S., Zhao, X. B., and Magliozzo, R. S. (2003) Rapid Formation of Compound II and a Tyrosyl Radical in the Y229F Mutant of *Mycobacterium tuberculosis* Catalase-Peroxidase Disrupts Catalase but not Peroxidase Function, *Journal of Biological Chemistry 278*, 44121-44127.

19. Smulevich, G., Jakopitsch, C., Droghetti, E., and Obinger, C. (2006) Probing the Structure and Bifunctionality of Catalase-Peroxidase (KatG), *Journal of Inorganic Biochemistry 100*, 568-585.

CHAPTER IV

Characterization of Dehaloperoxidase Compound ES and its Reactivity with Trihalophenols

Jeremiah Feducia, Rania Dumarieh, Lauren B. G. Gilvey, Tatyana Smirnova, Stefan Franzen, Reza A. Ghiladi

Abstract

Dehaloperoxidase (DHP), the oxygen-transport hemoglobin from the terebellid polychaete *Amphitrite ornata*, is the first globin identified to possess a biologically relevant peroxidase activity. DHP has been shown to oxidize trihalophenols to dihaloquinones in a dehalogenation reaction that uses hydrogen peroxide as a substrate. Herein, we demonstrate that the first detectable intermediate following the addition of hydrogen peroxide to ferric DHP contains both a ferryl heme and a tyrosyl radical, analogous to compound ES of cytochrome *c* peroxidase. Furthermore, we provide a detailed kinetic description for the reaction of pre-formed DHP Compound ES with the substrate 2,4,6-trichlorophenol, and demonstrate the catalytic competency of this intermediate in generating the product 2,4-dichloroquinone. Furthermore, using rapid-freeze-quench electron paramagnetic resonance spectroscopy we detected a signal at $g \approx 2.0058$ confirming the presence of a protein radical in DHP Compound ES and suggesting that this intermediate is analogous to the two-electron oxidized Compound ES of cytochrome c peroxidase. In the absence of substrate, DHP Compound ES evolves to a new species, Compound RH, which is functionally unique to dehaloperoxidase. We propose that this intermediate plays a protective role against heme bleaching. While unreactive toward further oxidation, Compound RH can be reduced and subsequently bind dioxygen, generating oxyferrous DHP, which may represent the catalytic link between peroxidase and oxygen-transport activities in this bifunctional protein.

IV.1. Introduction

As mentioned in Chapter 1, studies of DHP are of great interest as it is the first protein that acts as a hemoglobin and a peroxidase at the same time. What is more interesting is that DHP shares little sequence homology with hemoglobins but has the same three-dimensional fold. Although DHP shares neither sequence nor structural homology with any known peroxidase, it is only one order of magnitude slower than horseradish peroxidase in the dehalogenation of trihalophenol substrates and 1-2 orders of magnitude faster than hemoglobin. Therefore, an important question posed in the study by Feducia et al. (*1*) is whether DHP follows the same general peroxidase mechanism outlined in Chapter 1.

The conversion of trihalophenols to dihaloquinones by DHP in the presence of H_2O_2 is a two-electron oxidative dehalogenation process. However, the DHP intermediate identified to date is Compound II, which is a one-electron oxidized intermediate at the heme center. Thus it was important to employ advanced techniques such as stopped-flow UV-visible and RFQ EPR spectroscopies to look more carefully into the type of intermediates formed during the DHP catalytic cycle. There are several possible pathways through which a two-electron oxidation may occur. One possibility is that Compound II oxidizes a trihalophenol molecule to a trihalophenoxy radical. Then in another one-electron oxidation step, another Compound II molecule reacts with the trihalophenoxy radical yielding ferric DHP and a trihalocyclohexadienone cation, which then reacts with water to form the product (see Figure IV.1). This was a mechanism proposed by Osborne et al. (*2*) to explain the observation of a dimerized product upon the reaction of 4-chlorophenol with Mb in the presence of H_2O_2 and the requirement of two equivalents of Mb Compound II to convert one equivalent of TCP to DCQ.

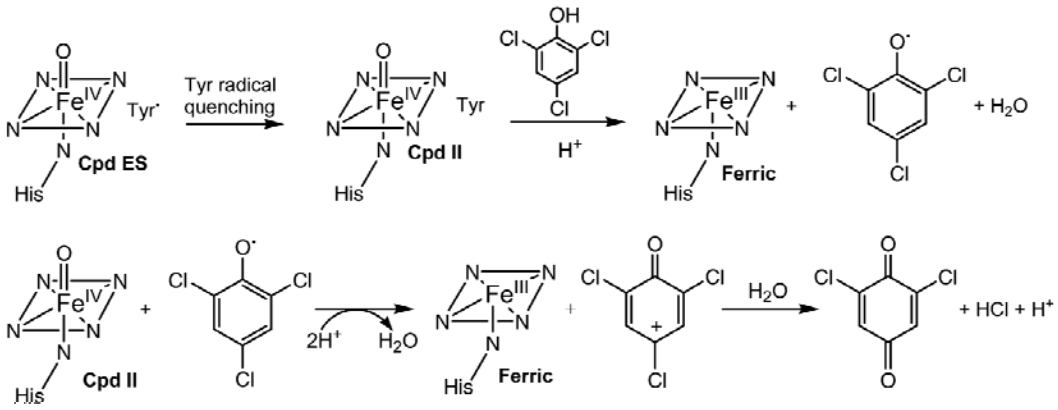

Figure IV.1: Proposed mechanism for the dehalogenation of trihalophenols by Mb (taken from Ref. (*2*))

Another possibility is that after the one-electron oxidation of trihalophenol to trihalophenoxy radical, the phenoxy radical disproportionates with another radical molecule to form trihalophenol and dihaloquinone. Ascorbate peroxidase follows a similar mechanism during the oxidation of ascorbate. After the formation of the one-electron oxidized intermediate (monohydroascorbate), it disproportionates to form ascorbate and dehydroascorbate. Finally, DHP could follow a mechanism similar to that of CcP where Compound ES, a two-electron oxidized intermediate, is responsible for the two-electron oxidation of trihalophenols. One of the advantages of this proposed mechanism is avoiding the formation of harmful radicals (since phenoxy radicals can bind to DNA (*3*)) either through a single two-electron oxidation step or sequential one-electron steps without the transient phenoxy radical dissociating from the enzyme.

In order to explore mechanistic hypotheses, we have undertaken a comprehensive UV-visible and electron paramagnetic spectroscopic study of the DHP intermediate formed from the reaction of the ferric enzyme with hydrogen peroxide under a variety of conditions using both stopped-flow and rapid-freeze-quench methods, and have determined this intermediate to be DHP Compound ES. We have further explored the stability of this Compound ES, and demonstrated the existence of a competitive pathway between product formation and decay to a novel species, termed Compound RH, which possesses attenuated levels of dehaloperoxidase activity. Our experimental design reveals mechanistic insights

and kinetic descriptions of the intermediates in DHP, which have not been previously reported. We propose an updated catalytic cycle which provides a clearer understanding of the link between peroxidase and oxygen transport activities unique to this bifunctional enzyme.

It is important to note here that my contribution to this work was the collection of the RFQ samples and obtaining the EPR spectra of DHP Compound ES at pH 5 and 7. However, the EPR results I obtained are discussed along with the stopped-flow spectroscopy studies that Dr. Feducia performed because they go hand-in-hand to elucidate the mechanism of DHP.

IV.2. Materials and Methods

Please refer to Ref. (*1*) for a description of how the DHP, TCP, and H_2O_2 samples were prepared. Ref. (*1*) also describes how the enzyme assays and the stopped-flow UV-visible spectrophotometric studies were performed.

Preparation of Reaction Intermediates by Freeze-Quench Methods. Rapid freeze-quench experiments were performed with a BioLogic SFM 400 Freeze-Quench apparatus by mixing a 50 μM enzyme solution (final concentration) with a 10-fold excess of H_2O_2 solution in 100 mM potassium phosphate buffer (pH 5 and 7) at 25 °C. Reaction times were as follows: pH 5 – 100, 400 ms, 3.6, 36, 60 s; pH 7 – 100, 500, 800 ms, 2, 12, 60 s. A standard 4 mm O.D. quartz EPR tube was connected to a Teflon funnel, and both the tube and the funnel were completely immersed in an isopentane bath at -110 °C. The reaction mixtures were quenched by spraying them into the cold isopentane, and the frozen material so obtained was packed at the bottom of the quartz tube using a packing rod equipped with a Teflon plunger. Samples were then transferred to a liquid nitrogen storage dewar until analyzed.

X-band EPR Spectroscopy. EPR spectra were recorded with an X-band (9 GHz) Varian E-9 EPR spectrometer (Varian, El Palo, CA). A standard 3 by 4 mm quartz EPR tube was filled with a sample and placed into a quartz finger dewar insert filled with liquid nitrogen. The temperature of the samples was maintained at 77 K for the duration of the data

acquisition, which required periodic refilling of the dewar due to the evaporation of the liquid nitrogen during longer acquisition runs. The typical spectrometer settings were as follows: field sweep 200 G, scan rate 3.33 Gauss/s, modulation frequency 100 KHz, modulation amplitude 4.0 G, and microwave power 2 mW. The exact resonant frequency of each EPR experiment was measured by an EIP-578 (PhaseMatrix, San Jose, CA) in-line microwave frequency counter and is indicated in the figure captions. Typically, 20 to 200 individual scans were averaged to achieve sufficient signal-to-noise for the spectra obtained at short-quench and long-quench times, respectively.

IV.3. Results

Stopped-flow UV-Visible Characterization of Compound ES in DHP (performed by Dr. Feducia). Single mixing stopped-flow UV-visible spectroscopic methods were employed to detect DHP Compound ES. At pH 7, upon rapid mixing (2 ms) of a solution of ferric DHP [UV-visible spectrum: 407 (Soret), 504, 538, 635 nm] with H_2O_2, a transient species was observed (Figure IV.2, Table IV.1) whose spectral features [UV-visible: 420 (Soret), 545, 585 nm] we ascribe to a ferryl-containing DHP intermediate based upon previous characterization (*4-6*) and comparison to other known Fe(IV)-oxo containing hemoproteins (*7, 8*). As the ferryl intermediate of Compound ES is likely indistinguishable from that of Compound II by UV-visible spectroscopy, we assign this intermediate here as DHP Compound ES here based upon these results and those of our EPR spectroscopic study (*vide infra*). Values of k_{obs} for formation of this new species were linearly dependent on [H_2O_2] (2.5 – 10 fold excess per heme), giving a bimolecular rate constant of (3.56 ± 0.02) x 10^4 $M^{-1}s^{-1}$. Under these conditions, and in the absence of substrate, DHP Compound ES decays to a stable species [UV-visible: 411 (Soret), 530, 564 nm; k_{obs} = 0.0167 ± 0.0003 s^{-1}], which we have termed Compound RH.

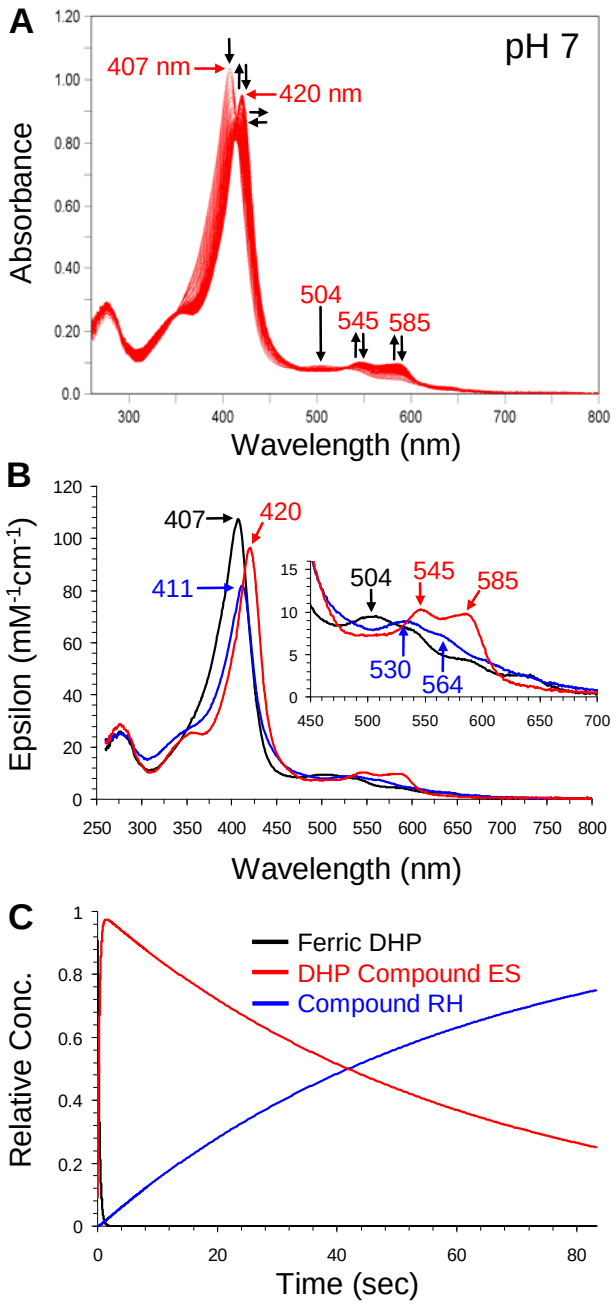

Figure IV.2: (A) Stopped-flow UV-visible spectroscopic monitoring of the reaction (900 scans, 85 sec) between DHP (10 µM) and a 10-fold excess of H_2O_2 at pH 7.0 (performed by Dr. Feducia). See experimental for details. (B) Calculated UV-visible spectra for both resting (black), Compound ES (red), and Compound RH (blue) DHP are shown; the rapid-scanning data from A were compiled and fitted to a double exponential reaction model using the Specfit global analysis program. (C) Relative concentration profile determined from the three component fit used in (B).

Table IV.1: UV-Visible Spectroscopic Data and Kinetic Parameters for the Oxidized Intermediates of DHP.

	pH 7		pH 5	
	λ_{max} (nm)	k_{obs} ($M^{-1}s^{-1}$) [a]	λ_{max} (nm)	k_{obs} ($M^{-1}s^{-1}$) [a]
WT DHP				
Ferric	407, 504, 538, 635	n/a	405, 504, 538, 636	n/a
Compound ES	420, 545, 585	$(3.56 \pm 0.02) \times 10^4$	419, 545, 585	$(2.78 \pm 0.01) \times 10^4$
Compound RH	411, 530, 564	0.0167 ± 0.0003 s^{-1}	410, 530, 590	0.0701 ± 0.0001 s^{-1}
Compound III	417, 542, 578	n.d.	417, 542, 578	n.d.

[a] $M^{-1}s^{-1}$ unless otherwise indicated; n/a = not applicable; n.d. = not determined

Similar reactivity is observed at pH 5: ferric DHP [UV-visible spectrum: 405 (Soret), 504, 538, 636 nm] is converted to Compound ES [UV-visible: 419 (Soret), 545, 585 nm; k_{obs} = $(2.78 \pm 0.01) \times 10^4$ $M^{-1}s^{-1}$], which further decays to Compound RH [UV-visible: 410 (Soret), 530, 590 nm; $k_{obs} = 0.0701 \pm 0.0001$ s^{-1}] (Figure S1). Hence, the rate of Compound RH formation is ~4 times greater at pH 5 than at pH 7.

Reaction of Pre-Formed Compound ES with TCP Substrate (performed by Dr. Feducia, see Ref. (1) for figures and more details). Double-mixing stopped-flow UV-visible studies were performed to explore the reactivity of Compound ES with TCP. After mixing 10 μM of ferric DHP with 10 equivalents of H_2O_2 and allowing for maximum formation of Compound ES (1.5 s incubation time at pH 7, and 0.9 s incubation time at pH 5), preformed Compound ES was mixed with 30 equivalents of TCP. The amount of product (DCQ) formed at pH 7 is similar to that formed at pH 5.

However, when the incubation time of DHP with H_2O_2 was extended to allow maximum formation of Compound RH which was then mixed with TCP, no substrate loss (at 311 nm) or product formation (at 275 nm) was observed. This result indicates that Compound RH has much less reactivity than ferric DHP or DHP Compound ES.

In-Situ Compound ES Formation in the Presence of TCP (performed by Dr. Feducia, see Ref. (1) for figures and more details). In contrast to the above experiments in which pre-formed Compound ES was reacted with TCP, double-mixing stopped-flow UV-visible spectroscopic methods was employed to examine if pre-incubation of ferric DHP with TCP, followed by the addition of a 10-fold excess of H_2O_2, led to the formation of DCQ product (275 nm) via a transiently formed Compound ES intermediate. Under these conditions, the

yield of DCQ product was nearly identical with that found for the reaction of fully pre-formed Compound ES with TCP (vide supra), at both pH 7 or pH 5.

Also, a pH-dependent difference with respect to the heme species observed was noted. At pH 7.0, Compound ES was distinctly formed upon the reaction of DHP (preincubated with TCP) with H_2O_2. Under these conditions, the rate of Compound ES formation was identical to that observed when ferric DHP is mixed with H_2O_2 in the absence of TCP. However, at pH 5.0, there was no distinct formation of Compound ES upon the reaction of DHP (preincubated with TCP) with H_2O_2.

Characterization of Protein Radicals in DHP Compound ES. Rapid-freeze-quench methods were employed to stabilize intermediates of the reaction between DHP (50 μM final) and a 10-fold excess of hydrogen peroxide at both pH 7 and pH 5 for consequent characterization by continuous wave (CW) EPR. X-band CW EPR spectra of DHP samples obtained at pH 7.0 with various quench times are shown in Figure IV.3. The shapes of all the EPR spectra measured from the samples collected at quenching times 500, 800 ms and 2 s were found to be identical with the only difference in the signal intensities. Maximal concentration of the radical is observed over the period of Compound ES formation (Figure IV.2c). The position of the signal is characterized by an average *g*-factor of 2.0058. The shape of the signal is best described by an anisotropic quintet. Based on the signal *g*-factor and a partially resolved hyperfine structure with a peak-to peak linewidth of about 21 G, this EPR signal was assigned to a tyrosyl radical (*9*). Samples with longer incubation times of 12 and 60 s have similar average *g*-factor, $g \approx 2.005$, and the same peak-to-peak linewidth of 21 G, however, do not show resolved hyperfine structure and have much lower intensity (concomitant with the loss of the ferryl UV-visible spectrum in our component analysis, Figure IV.2c).

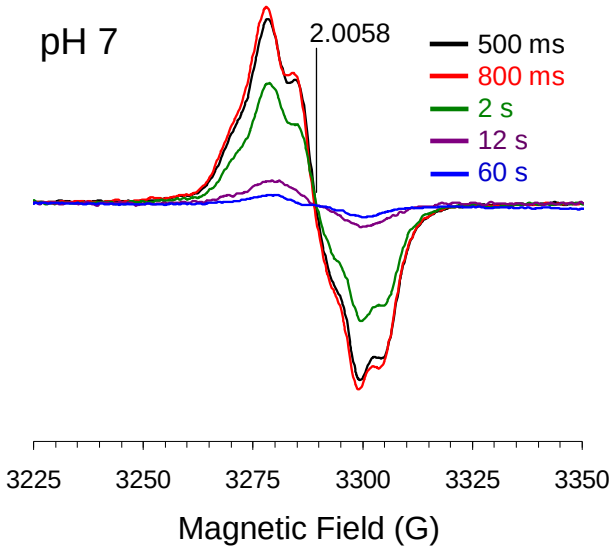

Figure IV.3: EPR spectra of the radical(s) in DHP Compound ES at pH 7. Rapid freeze-quench samples were prepared from the reaction of DHP (50 μM final) with a 10-fold excess of H_2O_2 at 25 °C, and rapidly frozen in an isopentane slurry. Spectra were obtained at 77 K using the spectrometer settings described in the experimental section. The resonant frequency of the experiments is 9.2330 GHz.

The EPR spectrum of Compound ES was similarly recorded at various quench times at pH 5 (Figure IV.4). The spectrum is centered at g = 2.0058 and shows a partially resolved hyperfine splitting described as an "anisotropic septet" (*10*). A very weak shoulder is observed at g = 2.035 (Figure S2) that could be an indication of the formation of a peroxyl radical since the samples were prepared under aerobic conditions (*11*), but the signal intensity is too low to warrant further speculation on its origin. At longer quench times when the component analysis indicates little to no remaining Compound ES by UV-visible spectroscopy (Figure S1c), the line shape of the EPR signal is drastically different, its signal intensity has dropped considerably, and the hyperfine splitting features are lost. Specifically, the signal has a very broad spectral feature in the $g \approx 2.04$ region and sharper features at g = 2.0085 and g = 1.995.

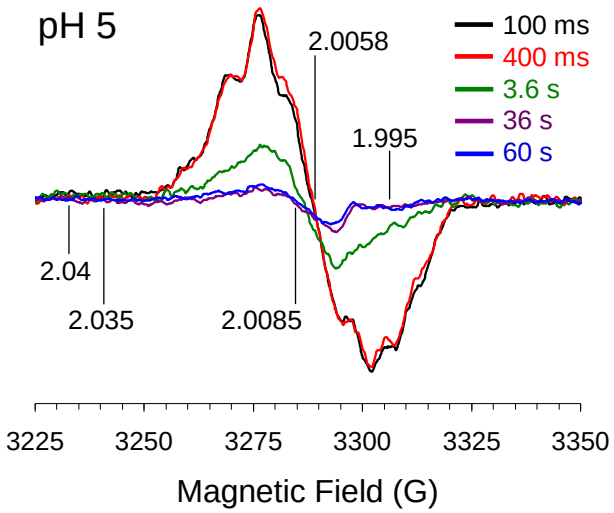

Figure IV.4: EPR spectra of the radical(s) in DHP Compound ES at pH 5. Rapid freeze-quench samples were prepared from the reaction of DHP (50 μM final) with a 10-fold excess of H_2O_2 at 25 °C, and rapidly frozen in an isopentane slurry. Spectra were obtained at 77 K using the parameters described in the experimental section.

Unfortunately, the low *g*-factor spectral resolution of these CW X-band experiments does not permit unambiguous identification of the radical species based on magnetic parameters alone. This ambiguity could be resolved by high-field (95 GHz) EPR experiments coupled with mutagenesis studies that are planned for the near future.

Formation and Reactivity of Compound RH (performed by Dr. Feducia, see Ref. (1) for more details). As described above, in the absence of reducing substrate, a new, unique species of DHP, termed Compound RH to denote that is a reversible heme intermediate, is formed upon the decay of Compound ES. In order to test the reactivity of the Compound RH species, single-mixing stopped-flow UV-visible spectroscopy was used to monitor the reaction between Compound RH (10 μM) and either a 10- or 100-fold excess of H_2O_2. In both cases, no reaction was observed (both pH 5 and 7 were investigated; data not shown). In spite of its inability to form high-valent iron-oxo intermediates, Compound RH still possesses attenuated levels of dehaloperoxidase activity, exhibiting a 6-fold lower reactivity with TCP as substrate when compared to ferric DHP.

While Compound RH displays a lack of reactivity with H_2O_2 by stopped-flow UV-visible spectroscopy, it is readily reduced with sodium dithionite at either pH 5 or 7 to yield ferrous (deoxy) DHP [UV-visible: 432 (Soret), 557, 626 nm], which upon exposure to dioxygen led to formation of oxyferrous DHP [UV-visible: 417 (Soret), 542, 578 nm]. Further oxidation with potassium ferricyanide, followed by desalting, allowed for the re-isolation of ferric DHP [UV-visible: 407 (Soret), 504, 538, 635 nm]. The activity of this 'regenerated'-ferric DHP was found to be nearly identical to that of as-isolated ferric DHP for TCP oxidation, suggesting that a pathway through Compound RH does not have any deleterious effect on dehaloperoxidase activity.

IV.4. Discussion

The conversion of trihalophenols to dihaloquinones is a two-electron oxidation. However, the intermediate that has been characterized to-date when ferric DHP reacts with H_2O_2 is Compound II, which is a one-electron oxidized heme center. Therefore, further characterization of the intermediates formed in the catalytic cycle of DHP is required. This paper provides evidence that the reactive species in DHP is Compound ES, which is a two-electron oxidized intermediate similar to that found CcP.

Stopped-flow UV-visible spectroscopy was used to characterize the intermediates formed upon the reaction of DHP with H_2O_2 at pH 5 and pH 7. The first detectable intermediate formed had spectral features that are clearly representative of a ferryl-containing species (Compound II or Compound ES). While Compound I was not detected, it could still be formed but reduced rapidly to Compound ES (vide infra). In the absence of substrate (TCP), Compound ES decays to the stable intermediate Compound RH (RH=Reversible Heme). However, in the presence of TCP, Compound ES is reduced back to the resting state (ferric DHP). Because preformed Compound ES (upon the reaction with TCP) produces the same amount of DCQ as *in situ* Compound ES does and at the same rate, it was concluded that Compound ES is the active oxidant of TCP.

Stopped-flow UV-visible and rapid-freeze-quench EPR spectroscopic methods were employed to characterize the high-valent iron(IV)-oxo and protein radical species,

respectively. After mixing ferric DHP with H_2O_2, the first resulting intermediate has a spectrum characteristic of a ferryl heme center. Since Compound I is not observed after DHP is reacted with H_2O_2, then there must be an endogenous reducing agent that rapidly reduces the porphyrin π-cation radical in Compound I. The crystal structure of DHP does not show any cofactors or other metals. Therefore, we used RFQ-CW-EPR to see whether we can detect any signals originating from amino acid residues. Indeed, at pH 5 and pH 7, we detected the signal of protein radical whose formation and decay profiles (detected by EPR) follow those of compound ES (detected by stopped-flow UV-visible spectroscopy). This paper provides the first evidence that Compound ES, which contains two oxidizing equivalents: one at the heme center and the other on an amino acid residue, is the reactive intermediate in DHP.

Analysis of the signal *g*-factor and the partially resolved hyperfine structure present in our EPR data, with a peak-to peak linewidth of about 21 G, suggests that the radical in DHP Compound ES likely resides on a tyrosine residue initially (*9*). The longer incubation times of 12 and 60 s exhibit a similar average *g*-factor, $g \approx 2.005$, and the same peak-to-peak linewidth of 21 G; however, they do not show resolved hyperfine structure and have much lower intensity (concomitant with the loss of the ferryl UV-visible spectrum in our component analysis, Figure IV.2c). Thus, it is difficult to comment extensively on the origin of these signals observed at later times, especially at pH 5. These spectra could be attributed to a different Tyr-based radical than the one initially observed, or the signal could also be a mixture of Tyr and Trp based radicals (*12*). Another option to consider is a radical originating from a cysteine residue, which is usually characterized by large *g*-factor anisotropy that would be resolved in the X-band spectra (*13*-*15*). Although Cys-based radicals have been accepted as intermediates in metalloprotein cycles, they are not commonly observed by freeze-quench EPR spectroscopy. However, Cys-based radicals should not be completely ruled out as intermediates at the quenching times of 12 and 60 sec as they have been identified as forming in human Mb under similar conditions (*16*).

Of the five tyrosine residues which DHP possesses (Figure IV.5: Tyr^{16}, Tyr^{28}, Tyr^{34}, Tyr^{38}, Tyr^{107}), only two are reasonably close to the heme prosthetic group to be considered

likely candidates for reducing Compound I initially, Tyr^{34} and Tyr^{38}; the closest contact between Tyr^{34} and the heme edge is 5.56 Å (Tyr Cγ), whereas Tyr^{38} is 7.54 Å (phenolic oxygen). The remaining three tyrosine residues are greater than 10 Å (Tyr^{28}) or 15 Å (Tyr^{16} and Tyr^{107}) from the heme edge. Furthermore, the closest heme edge to Trp^{120} (10.53 Å) and Cys^{73} (16.29 Å) contacts are similarly distant, making them unlikely candidates as the residues responsible for the initial reduction of the transiently formed Compound I intermediate. Thus, based on both the available structural studies of DHP, and our present spectroscopic analysis, we suggest that the initial site of radical formation in DHP Compound ES is either Tyr^{34} or Tyr^{38}.

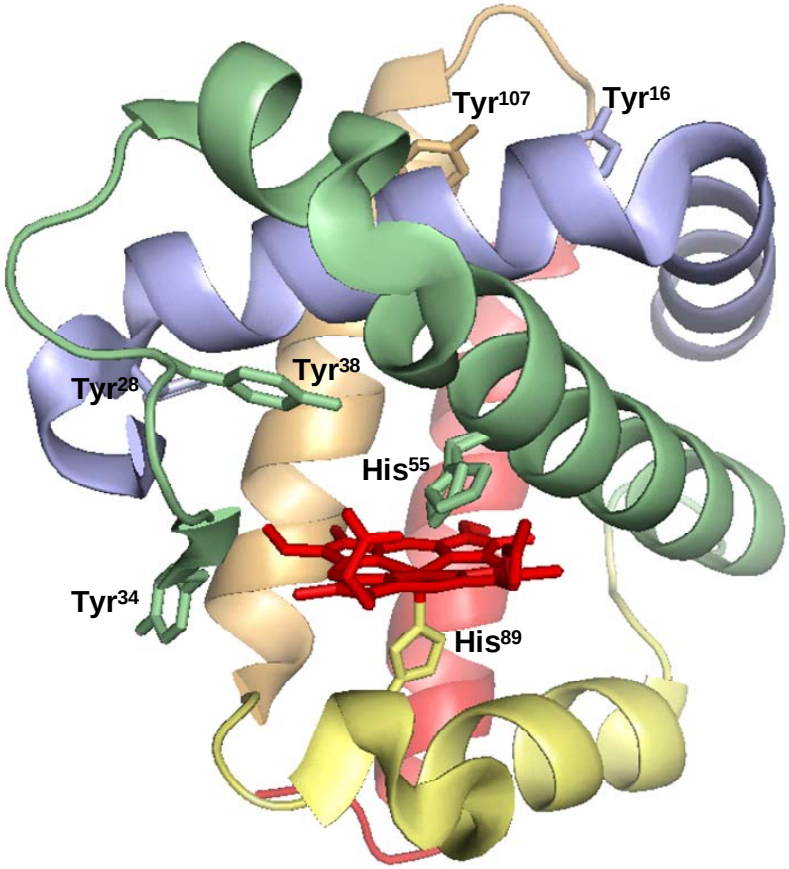

Figure IV.5: Figure of DHP displaying the location of tyrosines relative to the active site

While the definitive identification of the specific residue that gives rise to the initial protein radical in DHP Compound ES will be the subject of future high-field EPR investigations coupled with mutagenesis studies, the time-dependent changes observed in the protein radical signal, especially at pH 5, suggest either a change in the local electronic structure of the radical, or a migration of the radical out of the active site to other redox active protein side-chains upon decay of Compound ES. Radical migration in proteins has been observed before. For example, the reaction of sperm whale Mb with hydrogen peroxide yields covalent dimers that arise from the coupling of surface tyrosyl radicals (Tyr^{151}), which results from a radical migration out of the Mb active site (*17*). Similarly, it has been demonstrated that human Mb also forms a covalent dimer (*18*), but through surface cysteines (Cys^{110}) forming a disulfide link, consistent with our putative radical observed at long quench times at pH 5. DHP may possess a similar radical migration pathway, with surface radicals leading to the oxidation of TCP that binds to DHP through a hypothesized external binding pocket. This would not be unlike CcP, whose initial Trp^{191} radical in Compound ES leads to a radical migration which is ultimately responsible for oxidizing substrate (cytochrome c) at the surface of the peroxidase (protein-protein interface) (*19*). Thus, as CcP may have evolved from traditional (heme-edge electron transfer) peroxidases an external binding interface for oxidizing cytochrome c, DHP may also similarly have evolved from Mb an external binding pocket for oxidizing trihalophenols. In accord with this hypothesis, tyrosine has been proposed to play a role in the peroxidase mechanism of Mb (*19*). This hypothesis will be particularly interesting if our supposition is that Tyr^{34} is the site of the radical in DHP Compound ES, as this residue is located at the surface of DHP, yet is also within close proximity to the heme (Figure IV.5), and thus could serve as a redox conduit between the hypothesized external binding pocket and the active site.

In the absence of substrate, Compound ES decays to the stable intermediate Compound RH, which is unreactive toward H_2O_2. While peroxidase inactivation in HRP and CcP is known to occur via heme bleaching, Compound RH can be reduced under mild conditions to ferrous DHP, which can then form oxyferrous DHP upon being exposed to oxygen. Compound RH is not observed in peroxidases or O_2-transport globins, such as

hemoglobin and myoglobin (*17, 20-23*). Therefore, Compound RH is unique to DHP perhaps due to its bifunctionality: the inactive dehaloperoxidase can be converted to an active oxygen transport protein via a reduction pathway that is specific for globins, not peroxidases. Inactivation of DHP is important in the absence of trihalophenol substrate to avoid non-specific oxidation of other metabolites. However, inactivation via heme bleaching (as is the case in peroxidases) could be costly for DHP, which also functions as the hemoglobin in *A. ornata*.

Based upon the results obtained from these stopped-flow UV-visible and RFQ-EPR spectroscopic experiments, and through modification of previously established mechanisms for the general function of peroxidases, we propose the following catalytic cycle for the *in vitro* peroxide-dependent oxidation of ferric DHP from *A. ornata* in the presence and absence of trihalphenol (Scheme IV.1). Ferric DHP reacts with one equivalent of H_2O_2, transiently forming Compound I (step i), which then undergoes rapid endogenous electron transfer to generate the observed Compound ES intermediate and protein radical (step ii). A bifurcation in the mechanism occurs which is dependent upon substrate: in the presence of trihalophenol, DHP Compound ES is reduced by two electrons, thereby regenerating the ferric state of the enzyme, and forming the dihaloquinone product (step iii-a). In the absence of substrate, however, Compound RH is formed (iii-b) by an as-yet understood process, and can subsequently be reduced to the ferrous enzyme (iv) and bind dioxygen to form the oxyferrous intermediate (v). Autoxidation of oxyferrous DHP leads to the formation of the ferric enzyme (vi). The existence, and by extension identity, of a possible sixth ligand in Compound RH is unknown at this time, and this ambiguity is represented by the bound X in Scheme IV.1. We tentatively assign the oxidation state of Compound RH as a ferric heme based upon the evidence that: i) Compound RH exhibits a 'ferric-like' heme spectrum that neither matches the ferryl nor ferrous spectra of DHP (Table 1), ii) Compound RH forms from the decay of an iron(IV)-oxo species, which for most heme proteins yields a ferric enzyme, and iii) the fact that Compound RH can be reduced to the ferrous enzyme, implying that it is not a ferrous heme to begin with. Further studies will be necessary to definitively assign the oxidation state of the heme in Compound RH.

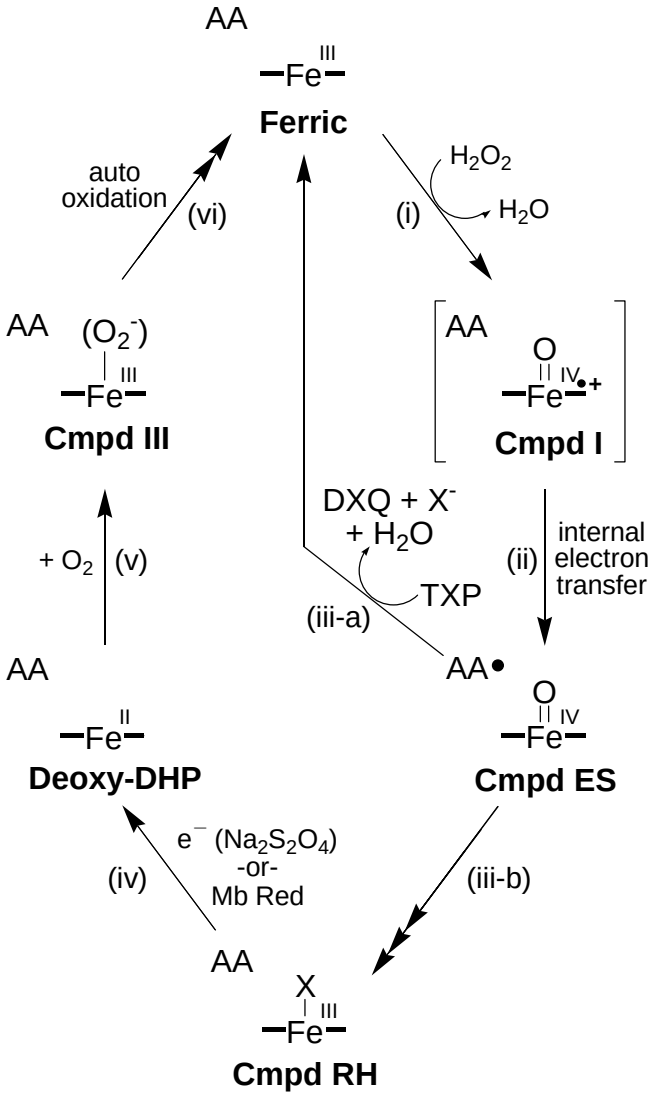

Scheme IV.1: Proposed Catalytic Cycle for Dehaloperoxidase.

Conclusion

The present study addresses a number of key questions pertaining to the nature and catalytic competency of the Compound ES intermediate in DHP. Our spectroscopic and biochemical characterization of DHP Compound ES suggests that this species is similar to the two-electron oxidized Compound ES of CcP in that it possesses both a ferryl heme center and a protein radical. Furthermore, our results are consistent with Compound ES being an active species responsible for trihalophenol oxidation, as opposed to Compound I. A

peroxidase-attenuated species unique to DHP, namely Compound RH, was also identified, and a role for its formation as a protective species against unwanted oxidation chemistry was hypothesized. Unreactive toward further oxidation, it was found that reduction of Compound RH regenerates oxyferrous DHP, and suggests that the recovery of the oxygen-transport function from an attenuated peroxidase species via reduction (possibly globin reductase) is a consequence of the bifunctional nature of this protein, and may represent the chemical process that links the oxygen transport and peroxidase activities in dehaloperoxidase.

Acknowledgments. We acknowledge financial support for this work from Army Research Office Grant 52278-LS.

Supporting Information

Characterization of Dehaloperoxidase Compound ES and its Reactivity with Trihalophenols

Contents

Figure IV.S1. (A) Stopped-flow UV-visible spectroscopic monitoring of the reaction (900 scans, 85 sec) between DHP (10 μM) and a 10-fold excess of H_2O_2 at pH 5.0. See experimental for details. (B) Calculated UV-visible spectra for both resting (black), Compound ES (red), and Compound RH (blue) DHP are shown; the rapid-scanning data from A were compiled and fitted to a double exponential reaction model using the Specfit global analysis program. (C) Relative concentration profile determined from the three component fit used in (B).

Figure IV.S2. EPR spectra of the radical(s) in DHP Compound ES at pH 5. The weak shoulder observed at a the freeze-quench time of 400 ms is amplified 5-fold to better show the low signal feature at g = 2.035. Rapid freeze-quench samples were prepared from the reaction of DHP (50 μM final) with a 10-fold excess of H_2O_2 at 25 °C, and rapidly frozen in an isopentane slurry. Spectra were obtained at 77 K using the parameters described in the experimental section.

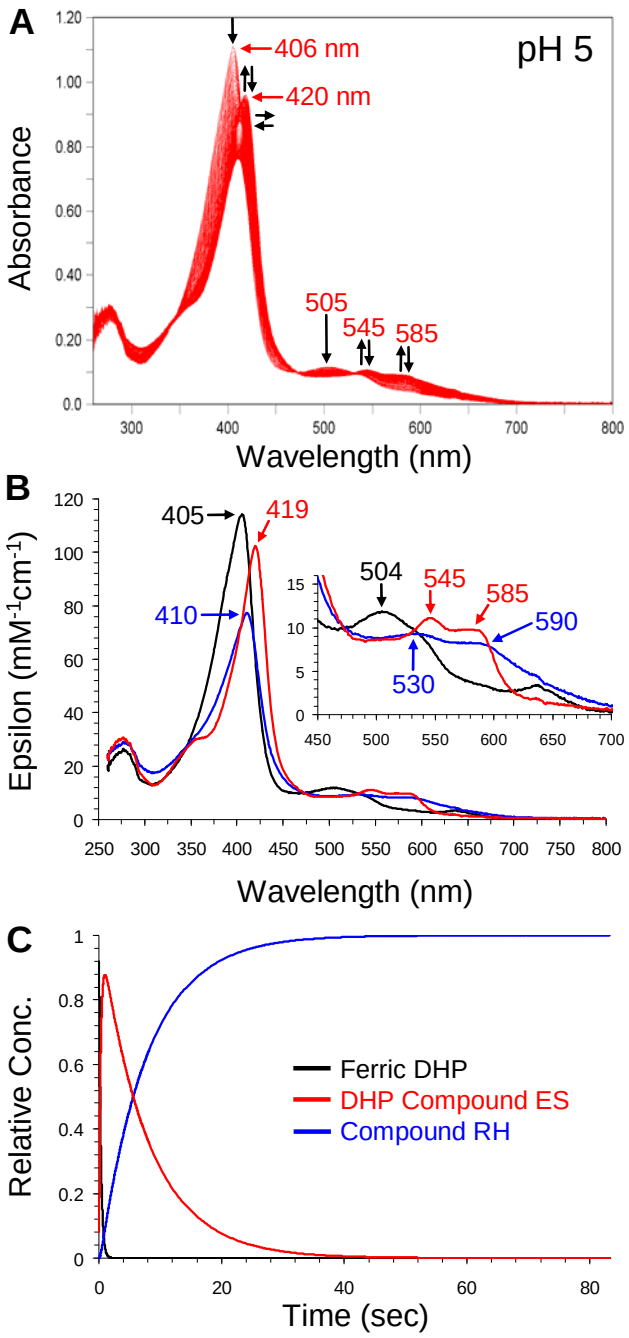

Figure IV.S1: (A) Stopped-flow UV-visible spectroscopic monitoring of the reaction (900 scans, 85 sec) between DHP (10 μM) and a 10-fold excess of H_2O_2 at pH 5.0. See experimental for details. (B) Calculated UV-visible spectra for both resting (black), Compound ES (red), and Compound RH (blue) DHP are shown; the rapid-scanning data from A were compiled and fitted to a double exponential reaction model using the Specfit global analysis program. (C) Relative concentration profile determined from the three component fit used in (B).

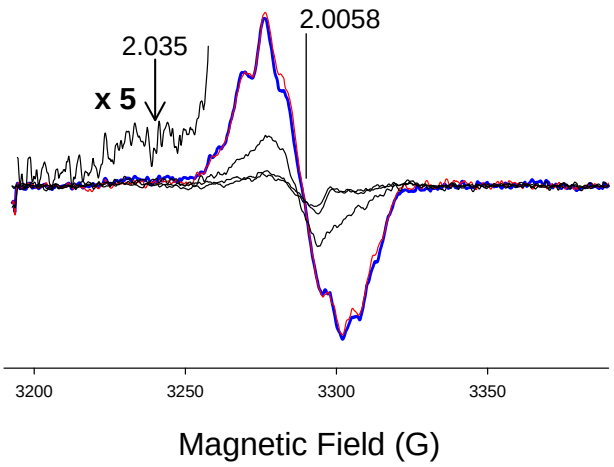

Figure IV.S2: EPR spectra of the radical(s) in DHP Compound ES at pH 5. The weak shoulder observed at a the freeze-quench time of 400 ms is amplified 5-fold to better show the low signal feature at g = 2.035. Rapid freeze-quench samples were prepared from the reaction of DHP (50 μM final) with a 10-fold excess of H_2O_2 at 25 °C, and rapidly frozen in an isopentane slurry. Spectra were obtained at 77 K using the parameters described in the experimental section.

REFERENCES

1. Feducia, J., Dumarieh, R., Gilvey, L. B. G., Smirnova, T., Franzen, S., and Ghiladi, R. A. (2009) Characterization of Dehaloperoxidase Compound ES and Its Reactivity with Trihalophenols, *Biochemistry 48*, 995-1005.

2. Osborne, R. L., Coggins, M. K., Walla, M., and Dawson, J. H. (2007) Horse Heart Myoglobin Catalyzes the H_2O_2-Dependent Oxidative Dehalogenation of Chlorophenols to DNA-Binding Radicals and Quinones, *Biochemistry 46*, 9823-9829.

3. Dai, J., Sloat, A. L., Wright, M. W., and Manderville, R. A. (2005) Role of Phenoxyl Radicals in DNA Adduction by Chlorophenol Xenobiotics Following Peroxidase Activation, *Chemical Research in Toxicology 18*, 771-779.

4. Belyea, J., Gilvey, L. B., Davis, M. F., Godek, M., Sit, T. L., Lommel, S. A., and Franzen, S. (2005) Enzyme Function of the Globin Dehaloperoxidase from *Amphitrite ornata* is Activated by Substrate Binding, *Biochemistry 44*, 15637-15644.

5. Franzen, S., Belyea, J., Gilvey, L. B., Davis, M. F., Chaudhary, C. E., Sit, T. L., and Lommel, S. A. (2006) Proximal Cavity, Distal Histidine, and Substrate Hydrogen-Bonding Mutations Modulate the Activity of *Amphitrite ornata* Dehaloperoxidase, *Biochemistry 45*, 9085-9094.

6. Franzen, S., Gilvey, L. B., and Belyea, J. L. (2007) The pH Dependence of the Activity of Dehaloperoxidase from *Amphitrite ornata*, *Biochimica Et Biophysica Acta-Proteins and Proteomics 1774*, 121-130.

7. Laurenti, E., Ghibaudi, E., Todaro, G., and Ferrari, R. P. (2002) Enzymatic Degradation of 2,6-Dichlorophenol by Horseradish Peroxidase: UV-Visible and Mass Spectrophotometric Characterization of the Reaction Products, *Journal of Inorganic Biochemistry 92*, 75-81.

8. Laurenti, E., Ghibaudi, E., Ardissone, S., and Ferrari, R. P. (2003) Oxidation of 2,4-Dichlorophenol Catalyzed by Horseradish Peroxidase: Characterization of the Reaction Mechanism by UV-Visible Spectroscopy and Mass Spectrometry, *Journal of Inorganic Biochemistry 95*, 171-176.

9. Svistunenko, D. A., and Cooper, C. E. (2004) A New Method of Identifying the Site of Tyrosyl Radicals in Proteins, *Biophysical Journal 87*, 582-595.

10. Svistunenko, D. A. (2005) Reaction of Haem Containing Proteins and Enzymes with Hydroperoxides: The radical view, *Biochimica Et Biophysica Acta-Bioenergetics 1707*, 127-155.

11. Lund, M. N., Luxford, C., Skibsted, L. H., and Davies, M. J. (2008) Oxidation of Myosin by Haem Proteins Generates Myosin Radicals and Protein Cross-Links, *Biochemical Journal 410*, 565-574.

12. Svistunenko, D. A., Dunne, J., Fryer, M., Nicholls, P., Reeder, B. J., Wilson, M. T., Bigotti, M. G., Cutruzzola, F., and Cooper, C. E. (2002) Comparative Study of Tyrosine Radicals in Hemoglobin and Myoglobins Treated with Hydrogen Peroxide, *Biophysical Journal 83*, 2845-2855.

13. Lawrence, C. C., Bennati, M., Obias, H. V., Bar, G., Griffin, R. G., and Stubbe, J. (1999) High-Field EPR Detection of a Disulfide Radical Anion in the Reduction of Cytidine 5 '-Diphosphate by the E441Q R1 Mutant of *Escherichia coli* Ribonucleotide Reductase, *Proceedings of the National Academy of Sciences of the United States of America 96*, 8979-8984.

14. Hoffman, M. Z., and Hayon, E. (1972) One-Electron Reduction Of Disulfide Linkage in Aqueous-Solution - Formation, Protonation, and Decay Kinetics of RSSR- Radical, *Journal of the American Chemical Society 94*, 7950-&.

15. Chan, P. C. (1973) Pulse-Radiolysis Study of Optical-Absorption and Kinetic Properties of Dithiothreitol Free-Radical, *Journal of the American Chemical Society 95*, 5504-5508.

16. Witting, P. K., Douglas, D. J., and Mauk, A. G. (2000) Reaction of Human Myoglobin and H_2O_2: Involvement of a Thiyl Radical Produced at Cysteine 110, *Journal of Biological Chemistry 275*, 20391-20398.

17. Fenwick, C. W., and English, A. M. (1996) Trapping and LC-MS Identification of Protein Radicals Formed in the Horse Heart Metmyoglobin-H_2O_2 Reaction, *Journal of the American Chemical Society 118*, 12236-12237.

18. Hirota, S., Azuma, K., Fukuba, M., Kuroiwa, S., and Funasaki, N. (2005) Heme Reduction by Intramolecular Electron Transfer in Cysteine Mutant Myoglobin Under Carbon Monoxide Atmosphere, *Biochemistry 44*, 10322-10327.

19. Smith, A. T., and Veitch, N. C. (1998) Substrate Binding and Catalysis in Heme Peroxidases, *Current Opinion in Chemical Biology 2*, 269-278.

20. Keilin, D., and Hartree, E. F. (1950) Reaction of Methaemoglobin with Hydrogen Peroxide, *Nature 166*, 513-514.

21. George, P., and Irvine, D. H. (1951) Reaction of Metmyoglobin with Hydrogen Peroxide, *Nature 168*, 164-165.

22. Giulivi, C., and Cadenas, E. (1998) Heme Protein Rradicals: Formation, Fate, and Biological Consequences, *Free Radical Biology and Medicine 24*, 269-279.

23. Alayash, A. I., Ryan, B. A. B., Eich, R. F., Olson, J. S., and Cashon, R. E. (1999) Reactions of Sperm Whale Myoglobin with Hydrogen Peroxide - Effects of Distal Pocket Mutations on the Formation and Stability of the Ferryl Intermediate, *Journal of Biological Chemistry 274*, 2029-2037.

CHAPTER V

Mutagenesis Studies of Dehalopeoxidase A and B: Compound I Formation and the Tyrosine Radical in Compound ES

Rania Dumarieh, Jennifer D'Antonio, Alexandra Liang, Tatyana Smirnova, Dimitri Svistunenko and Reza A. Ghiladi

Abstract

Dehaloperoxidase (DHP), the oxygen-transport hemoglobin from the terebellid polychaete *Amphitrite ornata*, is the first globin identified to possess a biologically relevant peroxidase activity. Ferric DHP has been shown to oxidize trihalophenols to dihaloquinones in a dehalogenation reaction that utilizes hydrogen peroxide as the oxidant. Rather than a traditional Compound I intermediate, the catalytically competent species in dehaloperoxidase appears to be Compound ES, a reactive intermediate that contains both a ferryl heme and a tyrosyl radical. By simulating the EPR spectrum of the tyrosyl radical in WT DHP A, Thompson et al [*J. Am. Chem. Soc. 132*, 17501-17510] proposed two different radicals as being both present in Compound ES, a primary tyrosyl radical that is characterized by a phenoxyl ring rotation angle of 45° or 75° and was suggested to correspond to either Tyr^{34} or Tyr^{28}, and a secondary radical that was suggested to reside on Tyr^{38}. In order to provide experimental support of these assignments, herein the present report focuses on altering radical formation in Compound ES via site-directed mutagenesis of these three tyrosine residues, Tyr^{28}, Tyr^{34} and Tyr^{38}, in both DHP A and B. Specifically, we have recombinantly expressed DHP A(Y34F), DHP A(Y38F), DHP A(Y34F/Y38F), DHP B(Y38F), DHP B(Y28F) and DHP B (Y28F/Y38F) and examined the reaction of the ferric enzyme of each mutant with hydrogen peroxide under a variety of conditions using stopped-flow UV-visible and rapid-freeze-quench EPR spectroscopic methods, and supported by biochemical assays. The spectroscopic results are presented in the context of the structures of DHP A and B, enabling unambiguous identification of the site of initial tyrosyl radical formation in dehaloperoxidase. The mutation of both Tyr^{34} and Tyr^{38} was required in order to identify Compound I using stopped-flow UV-visible spectroscopic methods. These two mutations were not sufficient, however, to fully arrest the formation of Compound ES, and the

additional mutation of Tyr^{28}, over 10 Å from the heme active site, was required to prevent any protein radical from being observed. Preferential site localization of the tyrosyl radical was also noted, suggesting that external binding of the trihalophenol substrate may occur in proximity to Tyr^{34} and Tyr^{28} for DHP A and B, respectively. Formation of the peroxidase-attenuated species Compound RH from the decay of Compound ES was only noted when Tyr^{38} was present, and this observation was rationalized by considering the effect of this residue on the conformation of the distal histidine. The novel structure-activity relationship of the tyrosyl radical reported herein for DHP highlights its chemical reactivity that may enable the single heme active site of dehaloperoxidase to function both as an oxygen-transport globin and as a peroxidase, and these results will be interpreted in light of the proposed mechanism of function of dehaloperoxidase.

V.1. Introduction

Peroxidases represent a class of enzymes that are ubiquitous in nature and essential to a wide variety of critically important life processes. As oxidoreductases, peroxidases heterolytically cleave the peroxidic bond, reducing hydrogen peroxide (or organic hydroperoxides) concomitant with the oxidation of both organic and inorganic substrates via one or two-electron steps. The majority of known peroxidases contain the heme prosthetic group, and have been divided into two major superfamilies: gene duplicated bacterial peroxidases (class I), secretory fungal peroxidases (class II), and classical, secretory plant peroxidases (class III) have been grouped by Welinder into the bacterial, fungal, and plant superfamily (*1*), whereas more recently Obinger and co-workers have coined the 'peroxidase-cyclooxygenase' superfamily (*2*), comprised of mammalian peroxidases (e.g. myeloperoxidase and lactoperoxidase), cyclooxygenases, peroxinectins and peroxidasins. These phylogenic relationships are primarily based upon gene and/or protein sequence alignments, and structural homology. Generally speaking, such comparative sequence analysis has allowed for the identification of putative peroxidase domains from genomic data, and represents a powerful tool for predicting the physiological role(s) of enzymes in various organisms. However, as the archetype of a potentially new emerging class of peroxidases termed the hemoglobin-peroxidases, dehaloperoxidase (DHP), the putative coelomic oxygen-transport hemoglobin from the terebellid polychaete *Amphitrite ornata* (*3-5*), defies such predictive grouping. DHP shares neither sequence nor structural homology with any of the classical peroxidases (e.g. cytochrome c peroxidase, horseradish peroxidase) (7), and has little sequence homology to other known hemoglobins. As such, its oxidoreductase and oxygen-transport role(s) *in vivo* cannot be inferred from primary biological sequence information. Moreover, its inclusion as a member of the globin superfamily is based solely upon its globular structure (6). Thus, as a representative of globins found in marine organisms, comparison of the mechanism and activity of DHP to other hemoglobins and peroxidases may aid in establishing the scientific foundation of protein structure-function relationships specific to bi/multi-functional proteins, and further

our understanding of marine peroxidases in relation to those of mammalian, plant, or bacterial origins.

The diversity of environmental haloaromatic toxins which act as repellents secreted by marine organisms such as *Notomastus lobatus* (polychaeta) (*6-8*) and *Saccoglossus kowalevskii* (hemichordata) (*9, 10*) represents a significant challenge to other infaunal organisms that co-inhabit benthic ecosystems. Examples of these biogenically-produced halometabolites include mono-, di-, and tribromophenols, mono- and dibromovinylphenols, and bromopyrroles. To overcome high levels of these volatile brominated secondary metabolites, *A. ornata* employs dehalogenating enzymes that enable it to tolerate certain biocidal compounds. DHP, as one such enzyme, possesses a broad substrate specificity for the oxidation of the mono-, di-, and trisubstituted halophenols that possess bromine, chlorine, or fluorine substituents (*11, 12*), thus distinguishing DHP as the first globin shown to possess a biologically relevant peroxidase activity (*11*). The dehaloperoxidase function of this hemoglobin was first determined by fractionation of the *A. ornata* proteome to determine which component of the organism was capable of degrading bromophenols (*11*). The high specific activity of the purified protein signified that DHP was solely responsible for the observed oxidative dehalogenation reaction, and recombinant expression of the protein further indicated that such enzymatic activity is intrinsic to DHP (*12*).

Both known isoenzymes of DHP (A and B) have been shown to catalyze the oxidative degradation of 2,4,6-trihalogenated phenols in the presence of hydrogen peroxide to their corresponding 2,6-dihalo-1,4-benzoquinones, and the mechanism of this reaction has been the focus of a number of recent reports (*12-29*). Peroxidases generally function via the Poulos-Kraut mechanism (*30*) in which H_2O_2 reacts with a ferric heme to form Compound I, the iron(IV)-oxo porphyrin π-cation radical species that is formally oxidized by two electrons relative to the ferric resting state. Dehaloperoxidase also forms Compound I, as recently investigated by Hoffman and co-workers using cryoreduction in conjunction with EPR spectroscopy (*28*), but it rapidly converts to a more stable species due to the presence of an endogenous reducing species. Using stopped-flow UV-visible and rapid freeze-quench EPR spectroscopic methods, we have previously demonstrated that both ferric DHP A and B react

with hydrogen peroxide to yield an iron(IV)-oxo heme center with an amino acid radical that is reminiscent of the two-electron oxidized intermediate termed Compound ES in CcP (*13, 29*). The catalytic competency of Compound ES for oxidizing the substrate 2,4,6-tricholorphenol (TCP) to 2,6-dichloro-1,4-benzoquinones (DCQ) has also been demonstrated, and peroxidase-like catalytic cycles for DHP that proceed through this species have been proposed (*13, 29*). Furthermore, Dawson and co-workers have reported that the overall two-electron oxidation of TCP by DHP proceeds through discrete one-electron steps (*24, 28*), which is consistent with the hypothesis that the trihalogenated substrate is oxidized by Compound ES. Interestingly, DCQ itself is not an innocent species, having been shown to react separately with both Compound ES and ferric DHP to yield oxyferrous DHP in either case (*29*). As deduced by spectroelectrochemistry, the unusually high reduction potential for a peroxidase of ~+205 mV reported for DHP likely facilitates reactions with DCQ that ultimately favor the reduction of the heme prosthetic group and formation of oxyferrous DHP B (*29, 31*). In the absence of a reducing co-substrate (either as TXP or DXQ), the formation of a species termed Compound RH, which is unique to dehaloperoxidase and has not found in any other globin, has been observed (*13, 29, 32*).

Although the above research and a number of other studies on DHP (*13, 19, 24, 33*) have helped to elucidate several of its mechanistic pathways, it is still not understood how this bi-functional protein can act as both a hemoglobin and a peroxidase, and a number of key questions regarding the nature of the catalytic intermediate(s) remain. One critical aspect of the dehaloperoxidase mechanism that remains unaddressed is the nature of the protein radical in Compound ES. Previous low-field electron paramagnetic resonance (EPR) spectroscopic studies suggested that the radical is located on a tyrosine residue near the heme center (*13, 29*). However, the localization of the protein radical to a specific residue in Compound ES was not assigned at that time due to the low resolution of the hyperfine structure. More recently, by simulating the EPR spectrum of the tyrosyl radical in WT DHP A, Thompson et al. (*34*) have proposed two different radicals as being both present in Compound ES. Specifically, a primary tyrosyl radical that is characterized by a phenoxyl ring rotation angle of 45° or 75° was suggested to correspond to either Tyr^{34} or Tyr^{28}, and a

secondary radical that was suggested to reside on Tyr^{38}. Interesting, the Tyr^{34} radical was shown to form with a very high relative yield (almost 100% of heme), atypical of other globins, and likely signifies the importance of Compound ES in the mechanism of DHP. Additionally, it was hypothesized that two alternative routes of Compound ES decay occur in DHP, and that the specific route is determined based upon the conformation of the distal histidine, His^{55}, which has been shown to exist in both 'open' and 'closed' conformations (*35-38*). In the less populated closed conformation, a Tyr^{38} radical was hypothesized to form, but in the major open conformation, Compound ES decays to Compound RH, a peroxidase-attenuated species that has been hypothesized to be protective against undesired peroxidase activity in the absence of substrate.

Thus, given the multiple roles that it plays in DHP, the focus of the present report is to examine the location, reactivity, and decay of the protein-based radical of DHP Compound ES, as this may have a bearing on the mechanism of function, the structure-activity relationship, and the locus of substrate oxidation in DHP. Of the five tyrosine residues in DHP A (Figure V.1: Tyr^{16}, Tyr^{28}, Tyr^{34}, Tyr^{38}, Tyr^{107}), only three are reasonably close to the heme prosthetic group to be considered likely candidates for reducing Compound I initially, Tyr^{34} and Tyr^{38}; the closest contact between Tyr^{34} and the heme edge is 5.56 Å (Tyr Cγ), whereas Tyr^{38} is 7.54 Å (phenolic oxygen) and that of Tyr^{28} is 10 Å. The remaining two tyrosine residues are greater than 15 Å (Tyr^{16} and Tyr^{107}) from the heme edge, making them unlikely candidates as the residues responsible for the initial reduction of a transiently formed Compound I intermediate. By comparison, DHP B only possesses four of the tyrosine residues found in DHP A, as this isoenzyme bears an Asn at position 34. Thus, the experimental strategy employed herein focuses on altering radical formation in Compound ES via site-directed mutagenesis of three tyrosine residues, Tyr^{28}, Tyr^{34} and Tyr^{38}, in both DHP A and B. Specifically, we have recombinantly expressed DHP A(Y34F), DHP A(Y38F), DHP A(Y34F/Y38F), DHP B(Y38F), DHP B(Y28F) and DHP B (Y28F/Y38F) and examined the reaction of the ferric enzyme of each mutant with hydrogen peroxide under a variety of conditions using stopped-flow UV-visible and rapid-freeze-quench EPR spectroscopic methods, and supported by biochemical assays. The spectroscopic results are

presented in the context of the structures of DHP A and B, enabling identification of the site of initial tyrosyl radical formation in dehaloperoxidase. Evidence for the formation of DHP Compound I in specific tyrosine mutants will also be presented, thus providing additional support for the proposed mechanism of dehaloperoxidase. Furthermore, the relationship between Compound ES and Compound RH will be discussed in the context of mutants lacking specific active site tyrosine residues. Overall, the chemistry of the tyrosyl radical reported herein for DHP highlights novel and interesting reactivity that may enable the single heme active site of dehaloperoxidase to function both as an oxygen-transport globin and as a peroxidase.

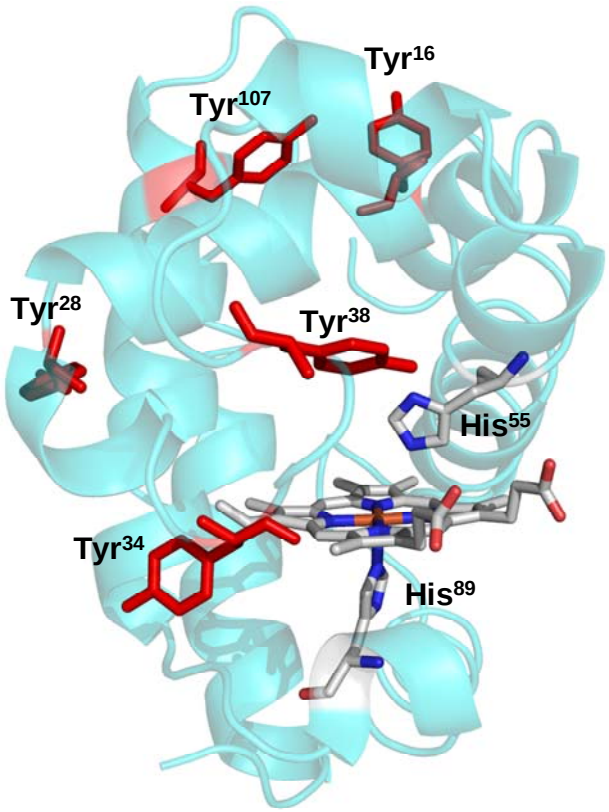

Figure V.1: Heme active site of DHP A in relation to all tyrosine residues present in the isoenzyme. The proximal and distal histidines, His^{89} and His^{55}, are provided for orientation. Coordinates (2QFK) were obtained from the Protein Data Bank and displayed using Pymol. DHP B lacks Tyr^{34}, which is substituted by an asparagine, but otherwise possesses the remaining four tyrosine residues.

V.2. Materials and Methods

Buffer salts and acetonitrile (HPLC grade) were purchased from Fisher Scientific. All other reagents and biochemicals, unless otherwise specified, were of the highest grade available from Sigma-Aldrich. The QIAprep® Spin Miniprep Kit was from QIAGEN Sciences (Valencia, CA) and the Quikchange® II site-directed mutagenesis kit was purchased from Stratagene (La Jolla, CA). The required oligonucleotides were synthesized by IDT DNA Technologies, Inc. EPR tubes were purchased from Norell (Landisville, NJ). Solutions of 2,4,6-trichlorphenol (TCP) were freshly prepared daily in 100 mM potassium phosphate (KPi) buffer (variable pH) and kept at 4 ^{o}C while protected from light. UV-visible spectra were recorded periodically to ensure that the TCP substrate had not degraded. Hydrogen peroxide solutions were also freshly made prior to each experiment: initially, a 10 mM stock solution of H_2O_2 was prepared and maintained at 4 ^{o}C (typically less than 15 minutes), during which all other protein/substrate solutions were loaded into the stopped-flow apparatus. When prepared in this manner, the stock H_2O_2 solution did not exhibit any degradation over this time period as determined by UV-visible spectroscopic analysis of the hydrogen peroxide absorbance at 240 nm (ε_{240} = 43.6 $M^{-1}cm^{-1}$). (*39*) The stock H_2O_2 solution was then diluted to the appropriate pre-mixing concentration and immediately loaded into the stopped-flow apparatus.

Plasmid Preparation, Protein Expression and Purification – All the mutations were generated with the Quikchange® II site-directed mutagenesis kit. Mutagenesis [melt (95 °C, 50 s), anneal (60 °C, 50 s), and extension (68 °C, 6 min] was performed for 18 cycles. The plasmid encoding WT DHP A (His tag) was used as a template to generate the following plasmids using mutagenic primers: pDHPA(Y38F) [5'- TTC AAA AAC TTT GTC GGC AAA TCT GAC CAA GAG CTC AAA TCG ATG GCC AAG-3' (sense) and 5'- CTT GGC CAT CGA TTT GAG CTC TTG GTC AGA TTT GCC GAC AAA GTT TTT GAA G-3' (antisense)], pDHPA(Y34F) [5'- G CGC CGC TTC TTC AAA AAC TAT GTC-3' (sense) and 5'- GAC ATA GTT TTT GAA GAA GCG GCG C- 3' (antisense)], and pDHPA(Y34F/Y38F) [5'- CCG GAC GAG CGC CGC TTC TTC AAA AAC TTT GTC GGC AAA TCT GAC-3' (sense) and 5'- GTC AGA TTT GCC GAC AAA GTT TTT GAA

GAA GCG GCG CTC GTC CGG- 3' (antisense)]. Similarly, the plasmid encoding WT DHP B (His tag) was used as a template to generate the following plasmids using mutagenic primers: pDHPB(Y28F) [5'- CGC ATT TTT GAA TAA GTT TCC GGA CGA GAA ACG CA -3' (sense) and 5'- TGC GTT TCT CGT CCG GAA ACT TAT TCA AAA ATG CG -3' (antisense)], and pDHPB(Y38F) [5'- CGC AAC TTC AAA AAC TTC GTC GGC AAA TCT GAC -3' (sense) and 5'- GTC AGA TTT GCC GAC GAA GTT TTT GAA GTT GCG -3' (antisense)]. The pDHPB(Y38F) plasmid was further used as the template for generating the double mutant pDHPB(Y28F/Y38F) with the mutagenic primers used originally to generate the pDHPB(Y28F) mutation. The plasmids were extracted using the QIAprep® spin miniprep kit, and the presence of the desired mutations and lack of secondary mutations were confirmed by sequencing. WT DHP A, WT DHP B, DHP A(Y34F), DHP A(Y38F), DHP A(Y34F/Y38F), DHP B(Y28F), DHP B(Y38F) and DHP B(Y28F/Y38F) (6x-His-tagged proteins) were expressed and purified as previously described (*13, 15, 29*) with only minor modifications.

Molecular Weight Determination – The molecular weight of the proteins employed in this study were experimentally determined via electrospray ionization mass spectrometry in positive-ion mode (Agilent Technologies 6210 LC-TOF, Santa Clara, CA). The protein sample was prepared in 50 mM ammonium acetate buffer, pH 7.0. The mobile phase consisted of HPLC grade solvents: water + 0.1% formic acid (v/v), and water:acetonitrile 5:95 + 0.1 % formic acid (v/v). The injection volume was 5 µL and the flow rate was 300 µL per minute.

Preparation of Ferric DHP – Ferric DHP was treated with an excess of potassium ferricyanide in order to obtain a homogeneous solution of the enzyme in the ferric state. Excess ferricyanide was removed using a PD-10 desalting column prepacked with Sephadex G-25 medium. The protein was concentrated using an Amicon Ultra centrifugal filter equipped with a 10,000 kDa cutoff molecular weight membrane, and the purity of DHP was determined as previously published. Only protein samples that exhibited Reinheitzahl values (R_z) greater than 4.0 were utilized in this study. The concentrations of the mutant enzymes

were determined spectrophotometrically based on the literature values for WT DHP A (ε_{406} = 116.4 mM^{-1} cm^{-1}) (*12*) and WT DHP B (ε_{407} = 117.6 mM^{-1} cm^{-1}) (*29*).

UV-Visible Spectroscopic Studies and Dehaloperoxidase Activity Assays – Optical spectra were recorded using quartz microcuvettes (1 cm pathlength) on a Cary 50 UV-Visible spectrophotometer equipped with thermostatted cell holders at 25 °C. The apparent values of K_m and k_{cat} for the DHP mutants for hydrogen peroxide at a fixed saturating concentration of the trichlorophenol substrate were calculated by triplicate measurements of initial velocity at each H_2O_2 concentration. The experimental data was fitted to the Michaelis-Menten model using the enzyme kinetics software GraFit (Erithacus Software). The enzymatic activity was assayed on the basis of the disappearance of co-substrate (trichlorophenol, 312 nm; tribromophenol, 316 nm) or formation of product (difluoroquinone, 330 nm) monitored for 15 min at 25 ºC. The 1-mL reaction mixture contained 0.5 μM of enzyme (ferric or oxyferrous), 150 μM of trihalophenol and varying H_2O_2 concentrations (5, 10, 50, 150, 250, 500, 750 μM) in 100 mM potassium phosphate buffer at pH 7.

Stopped-flow UV-Visible Spectrophotometric Studies – Experiments were performed on a Bio-Logic SFM-400 Triple Mixing Stopped-Flow instrument equipped with a diode array UV-Visible spectrophotometer, and were carried out at 20 °C in 100 mM KPi buffer (variable pH). Constant temperature was maintained using a circulating water bath. Data was collected (900 scans total) over a three time-domain regime (2.5 ms, 25 ms, 250 ms; 300 scans each) using the BioKinet32 software package (Bio-Logic). Single-mixing experiments were performed as follows: ferric DHP enzyme at a final concentration of 10 μM was reacted with 2.5 – 25 equivalents of H_2O_2. Experiments were performed in double-mixing mode using an aging line prior to the second mixing step. The design of the experiments allowed for the mixing of DHP with H_2O_2 for various aging times, followed by the second mix with either TCP/DCQ: DHP + H_2O_2 → Delay → + TCP/DCQ. Concentrations after mixing were $[DHP]_f$ = 10 μM, $[H_2O_2]_f$ = 100 μM, and $[TCP]_f$ = 300 μM or [DCQ] = 70 μM. All data were evaluated using the Specfit Global Analysis System software package (Spectrum Software Associates) and fit with SVD analysis as either one-step, two species or two-step, three

species irreversible mechanisms, where applicable. Kinetics data were baseline corrected using the Specfit autozero function.

Preparation of Reaction Intermediates by Freeze-Quench Methods – Rapid freeze-quench experiments were performed with a BioLogic SFM 400 Freeze-Quench apparatus by mixing a 50 μM enzyme solution (final concentration) with a 10-fold excess of H_2O_2 solution in 100 mM potassium phosphate buffer (pH 7) at 25 °C. Reaction times were varied and are reported in the figure legend. A standard 4 mm O.D. quartz EPR tube was connected to a Teflon funnel, and both the tube and the funnel were completely immersed in an isopentane bath at -110 °C. The reaction mixtures were quenched by spraying them into the cold isopentane, and the frozen material so obtained was packed at the bottom of the quartz tube using a packing rod equipped with a Teflon plunger. Samples were then transferred to a liquid nitrogen storage dewar until analyzed.

X-band EPR Spectroscopy – EPR spectra were recorded with an X-band (9 GHz) Varian E-9 EPR spectrometer (Varian, El Palo, CA). A standard 3 by 4 mm quartz EPR tube was filled with a sample and placed into a quartz finger dewar insert filled with liquid nitrogen. The temperature of the samples was maintained at 77 K for the duration of the data acquisition, which required periodic refilling of the dewar due to the evaporation of the liquid nitrogen during longer acquisition runs. The typical spectrometer settings were as follows: field sweep 200 G, scan rate 3.33 Gauss/s, modulation frequency 100 KHz, modulation amplitude 4.0 G, and microwave power 2 mW. The exact resonant frequency of each EPR experiment was measured by an EIP-578 (PhaseMatrix, San Jose, CA) in-line microwave frequency counter and is indicated in the figure caption. Typically, 20 to 200 individual scans were averaged to achieve sufficient signal-to-noise for the spectra obtained at short-quench and long-quench times, respectively.

V.3. Results

Overexpression, Purification and Enzymatic Activity of DHP Mutants – The plasmids encoding wild-type DHP A or B with an N-terminal poly-His tag (pDHPA or pDHPB) were subjected to PCR amplification using mutagenic primers. DNA sequencing of the resulting

mutated genes in their entirety confirmed the success of the site-directed mutagenesis and the absence of secondary mutations. Recombinant DHP proteins for the mutants listed in Table 1 were obtained by expression in *E. coli* as described elsewhere, with protein yields upwards of ~9 mg/L culture. A two-part purification strategy (immobilized metal affinity followed by ion-exchange chromatographies) resulted in purification levels >95% homogeneity, with the DHP mutants being indistinguishable by SDS-PAGE gel from their wild-type counterparts. The monomeric molecular weights of each of the dehaloperoxidase mutants were determined by electrospray ionization MS, and were as follows: DHP A(Y34F), 16392.46 (calc. 16392.50); DHP A(Y38F), 16392.40 (calc. 16392.50); DHP A(Y34F/Y38F), 16376.39 (calc. 16376.50); DHP B(Y28F), 16258.14 (calc. 16258.37); DHP B(Y38F), 16258.39 (calc. 16258.37); DHP B(Y28F/Y38F), 16242.47 (calc. 16242.37).

As was found for isoenzymes A and B, the mutants were initially isolated as a mixture of the ferric and oxyferrous forms. Treatment of the as-isolated mutants with an excess of potassium ferricyanide permitted the isolation of their ferric form. The electronic absorption spectra of the DHP mutants in the ferric metaquo state are presented in Figure V.2 (pH 7), and relevant spectral features, optical purity ratios (Reinheitzahl or R_z, defined as A_{Soret}/A_{280}), and A_{Soret}/A_{380} ratio analysis can be found in Table 1. With only minor differences between them, overall the spectra of the tyrosine mutants exhibit features typical of a high spin ferric heme similar to those previously observed for DHP A or B under identical conditions (*12, 13*). Analysis of the A_{Soret}/A_{380} ratio is able to demonstrate relative populations of 6-coordinate (6-c) vs. 5-c high spin (HS) heme. Generally, 5-c HS heme species exhibit a slightly blue shifted and smaller extinction Soret band than their 6-c HS counterparts, as well as a shoulder at 380 nm. As such, 5-c HS hemes will yield a smaller A_{Soret}/A_{380} ratio than their 6-c HS analogs. As can be seen from the data in Table 1, the relative amounts of 5-c HS heme are greater in WT DHP A, DHP A(Y34F), WT DHP B, and DHP B(Y28F), all of which possess a tyrosine residue at position 38 (Tyr38). However, the relative population of 6-c HS heme is greater in the remaining four mutants, DHP A(Y38F), DHP A(Y34F/Y38F), DHP B(Y38F), and DHP B(Y28F/Y38F), all of which have a phenylalanine, rather than tyrosine, at that position. Thus, the presence of Tyr^{38} leads to a

shift in the population of high spin heme towards 5-c HS, with the distal histidine (His^{55}) in the open conformation, whereas its absence leads to a shift in the relative population towards 6-c HS heme, with the heme in the closed conformation. The consequences of the Tyr^{38} mutation-induced changes in heme coordination that are linked to the conformational flexibility of the distal histidine are addressed with respect to Compound RH formation (see Discussion).

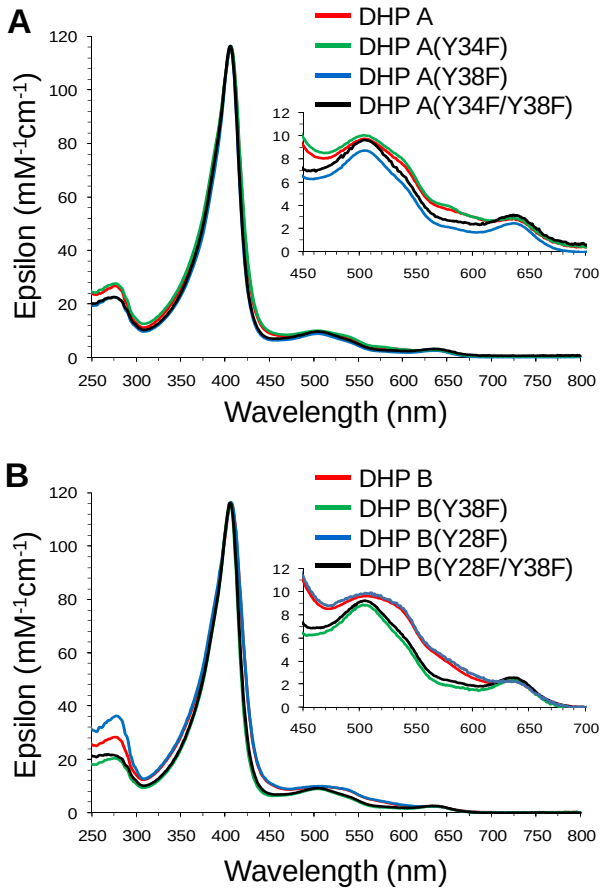

Figure V.2: UV-visible spectra of ferric DHP at pH 7.0. A) DHP A, DHP A(Y34F), DHP A(Y38F), DHP A(Y34F/Y38F); B) DHP B, DHP B(Y38F), DHP B(Y28F), DHP B(Y28F/Y38F)

Table V.1: UV-Visible Spectroscopic Data for DHP mutants at pH 7

	λ_{max} (nm)	A_{Soret}/A_{380}	Fe^{IV}=O Formed	Tyr• in Cmpd ES [b]	"Cmpd RH" formed [d]	Ref.
Ferric DHP A	407, 504, 538 (sh), 635	1.89	ES	Y34 (p), Y38 (s)	Yes	(*13*)
DHP A(Y34F)	408, 507, 535 (sh), 639	1.92	ES	Y38 (p), Y28 (s)	Yes	[a]
DHP A(Y38F)	406, 505, 541 (sh), 638	2.17	ES	Y34	No (bleach)	[a]
DHP A(Y34F/Y38F)	406, 505, 540 (sh), 635	2.00	I/ES	Y28	No (bleach)	[a]
Ferric DHP B	407, 508, 540 (sh), 633	1.81	ES	Y38 (p), Y28 (s)	Yes	(*29*)
DHP B(Y28F)	407, 510, 538 (sh), 640	1.84	ES	Y38	Yes	[a]
DHP B(Y38F)	406, 506, 540 (sh), 636	2.04	I/ES	Y28	No (bleach)	[a]
DHP B(Y28F/Y38F)	406, 504, 538 (sh), 636	2.04	I	n.d. [c]	No (bleach)	[a]

[a] = this work; [b] (p) = primary, (s) = secondary; [c] = none detected; [d] = spectral features may be similar, but not exactly identical, to Compound RH

For each of the DHP mutants, the hydrogen peroxide-dependent oxidative dehalogenation of 2,4,6-trichlorophenol (TCP) to yield the corresponding 2,6-dichloro-1,4-benzoquinone (DCQ) at pH 7 was monitored by UV-visible spectroscopy. Both enzyme and TCP co-substrate concentrations were held constant while the enzymatic reaction was initiated by the addition of a variable concentration of H_2O_2 as the substrate. In the absence of DHP (non-enzymatic control), no product was observed under the conditions examined, in agreement with previous reports that showed a requirement for the enzyme (*12, 13*). Kinetic parameters (k_{cat}, K_m, and catalytic efficiency, k_{cat}/K_m) for the dehaloperoxidase activity of the DHP mutants are presented in Table 2, together with those determined for wild-type DHP A and B under the same conditions for comparative purposes. All mutants exhibited saturable dehaloperoxidase activity under the conditions employed, and the data were fit to standard Michaelis-Menten kinetics using the method of initial rates for d[S]/dt, and k_{cat} was determined using the known epsilon value for TCP.

In general, all mutants exhibited an increase in catalytic rate (k_{cat}) when compared to the wild-type enzyme (Table 2). For isoenzyme A, mutation of Tyr^{34} to phenylalanine did not appear to significantly alter k_{cat} alone (0.77 s^{-1}), whereas the mutation of Tyr^{38} led to a modest 2-fold increase in k_{cat} (1.09 s^{-1}) when compared to WT DHP A (0.61 s^{-1}). However, the double mutant Y34F/Y38F exhibited an 8-fold increase (4.9 s^{-1}). With Tyr^{34} substituted by an asparagine in WT ferric DHP B, the isoenzyme exhibited a k_{cat} of 1.53 s^{-1}, which increased 3-5 fold depending upon the tyrosine mutant investigated (Y28F, 5.13 s^{-1}; Y38F,

8.53 s^{-1}; Y28F/Y38F, 5.37 s^{-1}). Taken together, the data suggest that the simultaneous mutation of the two tyrosine residues closest to the heme active site dramatically increases the ability of the enzyme to oxidize TCP, and was explored further using stopped-flow UV-visible spectroscopy (vide infra). Overall, K_m values for hydrogen peroxide were found to be a modest 2-3 fold higher for all but one of the tyrosine mutants investigated in Table 2 when compared to their wild-type counterparts. The one notable exception, DHP B(Y28F), exhibited a K_m value ~35-fold higher than WT DHP B. As this residue is greater than 10 Å from the heme active site, we rule out a direct interaction that would interfere with H_2O_2-binding. However, we surmise that the mutation of the solvent exposed tyrosine to the hydrophobic phenylalanine at position 28 may disrupt the 3_{10}-helical conformation of the adjacent residues Pro29–Asn34, which in turn could alter the E helix and lead to a weakening in H_2O_2-binding. The higher catalytic rates were offset by the higher K_m values which led to catalytic efficiencies (k_{cat}/K_m) that were only marginally different from the wild-type isoenzymes.

Table V.2: Kinetics data for the oxidation of 2,4,6-trichlorophenol as catalyzed by DHP in the presence of H_2O_2 at pH 7

Enzyme	$K_M H_2O_2$ (μM)	k_{cat} (s^{-1})	$k_{cat}/K_M H_2O_2$ (μM^{-1} s^{-1})	Ref
Ferric DHP A	23 ± 1	0.61 ± 0.01	0.027	(*13*)
DHP A(Y34F)	27 ± 5	0.77 ± 0.02	0.029	[a]
DHP A(Y38F)	68 ± 5	1.09 ± 0.05	0.016	[a]
DHP A(Y34F/Y38F)	56 ± 7	4.9 ± 0.1	0.09	[a]
Ferric DHP B	22 ±2	1.53 ± 0.03	0.070	(*29*)
DHP B(Y28F)	752 ± 48	5.13 ± 0.14	0.007	[a]
DHP B(Y38F)	60 ± 10	8.53 ± 0.33	0.143	[a]
DHP B(Y28F/Y38F)	47 ± 5	5.37 ± 0.07	0.114	[a]

[a] = this work

Stopped-flow UV-Visible Characterization of the Reaction of DHP A Mutants with H_2O_2. Single mixing stopped-flow UV-visible spectroscopic methods were employed to detect the high-valent iron-oxo species formed from the reaction of the tyrosine mutants of DHP A with hydrogen peroxide at pH 7. Upon rapid mixing (2 ms) of a solution of ferric DHP A(Y34F) [UV-visible spectrum: 407 (Soret), 507, 535 (sh), 639 nm] with a 10-fold

excess of H_2O_2, a transient species was observed (Figure V.3) whose spectral features [UV-visible: 419 (Soret), 545, 584 nm] we ascribe to a ferryl-containing intermediate based upon previous characterization (*13, 24, 29, 32, 33, 40, 41*) of this species in WT DHP. As the ferryl intermediate of Compound ES in DHP is indistinguishable from that of Compound II by UV-visible spectroscopy (*42*), we assign this intermediate here as DHP A(Y34F) Compound ES here based upon these results and those of our EPR spectroscopic study (*vide infra*). Values of k_{obs} for formation of this new species were linearly dependent on [H_2O_2] (2.5 – 25 fold excess per heme), giving a bi-molecular rate constant of (4.94 ± 0.02) x 10^4 $M^{-1}s^{-1}$. No decay of DHP A(Y34F) Compound ES to Compound RH was observed over the 3 second observation window under these conditions. Similar reactivity was observed for DHP A(Y38F): ferric DHP A(Y38F) [UV-visible spectrum: 406 (Soret), 505, 541 (sh), 638 nm] was also converted to Compound ES [UV-visible: 419 (Soret), 545, 585 nm; k_{obs} = (8.69 ± 0.03) x 10^4 $M^{-1}s^{-1}$] (Figure S1), again with no observation of Compound RH after 3 seconds. As Compound ES was observed in both the Y34F and Y38F mutants of DHP A in a similar manner as to WT DHP A, the individual mutations do not appear to significantly alter the nature of the intermediates formed as observable by UV-visible spectroscopy.

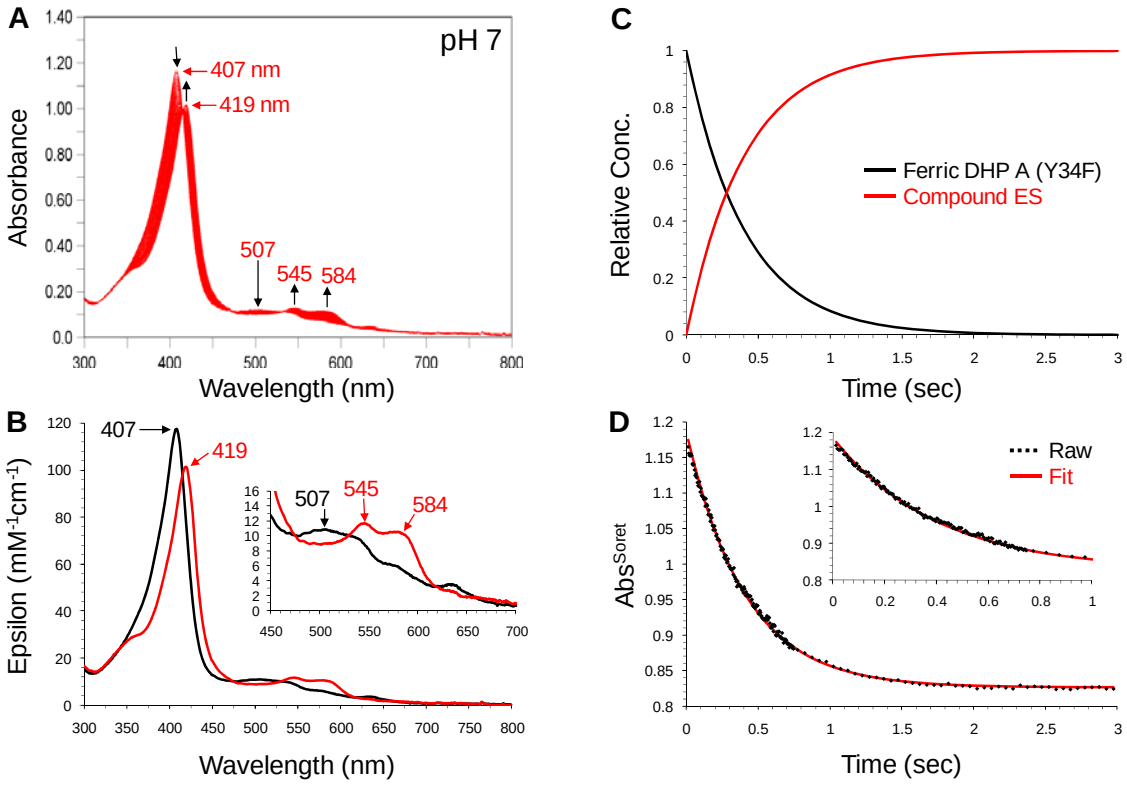

Figure V.3: (A) Stopped-flow UV-visible spectroscopic monitoring of the reaction (400 scans, 3 sec) between DHP A(Y34F) (10 μM) and a 10-fold excess of H_2O_2 at pH 7.0. See experimental for details. (B) Calculated UV-visible spectra for both resting (black) and Compound ES (red) DHP A(Y34F) are shown; the rapid-scanning data from A were compiled and fitted to a single exponential reaction model using the Specfit global analysis program. (C) Relative concentration profile determined from the two component fit used in (B). (D) The single wavelength trace (407 nm) of (A) and its fit from (B).

However, when the double mutant DHP A(Y34F/Y38F) was rapidly reacted with hydrogen peroxide under the conditions employed above (Figure V.4), a new species was formed [UV-visible: 405 (Soret; ε = 78 $mM^{-1}cm^{-1}$), 505 (broad shoulder), 643 nm; k_{obs} = (1.13 ± 0.02) x 10^5 $M^{-1}s^{-1}$] whose spectral features were distinct from those of the starting ferric enzyme [UV-vis: 406 (Soret; ε = 118 $mM^{-1}cm^{-1}$), 505, 540 (sh), 635 nm], from the aforementioned Compound ES/II species, and from Compound RH [UV-vis: 411, 530, 564 nm; WT DHP A]. However, the spectral features are highly reminiscent of Compound I in other hemoproteins, including native Mb (*43*) and its His^{64} mutants (*44*), HRP (*45*),

Arthromyces ramosus peroxidase (*46*), peanut peroxidase (*47*), soybean peroxidase (*48*), and *Rhodnius prolixus* nitrophorin 2 (*49*). Thus, on the basis of spectral similarities to Compound I in other hemoproteins, such as the distinct hypochromicity of the Soret band as well as the appearance of a visible feature ~640-50 nm (*43, 50*), we assign this intermediate observed here as DHP A(Y34F/Y38F) Compound I. Although observable, this species rapidly decayed (k_{obs} = 5.4 ± 0.1 s^{-1}) in the absence of an exogenously added substrate to a more stable state [UV-vis: 414 nm (Soret), 505 (sh), 540, 589 (sh)] whose spectral features were not directly assignable to Compound II/ES. This state may represent an equilibrium mixture of Compounds I & ES, the latter being identified by our EPR study (vide infra) as well as by the red shift of the Soret band. At longer reaction times (up to 85 seconds), this state was unstable as evidenced by the UV-visible spectrum undergoing bleaching with minimal shifts in the absorbance maxima. As such, this decay was not further explored as it may represent a pathway not relevant to the catalytic cycle of DHP and its scope is outside the context of the present study.

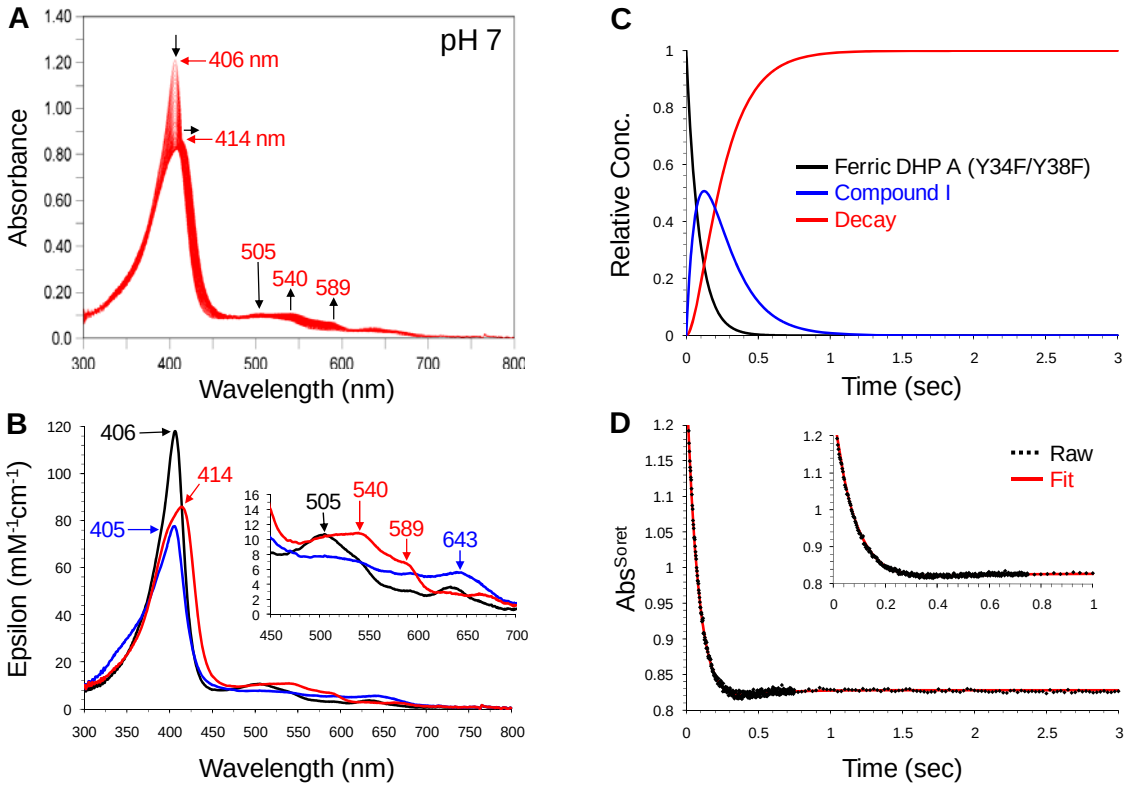

Figure V.4: (A) Stopped-flow UV-visible spectroscopic monitoring of the reaction (400 scans, 3 sec) between DHP A(Y34F/Y38F) (10 μM) and a 10-fold excess of H_2O_2 at pH 7.0. See experimental for details. (B) Calculated UV-visible spectra for both resting (black), Compound I (blue) and the decay species (red) of DHP A(Y34F/Y38F) are shown; the rapid-scanning data from A were compiled and fitted to a double exponential reaction model using the Specfit global analysis program. (C) Relative concentration profile determined from the three component fit used in (B). (D) The single wavelength trace (406 nm) of (A) and its fit from (B).

Stopped-flow UV-Visible Characterization of the Reaction of DHP B Mutants with H_2O_2. Under the same stopped-flow methods as those employed above, the formation of high-valent iron-oxo species in the tyrosine mutants of DHP B upon reaction with hydrogen peroxide at pH 7 was investigated. Rapid mixing of a solution of ferric DHP B(Y28F) [UV-visible spectrum: 407 (Soret), 510, 538 (sh), 640 nm] with a 10-fold excess of H_2O_2, a transient species was observed (Figure S2) whose spectral features [UV-visible: 419 (Soret), 545, 584 nm] we assign as the ferryl intermediate of Compound ES in DHP B(Y28F) based upon the spectroscopic arguments presented above for DHP A, as well as the results of our

EPR spectroscopic study (*vide infra*). Values of k_{obs} for formation of this new species were linearly dependent on $[H_2O_2]$ (2.5 – 25 fold excess per heme), giving a bimolecular rate constant of (1.56 ± 0.08) x 10^5 $M^{-1}s^{-1}$. The partial decay of DHP B(Y28F) Compound ES to a new species reminiscent of DHP B Compound RH was observed over the 3 second observation window under these conditions (k_{obs} = 6.2 ± 0.1 s^{-1}), and was complete after 85 seconds (vide infra). As Compound ES was observed for the Y28F mutant of DHP B, which also possesses the Y34N substitution, suggests that the Tyr→Phe mutation at position 28 does not appear to significantly alter the nature of the Compound ES intermediate formed (by UV-visible spectroscopy) when compared to WT DHP B.

However, when the mutant DHP B(Y38F) [UV-vis: 406 (Soret; ε = 119 $mM^{-1}cm^{-1}$), 506, 540 (sh), 636 nm] was rapidly reacted with hydrogen peroxide under the conditions employed above (Figure S3), a new species was formed [UV-visible: 405 (Soret; ε = 71 $mM^{-1}cm^{-1}$), 520 (broad), 644 nm; k_{obs} = (1.46 ± 0.08) x 10^5 $M^{-1}s^{-1}$] whose spectral features (Soret hypochromicity and λ_{max}) matched very well with those reported for DHP A(Y34F/Y38F) Compound I. Given that both DHP B(Y38F) and DHP A(Y34F/Y38F) both lack tyrosine residues at positions 34 and 38, it is not surprising that both exhibit the same chemistry and formed Compound I upon reaction with hydrogen peroxide. DHP B(Y38F) Compound I was found to be unstable, and rapidly converted (k_{obs} = 6.5 ± 0.1 s^{-1}) in the absence of an exogenously added substrate to a more stable state [UV-vis: 411 nm (Soret), 518, 540 (sh), 587 (sh)] whose spectral features were not assignable. The red shift of the Soret band suggests that Compound ES may have been partially formed (perhaps in equilibrium with Compound I), and was supported by the presence of a tyrosyl radical by EPR spectroscopy (vide infra). At longer observation times (up to 85 seconds), heme bleaching was noted (see Table 1).

A Compound I intermediate [UV-vis: 406 (Soret; ε = 64 $mM^{-1}cm^{-1}$), 528, 645 nm; k_{obs} = (1.64 ± 0.14) x 10^5 $M^{-1}s^{-1}$] was also observed upon reaction of DHP B(Y28F/Y38F) [UV-vis: 406 (Soret; ε = 118 $mM^{-1}cm^{-1}$), 504, 538 (sh), 636 nm] with a 10-fold excess of hydrogen peroxide (Figure V.5). Rapid decay (k_{obs} = 6.4 ± 0.1 s^{-1}) of this Compound I species yielded DHP that exhibited a ferric-like absorption spectrum [UV-vis: 404 nm

(Soret), 518, 542 (sh)] which lacked the red shifted Soret band that was observed in the decay products of the above mutants of DHP, and suggested the lack of an identifiable Compound ES species in this mutant. In agreement with this data, no tyrosyl radical was detectable in the EPR spectroscopic study of DHP B(Y28F/Y38F) (vide infra; Table 1). Heme bleaching was again noted at longer observation times (data not shown).

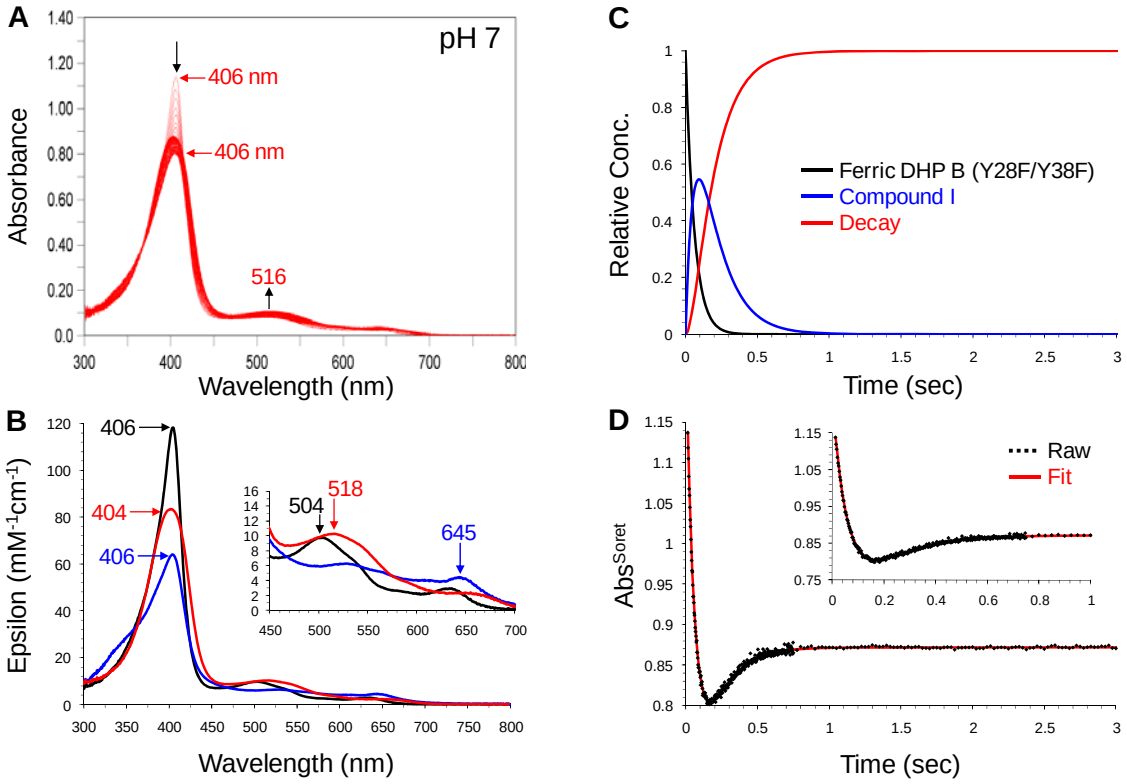

Figure V.5: (A) Stopped-flow UV-visible spectroscopic monitoring of the reaction (400 scans, 3 sec) between DHP B(Y28F/Y38F) (10 μM) and a 10-fold excess of H_2O_2 at pH 7.0. See experimental for details. (B) Calculated UV-visible spectra for both resting (black), Compound I (blue) and the decay species (red) of DHP B(Y28F/Y38Fare shown; the rapid-scanning data from A were compiled and fitted to a double exponential reaction model using the Specfit global analysis program. (C) Relative concentration profile determined from the three component fit used in (B). (D) The single wavelength trace (406 nm) of (A) and its fit from (B).

Characterization of Protein Radicals in Mutants of DHP A and B. Rapid-freeze-quench methods were employed to stabilize intermediates of the reaction between the

tyrosine mutants of DHP A or B (50 μM final) and a 10-fold excess of hydrogen peroxide at pH 7 for consequent characterization by continuous wave (CW) EPR. The X-band CW EPR spectra were obtained at various quench times for DHP A(Y34F) (Figure V.6), DHP A(Y38F) (Figure S4), and DHP A(Y34F/Y38F) (Figure S5). Free radicals were detected in both single mutants, as well as in the double mutant. Figure V.7, which displays the radical signals of the three mutants 0.5 seconds after mixing, clearly demonstrates that the radicals are different in all three cases – both the linsheapes and the g-factors measured at the crossover with the baseline are notably different. Specifically, the signals were characterized by an effective *g*-value of 2.0043 for DHP A(Y34F), 2.0046 for DHP A(Y38F), and 2.0074 for DHP A(Y34F/Y38F), with both the shape and intensity of the signal change as a function of quench time. At the longest quench times (60 s), when our component analyses suggested little to no remaining Compound ES present by UV-visible spectroscopy, the EPR signal intensity was observed to have dropped significantly, particularly for DHP A(Y34F/Y38F).

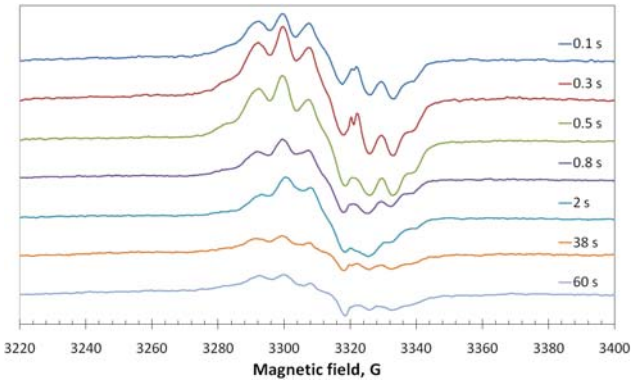

Figure V.6: The EPR spectra of the free radical freeze-quenched variable time after mixing 50 μM DHP A(Y34F) with 50 μM H_2O_2. The instrumental conditions for the spectra were: microwave frequency ν = 9.2977 GHz, microwave power P = xxx mW, modulation amplitude A_m = 4 G, spectra scan rate v = xxx G/s, number of scans per spectrum NS = 1.

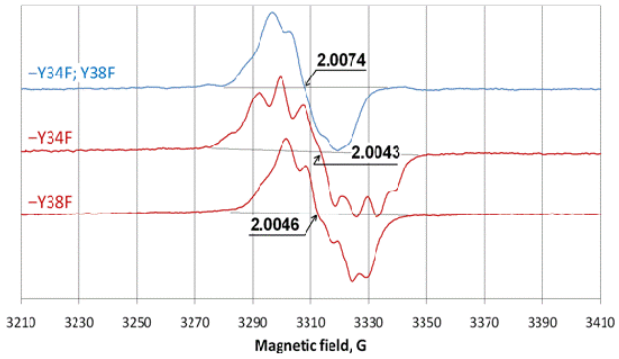

Figure V.7: The free radical EPR spectra of the three DHP A mutants after reaction with H_2O_2 at pH 7. In all three cases, the samples were freeze-quenched 0.5 s after mixing and the enzyme and H_2O_2 concentrations were 50 μM in the mixtures. Instrumental conditions are as specified in Figure V.6.

Previously, we observed that the protein radical in DHP A Compound ES exhibited an anisotropic quintet at pH 7, and an anisotropic septet at pH 5 (both at g = 2.0058) (*13*). More recently, we have demonstrated that two different tyrosyl radicals are formed in DHP A (*34*). On the basis of the EPR lineshapes of these two radicals, they were assigned to Y34 (the major, 'principal' species, seen as a sole free radical type at pH 7) and to Y38 (seen only at lower pH). Kinetic dependences of the radicals and of the ferric heme states of the enzyme, measured at different pH values, were in accordance with the view that the two radicals are formed in relationship with the distal His conformation. The current work with the mutants of DHP A (and DHP B, vide infra) confirms these assignments of the radicals: notably, the free radical spectrum in the DHP A(Y38F) mutant (Figures 7 & S4) is identical to the 'principal' radical previously assigned to Y34 in WT DHP A (Figure S6). When Y34 is replaced by phenylalanine as in DHP A(Y34F), the spectrum becomes identical to the 'pH 5 radical' signal previously assigned to Y38 in WT DHP A (Figure S7).

The spectral lineshape in Figure S7 is not a single species EPR signal. It consists of the Y38 radical signal, plus an additional one. In our previous work (*34*), we assumed that this additional signal was from the 'principal radical' Y34, and subtraction of the latter allowed us to identify what we believed was the pure lineshape of the Y38 radical spectrum. It appears now that in the mutant lacking Y34, the lineshape of the free radical EPR signal is very close to the raw pH 5 EPR spectra of WT DHP A. Interestingly, the spectrum is better

resolved in the mutant even at pH 7, where the Y38 radical is not detectable in the wild type. This indicates that there is yet another, a third type, of free radical in DHP. It is reasonable to suggest that this third type of radical is the one that is observable in the double mutant DHP A(Y34F/Y38F), where both Y34 and Y38 are replaced with phenylalanine (Figures 7 & S5).

The location of this radical might be speculated on the basis of the results and analysis of the isoform B mutants. As seen in Figure V.8, the double mutant DHP A(Y34F/Y38F) exhibited the same spectrum as DHP B(Y38F) (Figure S8), the latter possessing an asparagine at position 34 for this isoenzyme. This is a strong indication that in these mutants of two different DHP isoforms, the radical site is the same residue. Which residue can this be? One possibility is that it might be one of the other tyrosines in the molecule. If we mutate this residue out, the spectrum should revert to the Y38 radical type. If, however, we mutate a different tyrosine residue, which is not the site of the radical, the spectrum should stay as in Figure 8. Figure V.9 shows that when Y28 is replaced with a phenylalanine as in DHP B(Y28F) (Figure S9), the spectrum observed is similar to the one we interpreted before as the Y38 radical signal in DHP A. Therefore, we conclude that the EPR signals in Figure 8 originate from the Y28 site in DHP A(Y34F/Y38F) and DHP B(Y38F). One might argue that the EPR signals in Figure 8 are not exactly superimposable. We explain this by the fact that the DHP A signal was obtained as a result of spectral subtraction and the DHP B signal is a directly measured spectrum. In addition, the Y38 radical pure EPR lineshape is ‘contaminated’ with a Y34 radical signal in DHP A, and the same radical signal in DHP B is contaminated with a Y28 radical signal. Overall, however, it is important to highlight that all eight components in the lineshapes of the two signals coincide with a very good accuracy (Figure V.9). This is a strong indication that both spectra contain the same EPR signal.

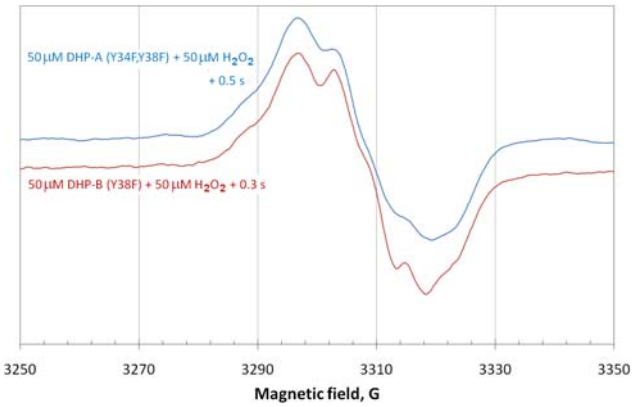

Figure V.8: The EPR spectra of the free radicals formed upon reaction of a 10-fold excess of H_2O_2 with 50 μM of DHP A (Y34F/Y38F) or DHP B(Y38F)

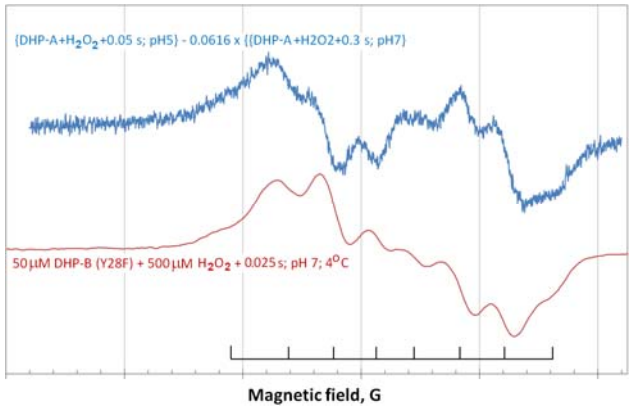

Figure V.9: The EPR spectra of the Y38 radical ('pH 5 radical') as a difference spectrum obtained by subtraction of the pH 7 signal from the pH 5 signal in WT DHP A and a spectrum detected for the Y28F mutant of DHP B under 10-fold molar excess of H_2O_2

Finally, when both Y28 and Y38 are muted to phenylalanine as in DHP B(Y28F/Y38F), the mutant did not exhibit any appreciable amount of free radicals upon reaction with H_2O_2. We surmise that this could be for the following alternative reasons: 1) The radical(s) are formed but dissipate via non-tyrosine residues much faster (damage to the protein and/or substrates must be much faster produced at similar peroxide concentrations); or 2) replacement of Y38 with a phenylalanine results in some changes in the distal side that result in the histidine permanently arrested in the closed conformation, and as a result H_2O_2 cannot access the active site and the reaction with peroxide proceeds extremely slowly. Based upon our stopped-flow UV-visible spectroscopic study, which clearly showed a rapid

reaction between H_2O_2 and the DHP B(Y28F/Y38F) mutant, we favor the possibility that the radicals do form but are rapidly dissipated in a manner that does not allow for their detection via conventional rapid-freeze-quench methodologies.

Lack of Formation of Compound RH. When the tyrosine mutants in the present study were reacted with a 10-fold excess of hydrogen peroxide in an identical manner that previously yielded Compound RH for the wild-type isoenzymes [DHP A, UV-vis: 411 (Soret), 530, 564 nm (*13*); DHP B, UV-vis: 411 (Soret), 554, 599 nm (*29*)], no clear formation of Compound RH was observed for the majority of the mutants after 85 seconds (Table 1; data not shown). Specifically, DHP A(Y38F), and DHP A(Y34F/Y38F) both exhibited bleached spectra (with minor 1-2 nm shifts in the Soret band) that were similar to Compound ES in the former, and to the 'mixed spectrum' species in the latter (data not shown). DHP B(Y38F) and DHP B(Y28F/Y38F) also exhibited bleaching of the spectrum that was formed after 3 seconds in the stopped-flow study (vide supra). Only DHP A(Y34F) [UV-vis: 416 (Soret), 560, 598 nm] and DHP B(Y28F) [UV-vis: 415 (Soret), 552, 598 nm] appeared to form a Compound RH-like species, however some caution is needed as neither spectrum matches exactly with authentic Compound RH from either isoenzyme, and may represent either incomplete Compound RH formation, or one whose electronic structure is different from that observed for the wild-type systems.

V.4. Discussion

Dehaloperoxidase isoenzymes A and B have been shown to catalyze the oxidative dehalogenation of 2,4,6-trihalogenated phenols to their corresponding 2,6-dihalo-1,4-benzoquinones in the presence of hydrogen peroxide. The overall reaction is consistent with the reactive species being a two-electron oxidized intermediate such as Compound I (ferryl + porphyrin π-cation radical) or Compound ES (ferryl + protein radical), with several reports identifying the latter species as being invoked in catalytic cycle of DHP as the active oxidant (*13, 24, 29*). Although the evidence for a tyrosyl radical in the Compound ES intermediate is compelling, determining the location of the protein radical is complicated by the presence of five tyrosine residues in DHP A, and four in isoenzyme B. Recently, it was proposed that two

free radicals are formed in DHP A upon reaction with H_2O_2 (*34*). To make these proposed assignments, the tyrosyl radical EPR spectrum of DHP A was simulated using parameters generated by the Tyrosyl Radical Spectra Simulation Algorithm (TRSSA) (*51*), which relies upon two input parameters, the phenoxyl ring rotation angle (θ) and the spin density on atom C1 of the radical (ρ_{C1}). These were used to calculate twelve different EPR spectral simulation parameters ($g_{x,y,z}$, $A^{\beta 1}{}_{x,y,z}$, $A^{\beta 2}{}_{x,y,z}$, and $\Delta H_{x,y,z}$) using semi-empirical dependences, then combined with another 18 (ϕ and $A_{x,y,z}$ for C3, C5, C2, and C6; $\phi^{\beta 1}$ and $\phi^{\beta 2}$) that are set invariant in the algorithm for all tyrosyl radicals, and were subsequently used to simulate the EPR spectra of Compound ES using *Simpow6* (*52*). The derived θ-value that led to an accurate simulation was then compared to tyrosine residues with similar θ angles using the Phenol Ring Rotation Angle Database, which when correlated with the known geometries of all the tyrosine residues from the available crystal structures of DHP, led to an assignment of the tyrosine candidate(s) likely to host the radical in wild-type dehaloperoxidase. However, in light of the limitations of simulating the poorly resolved hyperfine splitting observed for DHP A and B at low field, confirmation of the location of radical formation using experimental methods is necessary to unambiguously assign the nature of the protein radical in DHP Compound ES, and is thus the focus of the present report.

Of the five tyrosine residues which DHP possesses (Figure 1: Tyr^{16}, Tyr^{28}, Tyr^{34}, Tyr^{38}, Tyr^{107}), only three are reasonably close to the heme prosthetic group to be considered likely candidates for reducing Compound I initially, Tyr^{28}, Tyr^{34} and Tyr^{38}; the closest contact between Tyr^{34} and the heme edge is ~5.6 Å (Tyr Cγ), whereas Tyr^{38} is ~7.5 Å (phenolic oxygen), and Tyr^{28} is ~10.5 Å (Tyr Cδ). The remaining two tyrosine residues, Tyr^{16} and Tyr^{107}, are greater than 15 Å from the heme edge, making them unlikely candidates as the residues responsible for the initial reduction of a transiently formed Compound I intermediate. For DHP A, two different radicals were identified as being both present in Compound ES, a primary tyrosyl radical that is characterized by a phenoxyl ring rotation angle of 45° or 75° and was suggested to correspond to either Tyr^{34} or Tyr^{28}, and a secondary radical that was suggested to reside on Tyr^{38} (*34*). By extending this interpretation to the observed heterogeneity of the EPR lineshape in DHP B, which lacks a tyrosine at position

34, it was suggested that the radical initially forms in that isoenzyme on Tyr^{28} and Tyr^{38} (*29*). Thus, single and double mutants of DHP A and B were generated wherein these three tyrosine residues were mutated to phenylalanine, and were subsequently investigated by stopped-flow UV-visible and rapid-freeze-quench EPR spectroscopic methods to follow the formation of the high-valent iron(IV)-oxo and protein radical species, respectively, for the reaction of DHP with H_2O_2.

The single mutants of DHP A (as Y34F or Y38F) and the mutant DHP B(Y28F) all formed Compound ES upon reaction with hydrogen peroxide without the formation of an observable Compound I intermediate, similar to WT DHP A and B (*13, 29, 34*). The stopped-flow UV-visible spectroscopic data revealed that the formation of Compound I was observable only when both Tyr^{34} and Tyr^{38} were absent together, as in DHP A(Y34F/Y38F), DHP B(Y38F), and DHP B(Y28F/Y38F) [note: DHP B has an Asp substituted at position 34 rather than the Tyr that is found in isoenzyme A]. For DHP A(Y34F/Y38F) and DHP B(Y38F), the Compound I intermediate was found to partially convert to Compound ES, as indicated by both a red-shift of the Soret band and the presence of a tyrosyl radical EPR spectrum, suggesting the presence of yet another (secondary) endogenous reducing species. Only in DHP B(Y28F/Y38F) was no Compound ES observed by either UV-visible or RFQ-EPR spectroscopies, thus leading to the conclusion that while Tyr^{34} and Tyr^{38} may be the primary endogenous reductants of Compound I, Tyr^{28} was a viable one as well, albeit the rate of reduction was slower given its further position from the heme active site when compared to the other two residues.

Previously, we suggested that the time-dependent changes observed in the protein radical signal of WT DHP A Compound ES were indicative of either a change in the local electronic structure of the radical, or a migration of the radical out of the active site to other redox active protein side-chains upon decay of Compound ES. This latter possibility is not without precedent. The reaction of sperm whale Mb with hydrogen peroxide yields covalent dimers that arise from the coupling of surface tyrosyl radicals (Tyr^{151}), which results from a radical migration out of the Mb active site (*53*). Further, tyrosyl radicals have been proposed to play a role in the peroxidase mechanism of Mb (*54*). In CcP, the initial Trp^{191} radical in

Compound ES leads to a radical migration which is ultimately responsible for oxidizing substrate (cytochrome c) at the surface of the peroxidase (protein-protein interface) (*55*). Thus, as CcP may have evolved from traditional (heme-edge electron transfer) peroxidases an external binding interface for oxidizing cytochrome c, DHP may also similarly have evolved from Mb an external binding pocket for oxidizing trihalophenols. It is noteworthy that the protein radical signal of DHP A(Y38F) exhibited minimal time-dependent changes when compared to those observed for DHP A(Y34F), suggesting that the radical in DHP A(Y38F) was more localized on Tyr^{34} when compared to the radical in DHP A(Y34F), which showed migration from Tyr^{38} to Tyr^{28}. Not surprisingly, similar time-dependent changes were observed for WT DHP B previously as those noted here for DHP A(Y34F). As Tyr^{38} is relatively buried when compared to Tyr^{34} and Tyr^{28}, these observations can be interpreted in light of the hypothesized external binding pocket for trihalophenol substrates. If TXP oxidation occurs externally on the surface of dehaloperoxidase, then surface tyrosine residues such as Tyr^{34} and Tyr^{28} would be able to serve as a redox conduit between the hypothesized external binding pocket and the heme active site. In WT DHP A and DHP A(Y38F), both possess the surface accessible Tyr^{34} residue, which is the closest tyrosine to the heme active site, and therefore do not require further radical migration to effect substrate oxidation. In WT DHP B and DHP A(Y34F), both lack the surface accessible Tyr^{34} residue, and the radical forms on the next closest tyrosine residue, Tyr^{38}, before migrating to the closest surface-accessible tyrosine, Tyr^{28}. No radical migration from Tyr^{38} to Tyr^{16} nor Tyr^{107} was observed, likely due to the >16 Å distance between these residues. Interestingly, although Tyr^{28} was able to reduce Compound I and form Compound ES at a distance of 10.6 Å in DHP A(Y34F/Y38F), it was unable to reduce Tyr^{34} at the shorter distance of ~9.6 Å (i.e. no migration from Tyr^{34} to Tyr^{28}) in WT DHP A or DHP A(Y38F), indicative of a preferential localization of the radical on Tyr^{34} (perhaps due to thermodynamic considerations). Overall, these results can be interpreted in support of an external binding site for trihalophenol substrate that is in preferential proximity to Tyr^{34} in WT DHP A, and to Tyr^{28} in WT DHP B, although not necessarily mutually exclusive.

As previously reported, in the absence of a reducing substrate, a new species of DHP termed Compound RH was observed to form upon the decay of Compound ES in the wild-type enzyme (*13, 29*). The Compound RH species of DHP A [UV-vis: 411 (Soret), 530, 564 nm (*13*)] and DHP B [UV-vis: 411 (Soret), 554, 599 nm (*29*)] were shown to possess unique spectral features in the Q band region, as well as attenuated dehaloperoxidase activity. Recently, it has been suggested that the formation of Compound RH and of the Tyr^{38} radical are two alternative routes of Compound ES decay, and that the specific route that is taken depends on the conformation of the distal His^{55}, which has been observed in distinct 'open' and 'closed' conformations: in the less populated closed conformation (6c HS), the Tyr^{38} radical is formed, but in the major open conformation (5c HS), Compound ES decays, yielding Compound RH (*34*). The conformational flexibility of the distal histidine, His^{55}, therefore may impact radical formation as it relates to Compound RH formation in a manner that can be correlated with the UV-visible spectroscopic analysis (A_{Soret}/A_{380} ratio) that is a measure of the relative populations of 5- or 6c HS heme. Consistent with this hypothesis, only when Tyr^{38} was present leading to the distal histidine being present in the open conformation, as in WT DHP A, DHP A(Y34F), WT DHP B, and DHP (Y28F), was a Compound RH-like species formed. Moreover, these four DHP proteins exhibited an A_{Soret}/A_{380} ratio that represented a greater relative population of 5c HS heme. In the case of the other four DHP mutants [DHP A(Y38F), DHP A(Y34F/Y38F), DHP B(Y38F) and DHP B(Y28F/Y38F)], the absence of Tyr^{38} shifts the relative population of the heme towards 6c HS and a 'closed' conformation of the distal histidine. The closed conformation normally leads to a DHP biradical (Y38• and Y34•), however as these mutants lack Tyr^{38}, the biradical state was not achievable, and thus heme bleaching was the observed consequence.

While the exact nature of the Compound RH species will require further study, overall its formation appears to require the distal histidine to be in the open conformation, and mutations that effect protein structure, which in turn alters the ratio of 5c : 6c HS heme, may circumvent its formation and putative role as a protective species. We have surmised that when functioning as a peroxidase, DHP inactivation may be necessary to prevent non-specific oxidation of other metabolites from occurring when trihalophenol substrate is absent

(*13*). While heme bleaching is a normal route for peroxidase inactivation as in HRP (*56*), this could be metabolically costly for *A. ornata* given that DHP is its coelomic hemoglobin. Formation of Compound RH, however, could allow for dehaloperoxidase to be inactivated without sacrificing the protein to heme bleaching. As the oxyferrous form of the enzyme can be generated from Compound RH under reducing conditions (i.e. sodium dithionite), the Compound RH species may represent serve as a functional switch back to an oxygen transport protein via a reductive pathway while protecting *A. ornata* from deleterious and undesired peroxidase activity in the absence of trihalophenol.

Conclusion

The present study provides compelling evidence in support of a unique structure-function relationship in DHP that links together the conformational flexibility of the distal histidine with the location of the tyrosyl radical in Compound ES. By using a combination of single and double tyrosine mutants of DHP A and B to establish the spectral features of individual tyrosyl radicals, it was possible to deconvolute the EPR spectrum of Compound ES in the wild-type enzyme to provide unambiguous assignments of the tyrosine residues responsible for the *in situ* endogenous reduction of Compound I. The mutation of both Tyr^{34} and Tyr^{38} was required in order to identify Compound I using stopped-flow UV-visible spectroscopic methods. These two mutations were not sufficient, however, to fully arrest the formation of Compound ES. Remarkably, the additional mutation of Tyr^{28}, over 10 Å from the heme active site, was required to prevent any protein radical from being observed. Preferential site localization of the tyrosyl radical was also noted, suggesting that external binding of the trihalophenol substrate may occur in proximity to Tyr^{34} and Tyr^{28} for DHP A and B, respectively, and possibly indicative of a radical migration pathway in DHP analogous to that in CcP. Formation of the peroxidase-attenuated species Compound RH was only noted when Tyr^{38} was present. This observation was rationalized by considering the effect of this residue on the conformation of the distal histidine as revealed by the relative population of 5- and 6c HS heme present. Namely, the presence of Tyr^{38} leads to the pathway for Compound RH formation proposed by Thompson et al. (*34*) that is mediated by the distal

histidine in the open conformation. In the absence of Tyr[38], the biradical state that is normally associated with the closed conformation of the distal histidine cannot form, thereby leading to heme bleaching. Finally, the EPR spectroscopic data presented herein is in full agreement with, and provides experimental confirmation of, the simulations derived from the theoretical parameters predicted by the TRSSA. When combined with the phenol ring rotation angle database, the TRSSA represents a powerful predictive tool that can not only aid in assigning tyrosyl spectra, but can be used to rationally designing mutants for mechanistic investigations of electron-transfer pathways, for probing protein structure-function relationships, or for enzyme engineering.

Acknowledgments. We acknowledge financial support for this work by the North Carolina State University Molecular Biotechnology Training Program through an NIH T32 Biotechnology Traineeship grant (J. D.), and the Army Research Office Grant 57861-LS (R. G.). EPR instrumentation employed in this work has been supported by NIH S10RR023614, NSF CHE-0840501, and NCBC 2009-IDG-1015 (T. S.).

Supporting Information Available. Stopped-flow UV-visible spectroscopic monitoring of the reaction between DHP and a 10-fold excess of H_2O_2 at pH 7 for DHP A(Y38F) (Figure S1), DHP B(Y28F) (Figure S2), and DHP B(Y38F) (Figure S3), the RFQ-EPR spectra of the free radical in DHP A(Y38F) (Figure S4) and DHP A(Y34F/Y38F) (Figure S5), comparison of the EPR spectra of the Y34 radical in WT DHP A and in DHP A(Y38F) (Figure S6), comparison of the EPR spectra of the Y38 radical in WT DHP A and in DHP A(Y34F) (Figure S7), and the RFQ-EPR spectra of the free radical(s) in DHP B(Y38F) (Figure S4) and DHP B(Y28F) (Figure S5). This material is available free of charge via the Internet at http://pubs.acs.org

Supporting Information

Mutagenesis Studies of Dehalopeoxidase A and B: Compound I Formation and the Tyrosine Radical in Compound ES

Contents

Figure V.S1. (A) Stopped-flow UV-visible spectroscopic monitoring of the reaction (400 scans, 3 sec) between DHP A(Y38F) (10 μM) and a 10-fold excess of H_2O_2 at pH 7.0. See experimental for details. (B) Calculated UV-visible spectra for both resting (black) and Compound ES (red) DHP A(Y38F) are shown; the rapid-scanning data from A were compiled and fitted to a single exponential reaction model using the Specfit global analysis program. (C) Relative concentration profile determined from the two component fit used in (B). (D) The single wavelength trace (407 nm) of (A) and its fit from (B).

Figure V.S2. (A) Stopped-flow UV-visible spectroscopic monitoring of the reaction (400 scans, 3 sec) between DHP B(Y28F) (10 μM) and a 10-fold excess of H_2O_2 at pH 7.0. See experimental for details. (B) Calculated UV-visible spectra for both resting (black), Compound ES (red), and the decay product (green) of DHP B(Y28F) are shown; the rapid-scanning data from A were compiled and fitted to a double exponential reaction model using the Specfit global analysis program. (C) Relative concentration profile determined from the three component fit used in (B). (D) The single wavelength trace (408 nm) of (A) and its fit from (B).

Figure V.S3. (A) Stopped-flow UV-visible spectroscopic monitoring of the reaction (400 scans, 3 sec) between DHP B(Y38F) (10 μM) and a 10-fold excess of H_2O_2 at pH 7.0. See experimental for details. (B) Calculated UV-visible spectra for both resting (black), Compound I (blue), and the decay product (red) of DHP B(Y38F) are shown; the rapid-scanning data from A were compiled and fitted to a double exponential reaction model using the Specfit global analysis program. (C) Relative concentration profile determined from the three component fit used in (B). (D) The single wavelength trace (406 nm) of (A) and its fit from (B).

Figure V.S4. The EPR spectra of the free radical freeze-quenched variable time after mixing 50 μM DHP A(Y38F) with 50 μM H_2O_2. The instrumental conditions for the spectra were: microwave frequency ν = 9.2977 GHz, microwave power P = xxx mW, modulation amplitude A_m = 4 G, spectra scan rate ν = xxx G/s, number of scans per spectrum NS = 1.

Figure V.S5. The EPR spectra of the free radical freeze-quenched variable time after mixing 50 μM DHP A(Y34F/Y38F) with 50 μM H_2O_2. Instrumental conditions are as specified in Figure V.S4.

Figure V.S6. The EPR spectra of the Y34 radical in wild type DHP A (as reported in [Thompson et al., JACS 2010] and in the Y38F mutant. As the two spectra were measured on different EPR spectrometers operated at slightly different microwave frequencies, therefore they appear at different magnetic field values. The spectra were overplayed on the basis of common g-factors and the magnetic field values are not shown. The distance between the vertical gridlines are 20 G.

Figure V.S7. The EPR spectra showing the presence of the Y38 radical in wild type DHP A at pH 5 (as reported in [Thompson et al., JACS 2010] and in the DHP A(Y34F) mutant at pH 7. As in Figure S6, the two spectra were measured on different EPR spectrometers and the magnetic field values are not shown. The distance between the vertical gridlines are 20 G.

Figure V.S8. EPR spectra of the radical(s) in DHP B(Y38F) Compound ES at pH 7. Rapid-freeze quench samples were prepared from the reaction of ferric DHP B(Y38F) (50 μM final concentration) with a 10-fold molar excess of H_2O_2 at 25 °C, and rapidly frozen in an isopentane slurry. Spectra were recorded at 77 K using the spectrometer settings described in the Materials and Methods section. The cavity resonant frequency was 9.29651 GHz.

Figure V.S9. EPR spectra of the radical(s) in DHP B(Y28F) Compound ES at pH 7. Rapid-freeze quench samples were prepared from the reaction of ferric DHP B(Y28F) (50 μM final concentration) with a 10-fold molar excess of H_2O_2 at 25 °C, and rapidly frozen in an isopentane slurry. Spectra were recorded at 77 K using the spectrometer settings described in the Materials and Methods section. The cavity resonant frequency was 9.28311 GHz. The presence of a minor amount of quartz signal from the EPR tube that could not be fully subtracted is indicated by the asterisk.

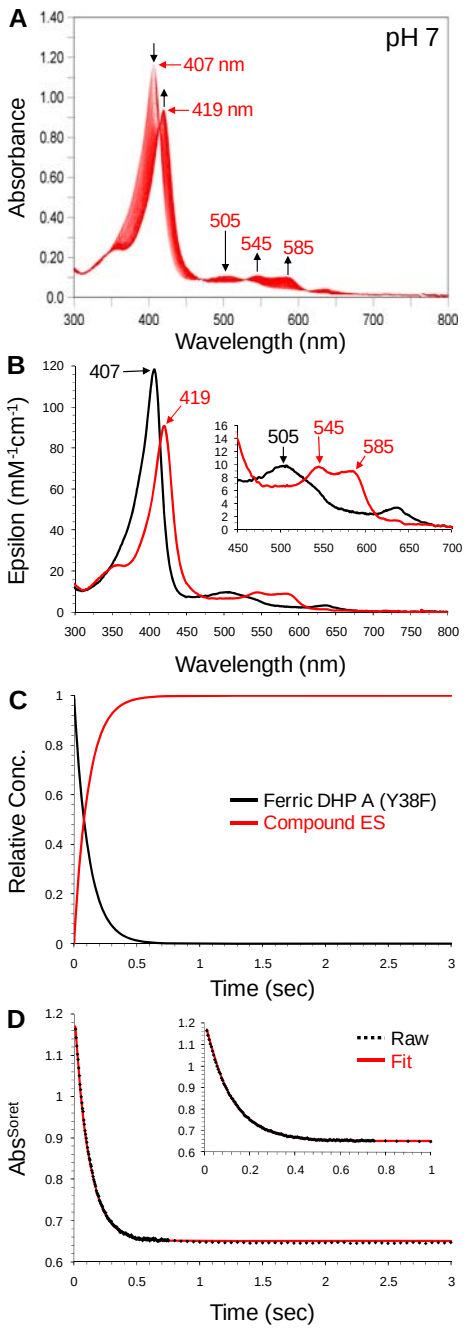

Figure V.S1: (A) Stopped-flow UV-visible spectroscopic monitoring of the reaction (400 scans, 3 sec) between DHP A(Y38F) (10 μM) and a 10-fold excess of H_2O_2 at pH 7.0. See experimental for details. (B) Calculated UV-visible spectra for both resting (black) and Compound ES (red) DHP A(Y38F) are shown; the rapid-scanning data from A were compiled and fitted to a single exponential reaction model using the Specfit global analysis program. (C) Relative concentration profile determined from the two component fit used in (B). (D) The single wavelength trace (407 nm) of (A) and its fit from (B).

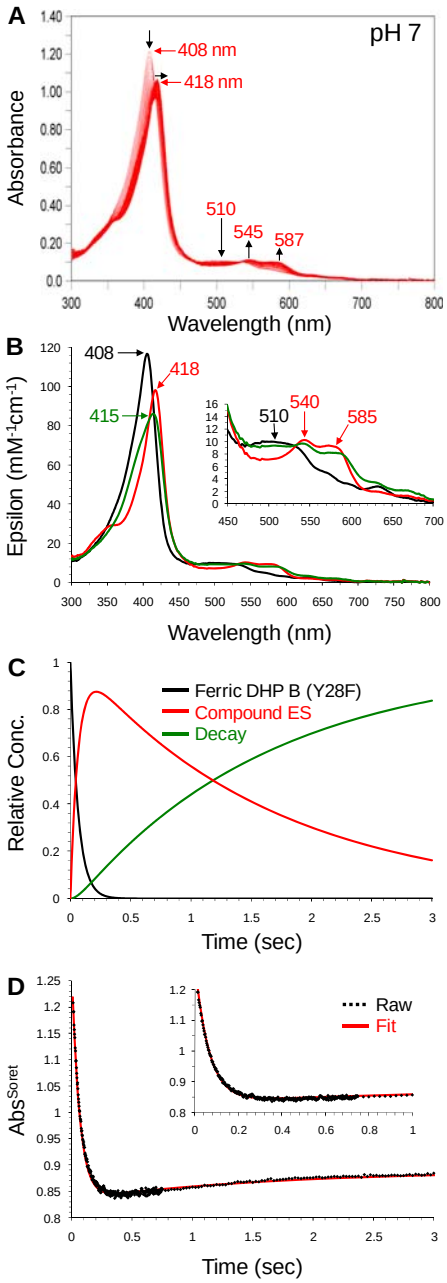

Figure V.S2: (A) Stopped-flow UV-visible spectroscopic monitoring of the reaction (400 scans, 3 sec) between DHP B(Y28F) (10 μM) and a 10-fold excess of H_2O_2 at pH 7.0. See experimental for details. (B) Calculated UV-visible spectra for both resting (black), Compound ES (red), and the decay product (green) of DHP B(Y28F) are shown; the rapid-scanning data from A were compiled and fitted to a double exponential reaction model using the Specfit global analysis program. (C) Relative concentration profile determined from the three component fit used in (B). (D) The single wavelength trace (408 nm) of (A) and its fit from (B).

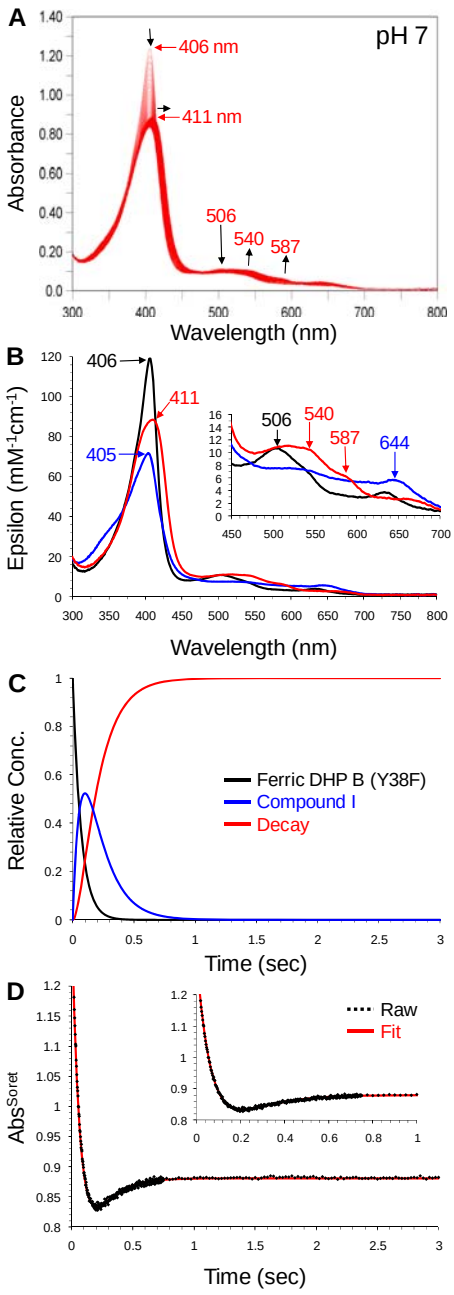

Figure V.S3: (A) Stopped-flow UV-visible spectroscopic monitoring of the reaction (400 scans, 3 sec) between DHP B(Y38F) (10 μM) and a 10-fold excess of H_2O_2 at pH 7.0. See experimental for details. (B) Calculated UV-visible spectra for both resting (black), Compound I (blue), and the decay product (red) of DHP B(Y38F) are shown; the rapid-scanning data from A were compiled and fitted to a double exponential reaction model using the Specfit global analysis program. (C) Relative concentration profile determined from the three component fit used in (B). (D) The single wavelength trace (406 nm) of (A) and its fit from (B).

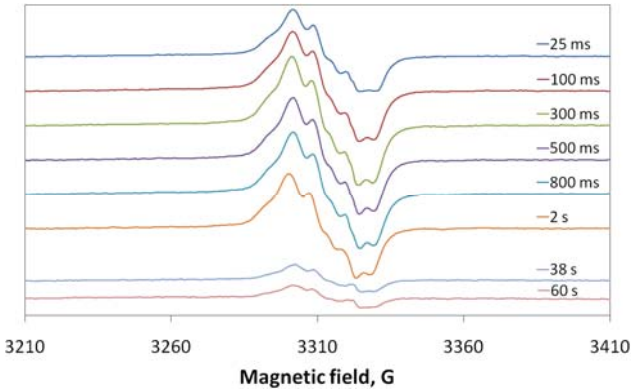

Figure V.S4: The EPR spectra of the free radical freeze-quenched variable time after mixing 50 μM DHP A(Y38F) with 50 μM H_2O_2. The instrumental conditions for the spectra were: microwave frequency ν = 9.2977 GHz, microwave power P = 2 mW, modulation amplitude A_m = 4 G, spectra scan rate v = 3.33 G/s.

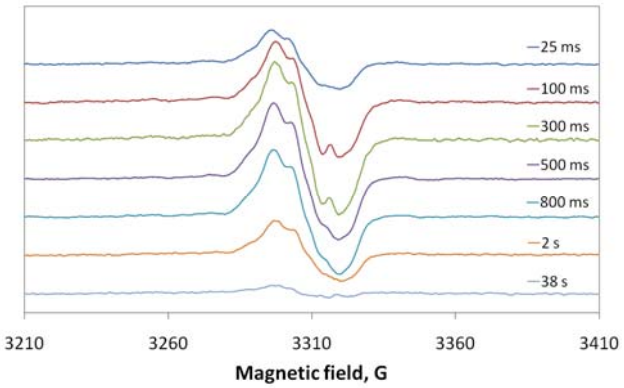

Figure V.S5: The EPR spectra of the free radical freeze-quenched variable time after mixing 50 μM DHP A(Y34F/Y38F) with 50 μM H_2O_2. Instrumental conditions are as specified in Figure V.S4.

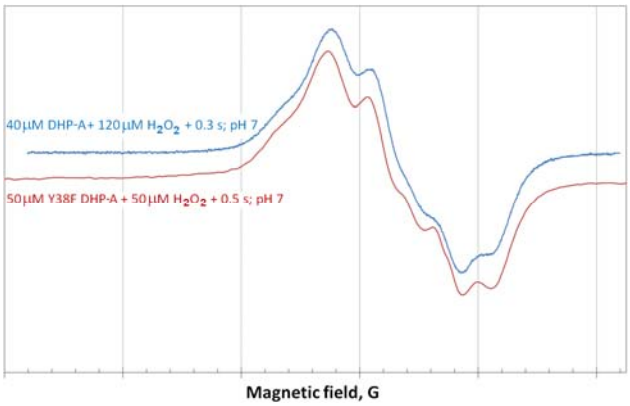

Figure V.S6: The EPR spectra of the Y34 radical in wild type DHP A (as reported in [Thompson et al., JACS 2010] and in the Y38F mutant. As the two spectra were measured on different EPR spectrometers operated at slightly different microwave frequencies, therefore they appear at different magnetic field values. The spectra were overplayed on the basis of common g-factors and the magnetic field values are not shown. The distance between the vertical gridlines are 20 G.

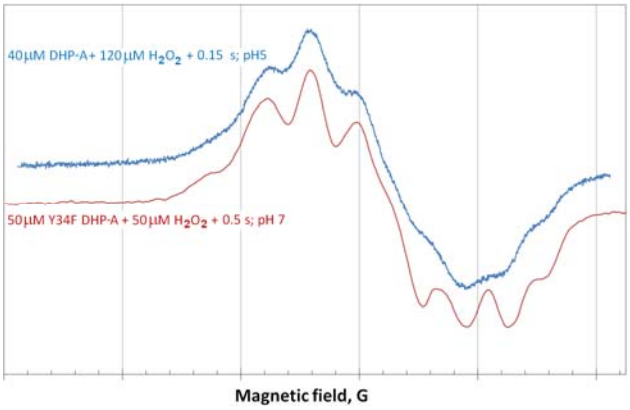

Figure V.S7: The EPR spectra showing the presence of the Y38 radical in wild type DHP A at pH 5 (as reported in [Thompson et al., JACS 2010] and in the DHP A(Y34F) mutant at pH 7. As in Figure S6, the two spectra were measured on different EPR spectrometers and the magnetic field values are not shown. The distance between the vertical gridlines are 20 G.

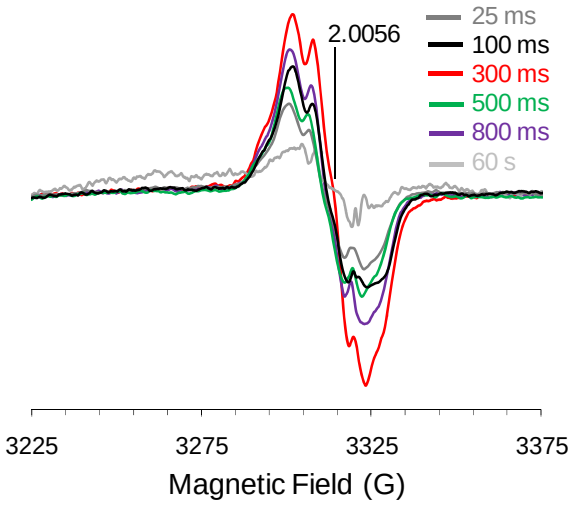

Figure V.S8: EPR spectra of the radical(s) in DHP B(Y38F) Compound ES at pH 7. Rapid-freeze quench samples were prepared from the reaction of ferric DHP B(Y38F) (50 µM final concentration) with a 10-fold molar excess of H_2O_2 at 25 °C, and rapidly frozen in an isopentane slurry. Spectra were recorded at 77 K using the spectrometer settings described in the Materials and Methods section. The cavity resonant frequency was 9.29651 GHz.

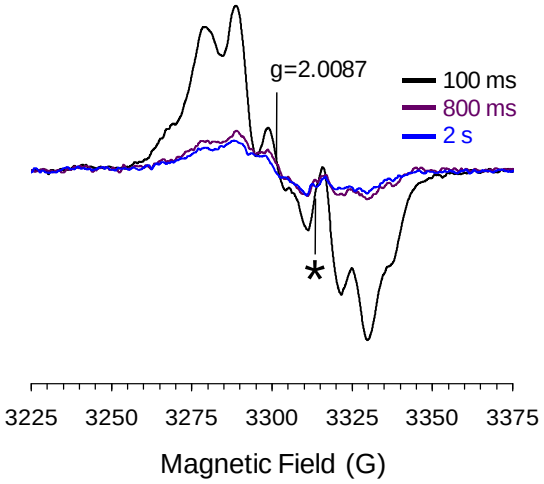

Figure V.S9: EPR spectra of the radical(s) in DHP B(Y28F) Compound ES at pH 7. Rapid-freeze quench samples were prepared from the reaction of ferric DHP B(Y28F) (50 µM final concentration) with a 10-fold molar excess of H_2O_2 at 25 °C, and rapidly frozen in an isopentane slurry. Spectra were recorded at 77 K using the spectrometer settings described in the Materials and Methods section. The cavity resonant frequency was 9.28311 GHz. The presence of a minor amount of quartz signal from the EPR tube that could not be fully subtracted is indicated by the asterisk.

REFERENCES

1. Welinder, K. G. (1992) Superfamily of Plant, Fungal, and Bacterial Peroxidases. *Curr Opin Struct Biol 2*, 388-393.

2. Zamocky, M., Jakopitsch, C., Furtmuller, P. G., Dunand, C., and Obinger, C. (2008) The peroxidase-cyclooxygenase superfamily: Reconstructed evolution of critical enzymes of the innate immune system. *Proteins 72*, 589-605.

3. Weber, R. E., Mangum, C., Steinman, H., Bonaventura, C., Sullivan, B., and Bonaventura, J. (1977) Hemoglobins of two terebellid polychaetes: Enoplobranchus sanguineus and Amphitrite ornata. *Comp Biochem Physiol A Comp Physiol 56*, 179-187.

4. Chiancone, E., Ferruzzi, G., Bonaventura, C., and Bonaventura, J. (1981) Amphitrite-Ornata Erythrocruorin.2. Molecular Controls of Function. *Biochim Biophys Acta 670*, 84-92.

5. Chiancone, E., Brenowitz, M., Ascoli, F., Bonaventura, C., and Bonaventura, J. (1980) Amphitrite-Ornata Erythrocruorin.1. Structural-Properties and Characterization of Subunit Interactions. *Biochim Biophys Acta 623*, 146-162.

6. Chen, Y. P., Lincoln, D. E., Woodin, S. A., and Lovell, C. R. (1991) Purification and Properties of a Unique Flavin-Containing Chloroperoxidase from the Capitellid Polychaete Notomastus-Lobatus. *J Biol Chem 266*, 23909-23915.

7. Roach, M. P., Chen, Y. P., Woodin, S. A., Lincoln, D. E., Lovell, C. R., and Dawson, J. H. (1997) Notomastus lobatus chloroperoxidase and Amphitrite ornata dehaloperoxidase both contain histidine as their proximal heme iron ligand. *Biochem 36*, 2197-2202.

8. Lincoln, D. E., Fielman, K. T., Marinelli, R. L., and Woodin, S. A. (2005) Bromophenol accumulation and sediment contamination by the marine annelids Notomastus lobatus and Thelepus crispus. *Biochem Syst Ecol 33*, 559-570.

9. King, G. M. (1986) Inhibition of Microbial Activity in Marine-Sediments by a Bromophenol from a Hemichordate. *Nature 323*, 257-259.

10. Fielman, K. T., and Targett, N. M. (1995) Variation of 2,3,4-Tribromopyrrole and Its Sodium Sulfamate Salt in the Hemichordate Saccoglossus-Kowalevskii. *Mar Ecol-Prog Ser 116*, 125-136.

11. Chen, Y. P., Woodin, S. A., Lincoln, D. E., and Lovell, C. R. (1996) An unusual dehalogenating peroxidase from the marine terebellid polychaete Amphitrite ornata. *J Biol Chem 271*, 4609-4612.

12. Osborne, R. L., Taylor, L. O., Han, K. P., Ely, B., and Dawson, J. H. (2004) Amphitrite ornata dehaloperoxidase: enhanced activity for the catalytically active globin using MCPBA. *Biochem Biophys Res Commun 324*, 1194-1198.

13. Feducia, J., Dumarieh, R., Gilvey, L. B., Smirnova, T., Franzen, S., and Ghiladi, R. A. (2009) Characterization of dehaloperoxidase compound ES and its reactivity with trihalophenols. *Biochem 48*, 995-1005.

14. Chen, Z., de Serrano, V., Betts, L., and Franzen, S. (2009) Distal histidine conformational flexibility in dehaloperoxidase from Amphitrite ornata. *Acta Crystallogr D Biol Crystallogr 65*, 34-40.

15. Davis, M. F., Gracz, H., Vendeix, F. A., de Serrano, V., Somasundaram, A., Decatur, S. M., and Franzen, S. (2009) Different modes of binding of mono-, di-, and trihalogenated phenols to the hemoglobin dehaloperoxidase from Amphitrite ornata. *Biochem 48*, 2164-2172.

16. Smirnova, T. I., Weber, R. T., Davis, M. F., and Franzen, S. (2008) Substrate binding triggers a switch in the iron coordination in dehaloperoxidase from Amphitrite ornata: HYSCORE experiments. *J Am Chem Soc 130*, 2128-2129.

17. Miksovska, J., Horsa, S., Davis, M. F., and Franzen, S. (2008) Conformational dynamics associated with photodissociation of CO from dehaloperoxidase studied using photoacoustic calorimetry. *Biochem 47*, 11510-11517.

18. Nienhaus, K., Nickel, E., Davis, M. F., Franzen, S., and Nienhaus, G. U. (2008) Determinants of substrate internalization in the distal pocket of dehaloperoxidase hemoglobin of Amphitrite ornata. *Biochem 47*, 12985-12994.

19. Franzen, S., Gilvey, L. B., and Belyea, J. L. (2007) The pH dependence of the activity of dehaloperoxidase from Amphitrite ornata. *Biochim Biophys Acta 1774*, 121-130.

20. de Serrano, V., Chen, Z., Davis, M. F., and Franzen, S. (2007) X-ray crystal structural analysis of the binding site in the ferric and oxyferrous forms of the recombinant heme dehaloperoxidase cloned from Amphitrite ornata. *Acta Crystallogr D Biol Crystallogr 63*, 1094-1101.

21. Franzen, S., Jasaitis, A., Belyea, J., Brewer, S. H., Casey, R., MacFarlane, A. W. t., Stanley, R. J., Vos, M. H., and Martin, J. L. (2006) Hydrophobic distal pocket affects NO-heme geminate recombination dynamics in dehaloperoxidase and H64V myoglobin. *J Phys Chem B 110*, 14483-14493.

22. Franzen, S., Belyea, J., Gilvey, L. B., Davis, M. F., Chaudhary, C. E., Sit, T. L., and Lommel, S. A. (2006) Proximal cavity, distal histidine, and substrate hydrogen-bonding

mutations modulate the activity of Amphitrite ornata dehaloperoxidase. *Biochem 45*, 9085-9094.

23. Belyea, J., Belyea, C. M., Lappi, S., and Franzen, S. (2006) Resonance Raman study of ferric heme adducts of dehaloperoxidase from Amphitrite ornata. *Biochem 45*, 14275-14284.

24. Osborne, R. L., Coggins, M. K., Raner, G. M., Walla, M., and Dawson, J. H. (2009) The mechanism of oxidative halophenol dehalogenation by Amphitrite ornata dehaloperoxidase is initiated by H2O2 binding and involves two consecutive one-electron steps: role of ferryl intermediates. *Biochem 48*, 4231-4238.

25. Osborne, R. L., Coggins, M. K., Walla, M., and Dawson, J. H. (2007) Horse heart myoglobin catalyzes the H2O2-dependent oxidative dehalogenation of chlorophenols to DNA-binding radicals and quinones. *Biochem 46*, 9823-9829.

26. Osborne, R. L., Raner, G. M., Hager, L. P., and Dawson, J. H. (2006) C. fumago chloroperoxidase is also a dehaloperoxidase: oxidative dehalogenation of halophenols. *J Am Chem Soc 128*, 1036-1037.

27. Osborne, R. L., Sumithran, S., Coggins, M. K., Chen, Y. P., Lincoln, D. E., and Dawson, J. H. (2006) Spectroscopic characterization of the ferric states of Amphitrite ornata dehaloperoxidase and Notomastus lobatus chloroperoxidase: His-ligated peroxidases with globin-like proximal and distal properties. *J Inorg Biochem 100*, 1100-1108.

28. Davydov, R., Osborne, R. L., Shanmugam, M., Du, J., Dawson, J. H., and Hoffman, B. M. (2010) Probing the oxyferrous and catalytically active ferryl states of Amphitrite ornata dehaloperoxidase by cryoreduction and EPR/ENDOR spectroscopy. Detection of compound I. *J Am Chem Soc 132*, 14995-5004.

29. D'Antonio, J., D'Antonio, E. L., Thompson, M. K., Bowden, E. F., Franzen, S., Smirnova, T., and Ghiladi, R. A. (2010) Spectroscopic and mechanistic investigations of dehaloperoxidase B from Amphitrite ornata. *Biochem 49*, 6600-16.

30. Poulos, T. L., and Kraut, J. (1980) The structure of cytochrome c peroxidase at 2.5 Å resolution. *J Biol Chem 255*, 575-580.

31. D'Antonio, E. L., Franzen, S., and Bowden, E. F. (2010) Redox Thermodynamics of the Fe(III)/Fe(II) Couple of Dehaloperoxidase-hemoglobin from *Amphitrite ornata*. submitted.

32. Du, J., Sono, M., and Dawson, J. H. (2010) Functional Switching of Amphitrite ornata Dehaloperoxidase from O_2-Binding Globin to Peroxidase Enzyme Facilitated by Halophenol Substrate and H_2O_2. *Biochem*, in press.

33. Belyea, J., Gilvey, L. B., Davis, M. F., Godek, M., Sit, T. L., Lommel, S. A., and Franzen, S. (2005) Enzyme function of the globin dehaloperoxidase from Amphitrite ornata is activated by substrate binding. *Biochemistry 44*, 15637-15644.

34. Thompson, M. K., Franzen, S., Ghiladi, R. A., Reeder, B. J., and Svistunenko, D. A. (2010) Compound ES of Dehaloperoxidase Decays via Two Alternative Pathways Depending on the Conformation of the Distal Histidine. *J Am Chem Soc 132*, 17501-17510.

35. Nicoletti, F. P., Thompson, M. K., Howes, B. D., Franzen, S., and Smulevich, G. (2010) New insights into the role of distal histidine flexibility in ligand stabilization of dehaloperoxidase-hemoglobin from Amphitrite ornata. *Biochem 49*, 1903-12.

36. de Serrano, V., D'Antonio, J., Franzen, S., and Ghiladi, R. A. (2010) Structure of dehaloperoxidase B at 1.58 A resolution and structural characterization of the AB dimer from Amphitrite ornata. *Acta Crystallogr D Biol Crystallogr 66*, 529-538.

37. Thompson, M. K., Davis, M. F., de Serrano, V., Nicoletti, F. P., Howes, B. D., Smulevich, G., and Franzen, S. (2010) Internal binding of halogenated phenols in dehaloperoxidase-hemoglobin inhibits peroxidase function. *Biophys J 99*, 1586-95.

38. Lebioda, L., LaCount, M. W., Zhang, E., Chen, Y. P., Han, K., Whitton, M. M., Lincoln, D. E., and Woodin, S. A. (1999) An enzymatic globin from a marine worm. *Nature 401*, 445.

39. Beers, R. F., Jr., and Sizer, I. W. (1952) A spectrophotometric method for measuring the breakdown of hydrogen peroxide by catalase. *J Biol Chem 195*, 133-140.

40. Franzen, S., Chaudhary, C., Belyea, J., Gilvey, L., Davis, M. F., Sit, T. L., and Lommel, S. A. (2006) Proximal cavity, distal histidine and substrate hydrogen-bonding mutations modulate the activity of Amphitrite ornata dehaloperoxidase. *Biochemistry 45*, 9085-9094.

41. Franzen, S., Gilvey, L. B., and Belyea, J. L. (2007) The pH dependence of the activity of dehaloperoxidase from Amphitrite ornata. *Biochim Biophys Acta-Prot Proteom 1774*, 121-130.

42. D'Antonio, J., and Ghiladi, R. A. (2011) Reactivity of Deoxy- and Oxyferrous Dehaloperoxidase B from Amphitrite ornata: Identification of Compound II and its Ferrous-Hydroperoxide Precursor. submitted.

43. Egawa, T., Shimada, H., and Ishimura, Y. (2000) Formation of compound I in the reaction of native myoglobins with hydrogen peroxide. *J Biol Chem 275*, 34858-34866.

44. Matsui, T., Ozaki, S., and Watanabe, Y. (1997) On the formation and reactivity of compound I of the His-64 myoglobin mutants. *J Biol Chem 272*, 32735-8.

45. Hewson, W. D., and Hager, L. P. (1979) Oxidation of horseradish peroxidase compound II to compound I. *J Biol Chem 254*, 3182-3186.

46. Farhangrazi, Z. S., Copeland, B. R., Nakayama, T., Amachi, T., Yamazaki, I., and Powers, L. S. (1994) Oxidation-reduction properties of compounds I and II of Arthromyces ramosus peroxidase. *Biochem 33*, 5647-52.

47. Rodriguez Maranon, M. J., Mercier, D., van Huystee, R. B., and Stillman, M. J. (1994) Analysis of the optical absorption and magnetic-circular-dichroism spectra of peanut peroxidase: electronic structure of a peroxidase with biochemical properties similar to those of horseradish peroxidase. *Biochem J 301 (Pt 2)*, 335-41.

48. Nissum, M., Schiodt, C. B., and Welinder, K. G. (2001) Reactions of soybean peroxidase and hydrogen peroxide pH 2.4-12.0, and veratryl alcohol at pH 2.4. *Biochim Biophys Acta 1545*, 339-48.

49. Singh, R., Berry, R. E., Yang, F., Zhang, H., Walker, F. A., and Ivancich, A. (2010) Unprecedented peroxidase-like activity of Rhodnius prolixus nitrophorin 2: identification of the [FeIV=O Por*]+ and [FeIV=O Por](Tyr38*) intermediates and their role(s) in substrate oxidation. *Biochem 49*, 8857-72.

50. Dunford, H. B., and Stillman, J. S. (1976) Function and Mechanism of Action of Peroxidases. *Coord Chem Rev 19*, 187-251.

51. Svistunenko, D. A., and Cooper, C. E. (2004) A new method of identifying the site of tyrosyl radicals in proteins. *Biophys J 87*, 582-595.

52. Nilges, M. SimPow6. Illinois EPR Research Center, http://ierc.scs.uiuc.edu/~nilges/software.html.

53. Fenwick, C. W., and English, A. M. (1996) Trapping and LC-MS identification of protein radicals formed in the horse heart metmyoglobin-H2O2 reaction. *J Am Chem Soc 118*, 12236-12237.

54. Witting, P. K., Mauk, A. G., and Lay, P. A. (2002) Role of tyrosine-103 in myoglobin peroxidase activity: Kinetic and steady-state studies on the reaction of wild-type and variant recombinant human myoglobins with H2O2. *Biochemistry 41*, 11495-11503.

55. Smith, A. T., and Veitch, N. C. (1998) Substrate binding and catalysis in heme peroxidases. *Current Opinion in Chemical Biology 2*, 269-278.

56. Gajhede, M. (2001) Horseradish Peroxidase, in *Handbook of Metalloprotein* (Messerschmidt, A., Huber, R., Poulos, T. L., and Weighardt, K., Eds.) pp 195-210, John Wiley & Sons, Inc., Chichester.